An experimental investigation of the “fate” of entrained peritectic minerals during adiabatic ascent of S-type granite magmas

By

Mbali Pertunia Mthethwa

Supervisor: Prof. Gary Stevens

Faculty of Science

March 2018

Declaration

By submitting this thesis/dissertation electronically, I declare that the entirety of the work contained therein is my own, original work that I am the sole author thereof (unless to the extent explicitly otherwise stated), that reproduction and publication thereof by Stellenbosch University will not infringe any third party rights and that I have not previously in its entirety or in part submitted it for obtaining any qualification.

Mbali P Mthethwa

Date: March 2018

Abstract

S-type granites generally display a wide range of trace and major element compositional variation, from tonalitic to leucogranitic compositions. A substantial volume of past research has investigated the mechanisms by which granitic magmas attain the wide compositional range that they display. The proposed theories fall into two broad categories: (i) processes that occur during magma ascent and crystallization, such as fractional crystallization and magma mixing, and (ii) processes that involve entrainment of crystals, or fragments of the source rock, to form part of the magma in the source during segregation. S-type granite magma compositions have been proposed to represent mixtures, in variable proportions, between melt and the peritectic assemblage produced by fluid-absent incongruent melting of metasediments. Despite strong geochemical arguments in support of this process, peritectic minerals are not commonly present in granites. This study used an experimental approach to investigate the fate of an entrained peritectic mineral assemblage, produced by the incongruent fluid-absent melting of biotite, in a monzogranitic S-type magma emplaced in the upper crust. The experiments were conducted at upper crustal, magmatic pressure-temperature conditions, in water pressurized, externally heated, Inconel cold-seal vessels using gold capsules. The starting materials consisted of 70 wt% of a synthetic silicate oxide and mineral mixture, which reacted to form the melt component of the magma at the experimental conditions, and 30 wt% of an assemblage of natural plagioclase, ilmenite and garnet, which was intended to represent the peritectic assemblage, with which the melt coexisted in the source. The results of phase equilibrium modelling and prior experimental studies indicate that the “melt” composition and peritectic assemblage used are consistent with the products of incongruent partial melting of a metapelite at approximately 10 kbar and 850 °C. The resultant starting material had an S-type monzogranitic composition. Experiments were carried out over a temperature range of 743 to 804 °C at a pressure of 1 kbar, with a run duration of 20 days. The results demonstrate that under the investigated P-T conditions, the magma undergoes two reaction mechanisms to bring the out-of-equilibrium, entrained high-

P-T peritectic crystals into equilibrium with the magma. These are, (i) a coupled dissolution-precipitation mechanism, which resulted in efficient equilibration of plagioclase and ilmenite. (ii) mineral-melt reactions that led to the replacement of the high-P-T phases by minerals that are stable at the conditions of the experiment. This process partially removed garnet from the run products, with biotite and cordierite produced at the expense of garnet. However, the garnet-melt reactions are significantly less efficient than dissolution-precipitation in bringing the garnet crystals into equilibrium with the magma. This is evident by the preservation of garnet cores armored by biotite reaction rims. The experiments show that, even including the slower reactions involving garnet, the rates of equilibration of the hypothetical peritectic crystals with the granitic magma at shallow crustal levels is very rapid. These processes appear to be highly efficient, and account for the predominantly magmatic nature of the above-mentioned minerals in crystalline granitic rocks. In the experimental run products, the magma was shown to have a sufficiently high melt volume, at the P-T conditions close to the solidus, to facilitate processes and reactions that bring out-of-equilibrium crystals into equilibrium with the magma. Furthermore, the results suggest that, where garnet crystals are present in crystalline granitic rocks they most likely represent a metastable phase at the conditions of intrusion. They also do not compositionally or texturally resemble the high-P-T peritectic phases, due to recrystallization in the deeper portions of the magma plumbing system. This research has explained why peritectic minerals are absent or very rare in crystalline granitic rocks. Additionally, the findings provide an understanding of why granitic rocks do not commonly contain restitic minerals, early formed magmatic phases that are not stable under the conditions of intrusion, nor peritectic minerals.

Uittreksel

S-tipe graniet rotse algemeen vertoon 'n wye groot en spoorelement komposisionele variasie van tonalitic om leucogranitic komposisies. Daar is 'n baie navorsing tot op hede te dokumenteer hoe granitiese magmas bereik die wye komposisionele variasie dat hulle vertoon. Die voorgestelde teorieë val in twee breë kategorieë: (i) prosesse wat plaasvind tydens magma trap en kristallisasie en (ii) prosesse wat meevoeren van kristal fragmente betrek om die magma in die bron. Maar laasgenoemde is die hoofstroom prosesse. Hierdie studie ondersoek deur 'n eksperimentele benadering die lot van entrained peritectic minerale versameling, wat deur die indruis vloeistof-afwesig smelt van biotiet, in 'n monzogranitic S-tipe magma ingeplaas in die boonste kors. Meevoeren van wisselende verhoudings van 'n peritectic minerale versameling in die smelt in die bron streek, voor magma trap, is vermoedelik 'n belangrike rol in graniet petrogenese speel. Daar word voorgestel dat die samestellingsvariasies vertoon deur gemiddelde tot S-tipe graniet rotse mafiese, is 'n gevolg van meevoeren van peritectic granaat, plagioklaas, ilmeniet, kwarts, cordierite en sillimanite om die smelt. Groot-element komposisionele tendense soos: (i) 'n sterk positiewe korrelasie tussen Ti en maficity (mol Fe + Mg.), 'N tendens wat algemeen in al granietrotse. (Ii) Toename in Ca en A / CNK met 'n toenemende maficity. (Iii) Die afname in Si en Ki met dalende maficity. Hierdie tendense ondersteun die lewensvatbaarheid van die peritectic samevoeging model. Maar mineralogiese en teksturele bewyse van hierdie peritectic fases is skaars in kristallyne granitiese gesteentes. Om vas te stel wat word van die entrained peritectic kristalle op vlak kors vlakke, is 'n sintetiese S-tipe monzogranitic magma samestelling gebruik as 'n vertrekpunt materiaal vir alle eksperimente. Die begin materiaal is saamgestel uit 70 wt.% sintetiese silikaatgel - (bedoel om die smelt fraksie verteenwoordig) en 30 wt.% hipotetiese hoë-P-T peritectic minerale versameling bestaande uit plagioklaas, granaat, en ilmeniet. Die begin materiaal is gesintetiseer sodat op die bereiking van eksperimentele P-T toestande, sal herhaal 'n silikaat smelt gegenereer by 850 °C en 10 kbar deur vloeistof-afwesig smelt van biotiet, saam sit met 'n peritectic versameling. Eksperimente is oor 'n temperatuur van 743-

804 °C en 'n konstante druk van 1 kbar gedra, met elke eksperiment hardloop vir 20 dae. Die resultate toon dat onder die ondersoek P-T toestande, die magma ondergaan drie reaksiemeganismes te buite-ewewig hipotetiese, entrained hoë-P-T peritectic kristalle in ewewig te bring. Dit is, (i) 'n gepaardgaande ontbinding-neerslag meganisme, wat-re evenwichtige komposisies van die hipoteties entrained plagioklaas en ilmeniet oor al ondersoek P-T voorwaardes en oorblyfsel granaat in die loop onder 804 °C. (ii) minerale-smelt reaksies waarin die granaat kristalle reageer met die smelt om biotiet, cordierite en hercynite-geproduseer produseer, net in die aanloop produk teen 804 °C. Maar die granaat-smelt reaksies is stadiger in vergelyking met die ontbinding-neerslag meganisme. Dit is duidelik deur die behoud van granaat kerne gepantserde deur biotiet reaksie vellings. Die eksperimente toon dat, afgesien van die oënskynlike stadiger reaksies met granaat, die pryse van ewewig van grof-gegranuleerde minerale met graniet magma op vlak kors vlakke is baie vinnig. Hierdie prosesse verskyn hoogs doeltreffend te wees, en is verantwoordelik vir die oorwegend magmatiese aard van die bogenoemde minerale in 'n hoë-vlak granitiese gesteentes. In die eksperimentele lopie produkte, is die magma getoon dat 'n voldoende hoë smelt volume het, op die P-T toestande naby aan die solidus, om prosesse of reaksies wat buite-ewewig kristalle bring in ewewig te fasiliteer. Verder het die resultate dui daarop dat, waar granaat kristalle teenwoordig is in kristallyne granitiese gesteentes hulle waarskynlik metastabiele fases in die magma wat ingedring en gekristalliseer is, en hulle doen ook nie compositioneel of texturally lyk die hoë-P-T entrained peritectic fases. Hierdie navorsing het duidelik waarom peritectic minerale afwesig of baie skaars in kristallyne granitiese gesteentes. Daarbenewens het die bevindinge toon hoekom ons nie moet verwag om óf restitic komponente, vroeg gevorm magmatiese fases of die peritectic minerale versameling in 'n hoë-vlak granitiese gesteentes sien.

Acknowledgements

This research was supported by the South African National Research Foundation (NRF) in the form of grants to Professor Gary Stevens through SARChI programme and an MSc bursary to Mbali Pertunia Mthethwa. To my supervisor, Prof. Gary Stevens thank you so much for the project, guidance, continuous support both academic and personal. Thank you for not giving up on this project when you had all the reasons to, your patience and kindness has truly humbled me. I would like to acknowledge Dr. Nicoli Gautier who provided samples from which the “peritectic” minerals used in this study were obtained, Dr Marcos Garcia Arias for his assistance with modelling calculations and Madelaine Frazenburg and Dr Angelique Laurie for assistance with analytical work (SEM).

I would also like to thank all my friends for their support. Special thanks to Michael Njah for all you did for me since the commencement of my MSc, without your continuous support and words of encouragement I would have given up. To Martins Njah, Golden Tefon and Linda Achop your support has humbled me, thank you so much. I would also like to thank my father Henry Mthethwa and my brother Simphiwe Mthethwa for being my pillars of strength and the greatest support system I would not have made it if you gave up on me. Finally, I would like to dedicate this to my late mother Mrs. Lindeni Precious Mthethwa; it is because of your courageous, strong-minded, hardworking and “never-give up” nature that made me to push myself even when I had no strength to do so. Thank you mama for investing in my education and everything you did for me may you soul rest in eternal peace.

Table of Contents

List of Figures

List of Tables

1 Introduction

Granites and migmatites are the most abundant rocks in the continental crust (Johannes, 1980). It is widely believed that these rocks are products of fluid-absent partial melting of crustal rocks in the lower and/or mid-crust (Clemens, 1990; Clemens and Watkins, 2001). Studies by Brown and Fyfe (1970), Stevens and Clemens (1993), Montel and Vielzeuf (1997), Stevens, et al. (1997) and Clemens and Droop (1998) have documented that high temperature fluid-absent incongruent melting of hydrous silicates (e.g. biotite/hornblende) is the most significant crustal melting process responsible for the generation of hot, voluminous, highly mobile granitic magmas. Large volumes of granitic magma generated by fluid-absent incongruent melting of biotite-bearing rocks have the ability to ascend to high crustal levels where they intrude to form granitic plutons or erupt to form felsic volcanic rocks (Clemens, 1990; Clemens and Droop, 1998; Petford et al., 2000). Clemens and Mawer (1992), Petford et al. (1993) and Petford et al. (2000) proposed that hot voluminous granitic magma produced by fluid-absent melting ascends to higher crustal levels through fractures, where the buoyant ascent of the magma is driven by the low density of the magma relative the surrounding rocks.

A consequence of the upward migration of granite magma from the deep crust to shallow crustal levels, as proposed by Clemens (1990), is the enrichment of the upper crust in heat producing elements (e.g. K, Th), while simultaneously leaving the lower crust dehydrated, refractory and enriched in mafic minerals. Consequently, granite magmatism is an important geodynamic processes in the crust, as it is the key mechanism by which crustal differentiation is achieved (Vielzeuf et al., 1990; Montel and Vielzeuf, 1997). The “footprints” of crustal differentiation are demonstrated by the formation of crustally-derived granitic rocks at high levels in the crust and the formation of Fe, Al & Mg enriched, relatively anhydrous granulite facies metamorphic rocks as the deep crustal residuum from which the granite magma segregated (Clemens, 1990).

The types of fluid-absent melting reactions involved in the generation of granitic magmas are proposed to be strongly dependent on source mineralogy and pressure-temperature (P-T)

conditions (Clemens and Wall, 1981; Clemens and Vielzeuf, 1987; Vielzeuf and Montel, 1994). For example, the partial melting of peraluminous metasedimentary source rocks involves incongruent breakdown of biotite through the general reaction: Bt + Pl1 + Sil + Qtz = Pl2 + Ilm + Grt + Kfs + melt (Stevens et al., 2007). The amount of melt that can be generated by fluid-absent melting reactions is controlled by the bulk composition of the source rock, the proportion of hydrous and anhydrous reactant phases and the P-T conditions of metamorphism (White et al., 2001; Brown and Korhonen, 2009). Based on predictive modeling (Clemens and Vielzeuf, 1987) and experimental considerations (Stevens et al., 1997; Vielzeuf and Montel, 1994), metagraywackes and metapelites are considered the most fertile source rocks for the generation of S-type granitic magmas. This is because these rocks contain quite a large fraction of hydrous minerals, whereas other metasedimentary rock types such as metaarenites are less fertile. Thermodynamic modelling studies by (Yakymchuk and Brown, 2014; Mayne et al., 2016) have investigated the effects of melt loss on the fertility of granitic source rocks in open systems. The results of the above-mentioned investigations revealed that melt withdrawal along the prograde P-T path reduces the fertility of the residual crust. Consequently, after each melt withdrawal episode, the residual source will produce lower melt volumes than would have been achieved over the same interval of temperature increase, with no melt loss.

Despite the large body of work on the genesis of S-type granites, the origins of the major and trace element compositional variations displayed by these rocks, especially those involving the more mafic end-members, remain a topic of extensive debate. Analysis of quenched experimental melts (e.g. Stevens et al., 2007), has shown that granitic melts generally have lower ferromagnesian contents than most crystalline S-type granite rocks. This compositional difference exists even between average S-type granites and melts generated by fluid-absent experiments over a temperature range of 850 – 900 °C, i.e. the inferred typical temperature range for peak metamorphic temperatures in the source region of granite rocks (Vielzeuf and Montel, 1994; Montel and Vielzeuf, 1997; Stevens et al., 2007). Experimental melts with high

amount of dissolved ferromagnesian (Fe, Mg) contents are only produced by melts generated at temperatures approaching 1000 °C with melt volumes typically in excess of 40 % (e.g. Patiño Douce and Johnston, 1991; Vielzeuf and Holloway, 1988). However, normal crustal melting typically does not exceed 900 °C because at this temperature, all the biotite would have reacted out and attainment of such high melt volumes requires complete breakdown of biotite before any melt loss occurs and this is unlikely to occur, as it requires unrealistic physical properties of granite source rocks (Clemens and Mawer, 1992). Consequently, the compositions of common S-type granites and granodiorites are too mafic to represent pure melts, hence they must reflect a mixture between leucocratic melt and a more ferromagnesian rich component. Melt inclusion studies corroborate the existence of such leucocratic melts in the granite source region. For example, the presence of strongly leucocratic melt and nanogranite inclusions in peritectic garnet crystals indicates that the growing garnet crystals trapped the melt during incongruent melting reactions. Consequently, the compositions of these trapped melts may be representative of the melt in the source at the time of anatexis (Cesare et al., 2011; Ferrero et al., 2012; Cesare et al., 2015). Nanogranite is a term given to inclusions made up of aggregates of quartz, K-feldspar, muscovite and biotite that are interpreted to represent crystallized anatectic melt inclusions (Cesare et al., 2015).

The models that have been proposed to account for the above-mentioned compositional variations displayed by granitic rocks fall into two broad categories. Some have attributed these compositional ranges to processes such as mixing between crustal melts and mantle derived melts of intermediate to mafic composition (Gray, 1984; Collins, 1996), crystal fractionation (Brown and Pressley, 1999; Couch, 2003) and wall-rock assimilation (De Paolo, 1981), which are proposed to occur during magma ascent and crystallization. The viability of these magma mixing and assimilation-fractional crystallization (AFC) mechanisms are challenged by the fact that mafic magmas will completely or nearly completely crystallize on contact with much cooler granite magmas, as well as the unrealistically high energy requirements of assimilation (Sparks and Marshal, 1986; Glazner, 2007). In addition, fractional

crystallization of biotite, the major ferromagnesian mineral in granites, cannot explain the geochemical trends defined by the rocks, which are typically characterized by a negative correlation between K_2O and FeO + MgO (maficity) (Stevens et al., 2007; Clemens and Stevens, 2012). Details of each of these considerations will be discussed in the sections that follow. Others have ascribed the generation of systematic major element compositional variations in granites to the entrainment of solid mineral fragments into the magma in the source region. These models are entrainment of restite and subsequent restite unmixing (RU) (Chappell and White, 1977, Chappell, 1996) and peritectic assemblage entrainment (PAE) (Stevens et al., 2007). The RU hypothesis entails entrainment of the entire restitic residuum in the source to the magma, with unmixing (separation of melt from residuum) creating the compositional range. In contrast, the PAE hypothesis involves entrainment of only the peritectic crystals produced by the biotite incongruent melting to the magma, with variable degrees of entrainment producing the compositional trends. The processes that involve entrainment in the source are considered the mainstream mechanisms responsible for diversifying the compositions of granitic magmas. However, the RU hypothesis is unlikely to represent an adequate mechanism to fully account for the major element compositional variations displayed by S-type granites (Wall et al., 1987; Clemens and Mawer, 1992; Stevens et al., 2007; Vernon, 2007). There are several reasons for this, as conceptualized by Chappell and White (1977). For example, the requirement that the source mobilize as a diatexitic magma requires that the critical melt fraction (van der Molen and Paterson, 1979) or second percolation threshold (i.e. melt volumes above 40-45 %, e.g. Vigneresse et al., 1996) be exceeded. Many source rocks are incapable of producing these melt fractions at realistic temperatures, and deliver a maximum melt yield, in the range of 20- 30 wt.. % (Montel and Vielzeuf, 1997; Brown, 2013), without taking the effect of incremental melt loss into account. Secondly, this model requires evacuation of the magma from the source prior to segregation of the entrained restite from the magma and requires diapiric ascent of granitic magmas. This type of magma transport is thermally and mechanically inefficient (Clemens and Mawer, 1992), with magma likely to stall relatively close to the source. Magma ascent to high levels in the

crust is likely to be achieved by ascent in dykes, which is substantially more efficient at moving hot magma through cooler rocks (Clemens and Mawer, 1992). Additionally, the RU hypothesis proposes that amphibolite facies xenoliths commonly found in granitic rocks represent unmelted or partially melted components of the source, which, along with the requirement of high melt fractions in the source, has led to the proposal that granitic magmas arise by low temperature fluid saturated melting (Chappell et al., 2000). The inferred relatively low temperatures of melting are at odds with the general view that most granitic magmas arise by incongruent breakdown of biotite at high temperatures (Vielzeuf and Holloway, 1988), as well as the clear ability of many granitic magmas to intrude at high levels in the crust and to erupt.

To date, the PAE model seems to be the most viable petrogenic mechanism to account for the geochemical trends displayed by granitic rock suites. For example, the very tightly correlated Ti vs. maficity (M = mol. Fe + Mg) trend observed in granite rocks irrespective of the type of source, in combination with the poor and negative correlation between K and maficity, demonstrates that these trends are not produced by fractionation of biotite (Stevens et al., 2007). It has been proposed that these trends result from entrainment of peritectic mineral assemblage in the source, which results in the Ti: maficity trend matching the stoichiometry of the incongruent biotite melting reaction (Clemens et al., 2011; Stevens et al., 2007). Arguing for and/or against any of the above-mentioned hypotheses is outside the scope of this study and the information is provided for contextual background. However, it can be argued that crustal melts produced at realistic temperatures have considerably lower maficity that even average granite compositions. Consequently, during crustal differentiation a process of some sort commonly allows the incorporation of some crystalline components into ascending granite magmas and probably plays an important role in shaping the chemical make-up of granitic rocks. However, since the first studies to propose that granitic magmas entrain significant components of the source (Chappell and White, 1977), one of the main research issues has been the difficulty of physically identifying these components in granitic rocks.

The type of source-“inherited”-material that this study has chosen to investigate is the peritectic mineral assemblage. Although peritectic phases are generally absent in high-level granite rocks, there is strong geochemical evidence that suggest their involvement in the petrogenesis of granites. Since the peritectic minerals are produced by the biotite partial melting reactions it is reasonable to expect that they are abundant in the source region and are likely to be entrained into the magma. Some publications (Clemens and Wall, 1988; Clemens and Droop, 1998, Clarke, 2007; Vernon, 2007; Vernon et al., 2009) have hypothesized that the entrained components do not survive during magma ascent, they either dissolve or react with the magma or they re-equilibrate with the magma through a coupled dissolution-precipitation mechanism (Villaros et al., 2009a).

Objectives of this study

This study has used experimental techniques to investigate the “fate” of the entrained peritectic mineral assemblage in a granitic magma that has ascended to shallow crustal levels. This research has addressed the following questions: i) what becomes of the entrained peritectic mineral assemblage, ii) what reaction mechanisms do granitic magmas utilize to bring out-of-equilibrium crystals into equilibrium; and iii) what are the minimum rates at which these reactions occur. Note that despite the focus on a hypothetical peritectic assemblage, the findings are likely to be equally relevant to entrainment of general residuum as conceptualized in the RU hypothesis, as well as to the entrainment of crystals produced by quenching of mafic magma on mingling with cooler granite magma.

2 Geochemistry of S vs. I-type granites

Chappell and White (1974) established a classification scheme for at least two types of granitic rocks, following their extensive study of the granites of the Lachlan Fold Belt in Australia. The authors discovered that the two rock types portrayed extensive mineralogical, geochemical and isotopic differences. Following this discovery, Chappell and White proposed the S- and I classification scheme. Rocks suites with strong peraluminous chemistry and sediment like initial strontium isotope ratios ($^{87}Sr/^{86}Sr_i > 0.708$) were classified as S-type granites, whereas those with more metaluminous chemistry and strontium isotope ratios in the range $^{87}Sr/^{86}Sr_i$ 0.704 – 0.706 were classified as I-type granites. The S and I prefix assigned to these rocks indicates that they are interpreted to have metasedimentary and meta-igneous source rocks, respectively.

S-type granites are now known to generally be the products of partial melting of metapelites and metagraywackes. The melting reactions involved in the generation of S-type granite magmas are well known through experimental studies (Vielzeuf and Montel, 1994; Stevens et al., 1997) and corroborating evidence from migmatitic granulites (Brown and Fyfe, 1970; Stevens and Van Reenen, 1992a; Sawyer, 1996; Johnson et al., 2001,2003). They are proposed to have the form Bt + Qtz + Pl1+ Sil = Pl2 + Grt + melt + Ilm ± Kfs in metapelites and Bt + Qtz + Pl1 = Pl2 + Grt + Opx + melt + Ilm + Kfs in metagraywackes. Clemens et al. (2011) proposed that I-type granites are products of partial melting of meta-volcanic rocks of intermediate composition e.g. andesite. The melting reaction is proposed to have the form Bt + Hbl + Qtz + Pl1 = melt + Pl2 + Cpx + Opx + Ilm ± Grt. S-type granites by virtue of their peraluminous compositions are associated with peraluminous minerals such as cordierite, muscovite, biotite and garnet, whilst I-type granites generally, have biotite and some cases hornblende and/or pyroxenes (Chappell and White, 2001).

2.1 Major element compositions

S-type granites display a compositional range from leucogranitic to tonalitic. They typically have high SiO_2 contents (65- ≤ 79 wt%), Na_2O < 3.2 wt% in rocks with ± 5 wt% K_2O and < 2.2 wt% in rocks with ± 2 wt% K_2O (Chappell and White, 1974; Chappell and White, 2001; Clemens, 2003). They are also characterized by variable FeO and MgO contents, from 0-to-8 wt% and 0-to-3.5 wt% respectively, Al_2O_3 can vary from 11- 17 wt% (Stevens at al., 2007). I-type granites can range in composition from granodiorites to leucogranites (Clemens et al., 2011). The more mafic I-type granite end-members can have >2.2 wt% Na_2O, the felsic end-members typically have Na_2O > 3.2 wt% (Chappell and White, 2001).

To further distinguish between the two rock types, Chappell and White (1974), use the Aluminum Saturation Index (ASI = mol.(Al_2O_3/ (CaO+Na_2O + K_20)) = ASI), with S-type granites displaying ASI values > 1.1 (peraluminous) and I –types displaying ASI values < 1.1(weakly peraluminous to metaluminous). A comparison of major element compositions and element ratios for S and I type granite rock suites are displayed in (Fig. 1). The data used for the construction of the plots was compiled from the literature. S-type granite data was taken from Kosciusko Batholith-Australia (Hine et al., 1978; Maas et al., 1997); Cape Granite Suite- South Africa (Scheepers and Armstrong, 2002); Himalaya (Scaillet et al., 1990; Inger and Harris, 1993; Ayres and Harris, 1997), Iberian Massif central (Williamson et al., 1997; Downes et al., 1997; Downes and Duthou, 1988); Krummendal batholith- Greenland (Kalsbeek et al., 2001). I-type granite data: Kosciusko (Hine et al., 1978), Moruya batholith- Australia (Griffin et al., 1978); North East China (Wu et al., 2003); Aegean Sea- Greece (Altherr and Siebel, 2002), South West China (Shen Liu et al., 2009) and Elba-Italy (Dini et al., 2002).

Aluminum saturation index (ASI) is one of the parameters that readily display the compositional differences between S and I-type granite suites. According to Chappell and White (1974), I-type granites exclusively have ASI values less than 1.1. However, compositions of the chosen granite rock suites show that leucocratic I-type granites have ASI values ≥1, with the most peraluminous rocks having ASI 1.3. Nonetheless, the mafic end

members of I-type granite suites have ASI values well < 1 (Fig. 1a). The rocks of the S-type granite suites examined in this study all plot above ASI 1.1. However, the leucocratic end members generally have lower ASI values than the mafic end-members. Thus, in S-type granites, the ASI value correlates positively with maficity, whereas I-type granites demonstrate the opposite trend. Clemens et al. (2011) proposed that the decrease in ASI values with increasing maficity in I-type granites results from entrainment of peritectic clinopyroxene. This necessitates the presence of hornblende as a reactant in the sources of these magmas. The trend towards more peraluminous character with increasing maficiy in S-type granites is proposed to arise by entrainment of a peritectic assemblage dominated by garnet (Stevens et al., 2007).

The data plotted in Figure 1 also demonstrates the distinct overlap in ASI values of leucocratic S and I type granitic rocks. However, on average at any given maficity value (mol. Mg +Fe) S-type granites still maintain higher ASI values than I-type granites. Clemens et al (2011) proposed that the overlap in ASI values for the two rock types was a consequence of similarities in the compositions of their parental melts. Both S and I-type granites show a very strong positive correlation between Ti and maficity (Fig.1b) and a substantial increase in Ca as rocks become more mafic (Fig.1c). However, it is worth noting that on average I-type granite rocks have higher Ca content than S-type granite rocks with similar maficity values. Elements such as K and Si (Fig.1d-e) display a negative correlation with maficity for both rock types. Clemens et al., (2011) proposed that the poor correlation between K_2O and maficity suggests that mineral phases that concentrate potassium (K) (e.g. biotite) must be reactant phases in melting reactions that generate magmas for both S and I type granite rocks. In S-type granites the increase in Ca, ASI and the decrease in Si with increasing maficity are proposed to be a consequence of entrainment of significant mixtures between peritectic garnet and either peritectic Ca-plagioclase an sillimanite respectively (Stevens et al., 2007). Additionally, the combined requirements of increasing ASI and Ca as well as decreasing Si and K as a function of increasing maficity is proposed to be met only by the entrainment of garnet to the melt.

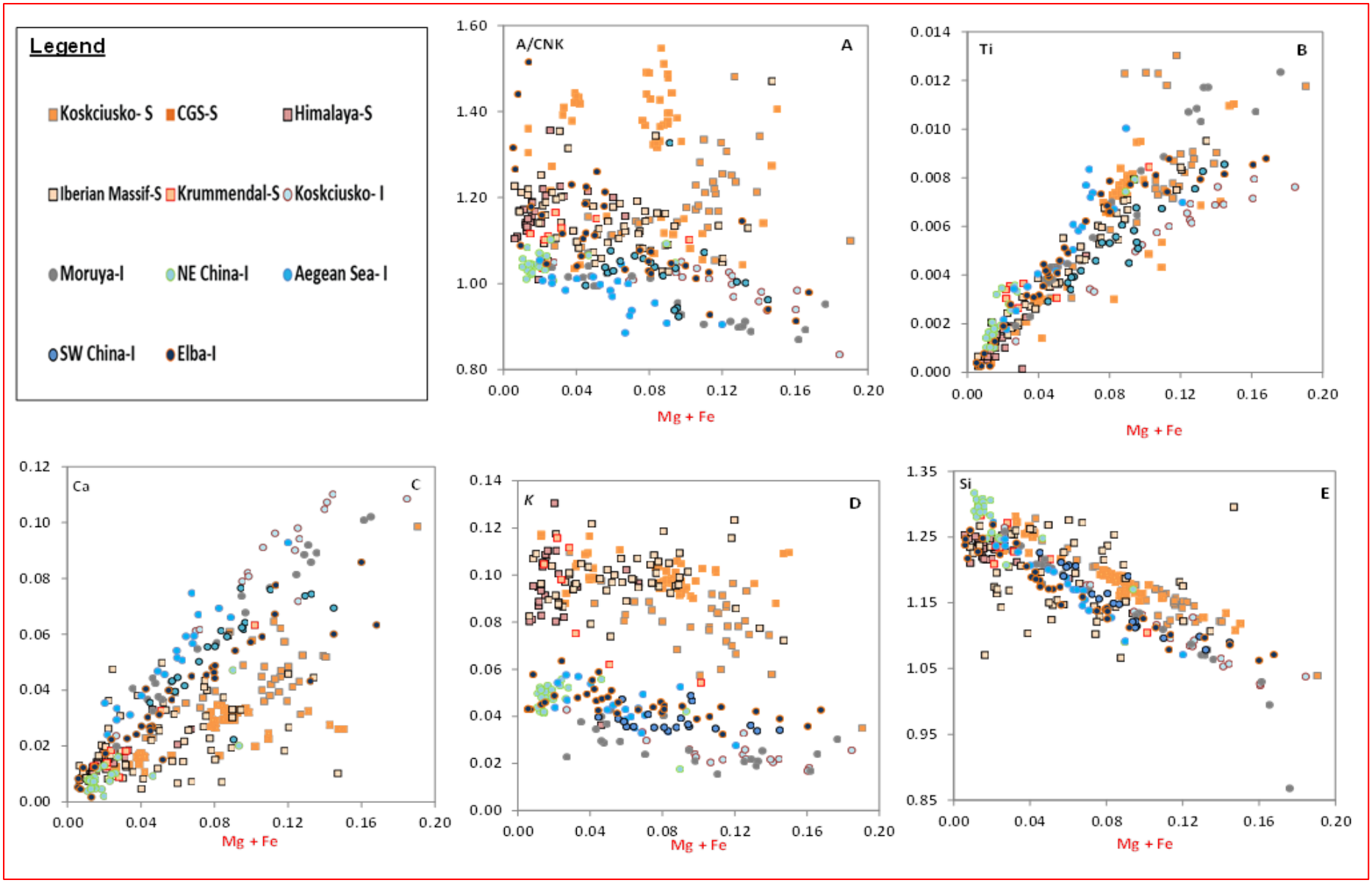

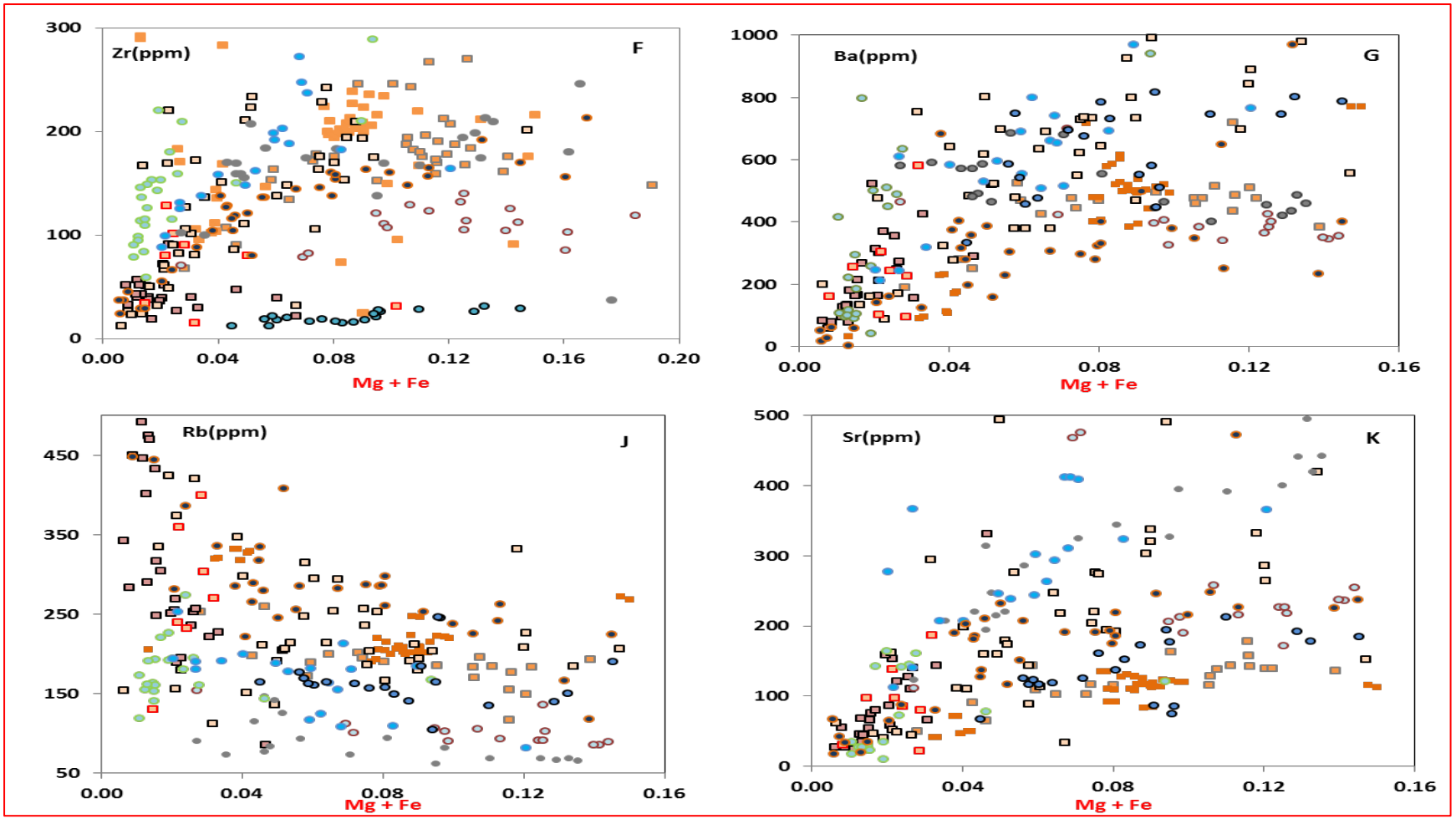

Figure 1: Plots illustrating major and trace element compositional trends for S- and I-type granitic rock suites plotted against maficity.

S-type suites are symbolized by squares and I-types by circles.

2.2 Trace element compositions

The accessory suite contained within S and I-type granites may be used as one of the key features to differentiate between the two rock types. S-type granites are associated with accessory phases such as inherited and magmatic zircon, monazite, and xenotime (Bea, 1996; Stevens et al., 2007; Villaros at et., 2009a). I type granite rocks are typically associated with sphene, predominantly magmatic zircon, allanite and apatite (Chappell and White, 2001; Broska, 2003). Both rocks contain ilmenite. Both S- and I-type granite rock suites show good correlation between Zr and maficity (Fig. 1f) (Clemens et al., 2011). Stevens et al. (2007) and Villaros et al. (2009), proposed that zircon, a common inclusion in biotite in high-grade metamorphic rocks is most likely entrained along with the peritectic assemblage due to its proximity to the sites of melting and small crystal size. Villaros et al. (2009b) further proposed that zircon and monazite crystals are most likely liberated and co-entrained with the peritectic assemblage during incongruent melting of biotite.

There is also a distinct overlap between Zr values of both rock types. However, on average I-type granites seem to have higher Zr concentrations than S-type granites with similar maficity values especially for more leucocratic end members. Clemens et al., (2011) attributed the above-mentioned trait to higher zircon solubility in I-type granite melts than in S-type magmas at similar temperatures. The concentration of elements such as Ba, Rb, and Sr (Fig. 1g-i) compatible in reactant phases of the biotite and/or hornblende incongruent melting reactions show a large scatter as a function of maficity. Villaros et al. (2009b) interpreted this scatter to be a consequence of the fact that these elements were liberated on melting and did not partition strongly into crystals in the residuum. The greatest scatter is seen at intermediate maficity values. This peak is proposed to represent magma compositions that formed at the highest degree of plagioclase and biotite consumption, but with less dilution by peritectic assemblage entrainment than is the case for magmas with higher maficity values (Villaros et al., 2009b). Clemens et al. (2011) reasoned that the scattered variation was merely a function of mineralogical variations in the source.

3 Models for compositional variations in S-type granites

3.1 Magma mixing

Mixing between a mafic and felsic magmas is considered by many workers to be a viable process to account for compositional diversity displayed by S-type granites of the Lachlan Fold Belt (LFB) in southeastern Australia (Vernon, 1983; Chappell, 1996; Collins, 1996; Maas et al., 1997). The magma-mixing hypothesis involves mixing of two or more magmas of different composition to form homogeneous hybrid magmas (Chappell, 1996; Vernon, 1983). Some authors (Keay et al., 1997, 1999; Didier, 1984; Gray, 1984) proposed that this mixing involves magma from a metasedimentary source providing the felsic component and magma from a mantle source providing the mafic component. The contribution of a juvenile mafic magma to the S-type granite magmas is estimated to range from 0 to between 10 and 40 % (Gray, 1984; Chappell and White, 1992; Collins, 1996, Keay et al., 1997). The occurrence of peraluminous microgranitoid enclaves in S-type granites and related volcanic rocks from this area, is commonly invoked as evidence of a small degree of hybridization between a peraluminous felsic magma and a more mafic magma (Didier, 1984; Reid et al., 1983; Chappell, 1996; Vernon, 2007). The mafic magma most likely played a role in shaping the composition of the S-type magma involved in the mixing, but had no influence on the composition of the host magma (Waight et al, 2000 a, b, 2001; Vernon, 2007).

According to Waight et al. (2000a,b, 2001); Clemens, (2003; 2012), the occurrence of mafic enclaves in granites is a result of magma mingling not mixing. “Mingling” refers to a physical interaction between two compositionally distinct magmas, resulting in the formation of a suspension of the minor phase in the major phase and both magmas retain their identities (Chappell, 1996; Clemens, 2012). Clemens (2012) documented that a small volume of true hybrid mafic to intermediate magmas may form adjacent to the site of intrusion of mafic magmas that provide a heat source for crustal melting. Whatever the proportion of the added mafic magma it is evidently not significant enough to effect major compositional changes to the S-type granitic magmas (Clemens, 2003). Sparks and Marshall (1986) stated that most

mafic xenoliths might possibly represent less evolved basaltic magma that solidified when commingled with a much larger volume of silicic magma.

A number of studies have documented that true mixing between compositionally different magmas is difficult to achieve, (Skjerlie and Patiño Douce, 1995). The above-mentioned authors documented that the rates of melt extraction are likely faster than diffusive homogenization, thus hindering the production of homogeneous hybrid melts. Sparks and Marshall (1986) documented that (i) Mingling between compositionally and thermally different magmas causes major changes in magma rheology. (ii) Thermal diffusion rates are orders of magnitudes faster than chemical diffusion rates, thus magmas must reach thermal equilibration before complete hybridization can occur by shearing and diffusion. (iii) The ability of magmas to mix successfully depends on their physical properties after thermal equilibration. The authors proposed that true hybridization could only occur when both magmas behave as liquids at the same temperature. In granitic magmas with low Reynolds number (< 2000), the large viscosity difference between the mafic and silicic magma will impede effective mixing (Huppert et al., 1984; Sparks and Marshall, 1986).

Gray (1984) proposed that radiogenic isotope variations in granites result from mixing of basaltic material and granitic melt derived from melting of a sedimentary source. Wall et al (1987) stated that mixing between felsic and mafic magma is the cause of linear trends in trace and major element Harker plots. Thus, if compositional variations in mafic S-type granites were indeed a result of magma mixing, it would be reasonable to expect radiogenic Sr and Nd isotopic ratios to portray a more mantle-like character with increasing maficity. Implying that, the most mantle-like isotopic compositions would characterize the most mafic granites (Clemens and Stevens, 2012), however, this is not the case as demonstrated by Fig. 2.

Farina and Stevens (2011) demonstrated that Sr isotopic variations observed in granite suites might be a reflection of: (i) compositional differences between magma batches produced from progressive partial melting of a single source, (ii) Isotopic disequilibrium due to slow diffusional

equilibration of plagioclase during partial melting of a crustal source rock. Therefore, failure to attain isotopic equilibrium in the source region before and during melt generation and magma extraction, results in magmas that are characterized by variable Sr isotopic compositions. The authors argued that the occurrence of mafic enclaves within granites does not necessarily invoke that isotopic variations owe their origin to any interaction between the mantle and crustal-derived magmas. Therefore, (Clemens, 2003; Farina and Stevens, 2011; Clemens et al., 2011; Clemens and Stevens, 2012) suggested that isotopic variations occur primarily because of source compositional heterogeneities, incomplete equilibration during anatexis in the source and the incremental assembly of granite plutons from many different magma batches.

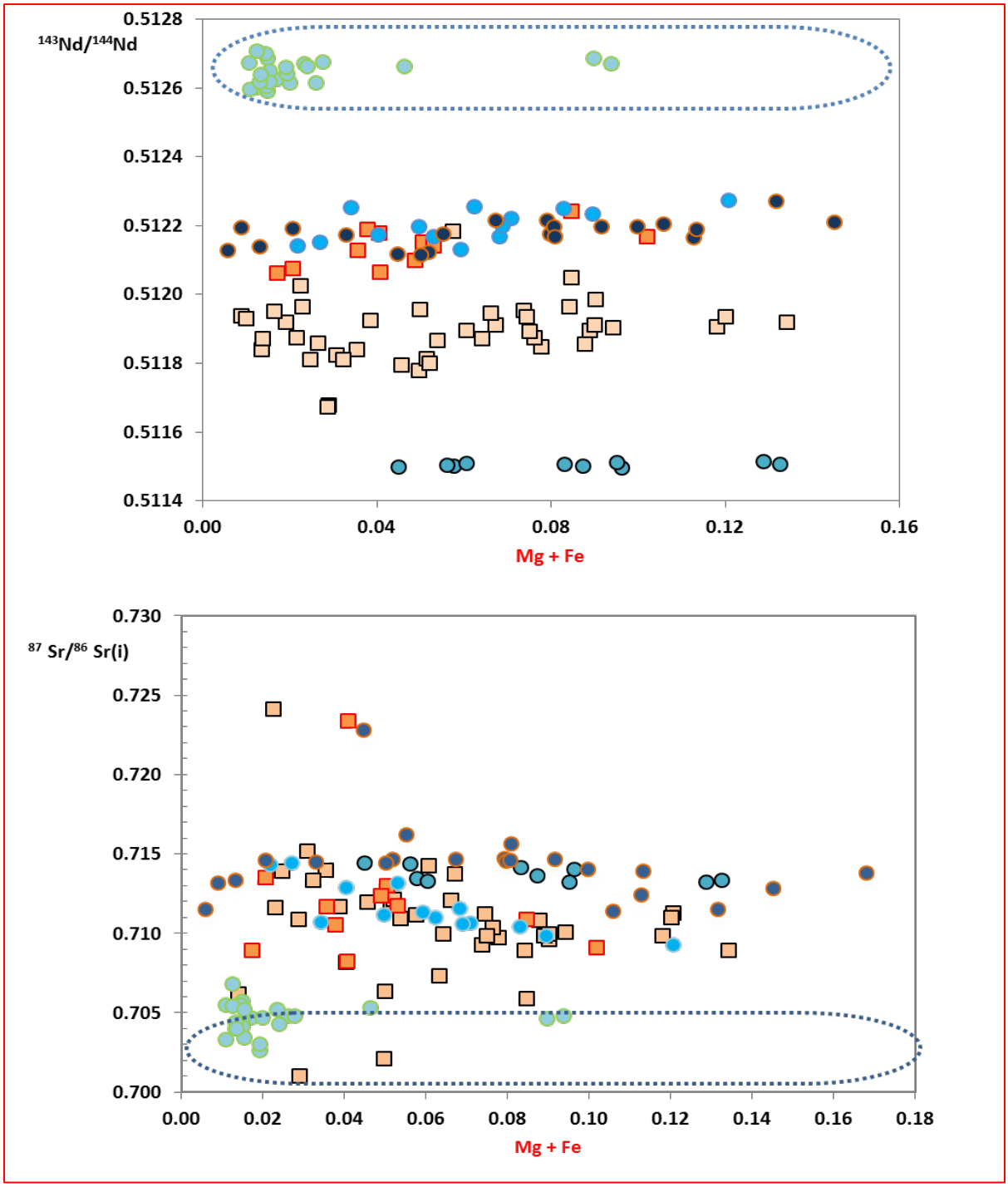

Figure 2: Nd and Sr isotopic compositions of selected S- and I-type granitic rock suites plotted against maficty. S-type granite suites are symbolized by squares and I-types by circles. References and legend are the same as in Fig 1.The blue dotted bands illustrate values that might be considered representative of mantle values. Note that neither granite type shows any clear correlation between maficity and isotopic composition.

3.2 Crystal Fractionation

Crystal fractionation (FC) is one of the processes proposed to play some role in shaping the compositional range exhibited by granites. In FC, the separation of crystals from magma is proposed to generate the compositional heterogeneities observed in high-level granite rocks (Chappell, 2004). (Couch, 2003; Chappell, 2004) documented that progressive separation of crystals from a magma driven by either some sort of flow or due to gravity typically produces more felsic (granitic) residual magmas. The ease with which such separation might occur is dependent on the density contrast between melt and crystals, the viscosity of the melt, the size of crystals and general dynamics of the magma chamber (Hawkesworth et al., 2000). The crystals have a bulk composition that differs from that of their host magma, thus progressive separation of crystals from the melt portion of the magma, causes the residual melt to continuously become the new effective bulk composition (Hawkesworth et al., 2000; Winter, 2014). If crystals separate from the melt as they form, the melt can no longer react with the crystals (Winter, 2014). Consequently, the crystals will remain out of compositional equilibrium with changing magmatic conditions, such that the resultant rock composition would be described as a series of fractionated melts, accumulated solids or as mixtures between cumulates and fractionated melts (Clemens and Stevens, 2012; Winter, 2014). Thus a range of magma compositions can be created from single parent magma by separation of varying amounts of crystals that formed in the magma chamber (Winter, 2014). However, some studies have documented that it is impossible for a reasonably sized granitic pluton to have formed by intrusion of one single magma batch (Petford et al., 2000; Glazner et al., 2004). It has been proposed that granitic plutons are constructed by multiple injections of discrete magma batches accompanied by partial solidification of each magma batch before intrusion of another. Such pulsed magma injections probably generate geochemical variations between batches (Petford et al., 2000; Glazner et al., 2004; Clemens et al., 2010; Clemens and Stevens, 2012). Because of the pulsed nature of the amalgamation of granitic plutons, granitic bodies inherit source derived chemical and isotopic characteristics (Clemens and Stevens,

2016). Additionally, it is has been proposed that high melt viscosities and slow chemical diffusion rates inhibit the efficiency of processes such as crystal settling and magma mixing and thus result in the preservation of original, source inherited heterogeneities (Glazner, 2014; Clemens, 2015; Clemens and Stevens, 2016). If crystals do segregate from the magma, this process is likely to only account for small-scale compositional variations, and not the observed pluton wide geochemical range displayed by high-level plutonic rocks (Reid et al., 1993).

The viability of fractional crystallization as a mechanism to account for major-element compositional range displayed by granite rocks has also been criticized from a major-element composition perspective. For example, Stevens et al, (2007), noted that all granite rocks are characterized by a strong positive correlation between Ti and maficity coupled with a negative correlation between K and maficity. As can be seen in Fig. 3, fractionation of biotite from silicic S-type granite melt would produce positive correlations between Ti and maficity and K and maficity. However, positive K vs. maficity trend is not a feature observed in granite rocks (Clemens and Stevens, 2012). Thus, the K and Ti vs. maficity trends displayed by different granite suites suggest that the maficity range within S-type granites cannot be a consequence of biotite fractionation. The mineralogy of granites supports this, ilmenite is a very common Ti-rich mineral in granites, which also contain a significant amount of Ti in biotite. Thus, the very good Ti:M correlation in most granite suites would require co-fractionation of ilmenite, biotite and other ferromagnesian silicates, despite the fact that these crystals have very different size and density properties. Based on the information documented above, it is clear that FC cannot be responsible for pluton-wide compositional variations displayed by granitic rocks. However, local FC is proposed to occur in plutonic granitic magmas at or just below their final emplacement region, to produce volatile-enriched near-roof zones (Clemens et al., 2010).

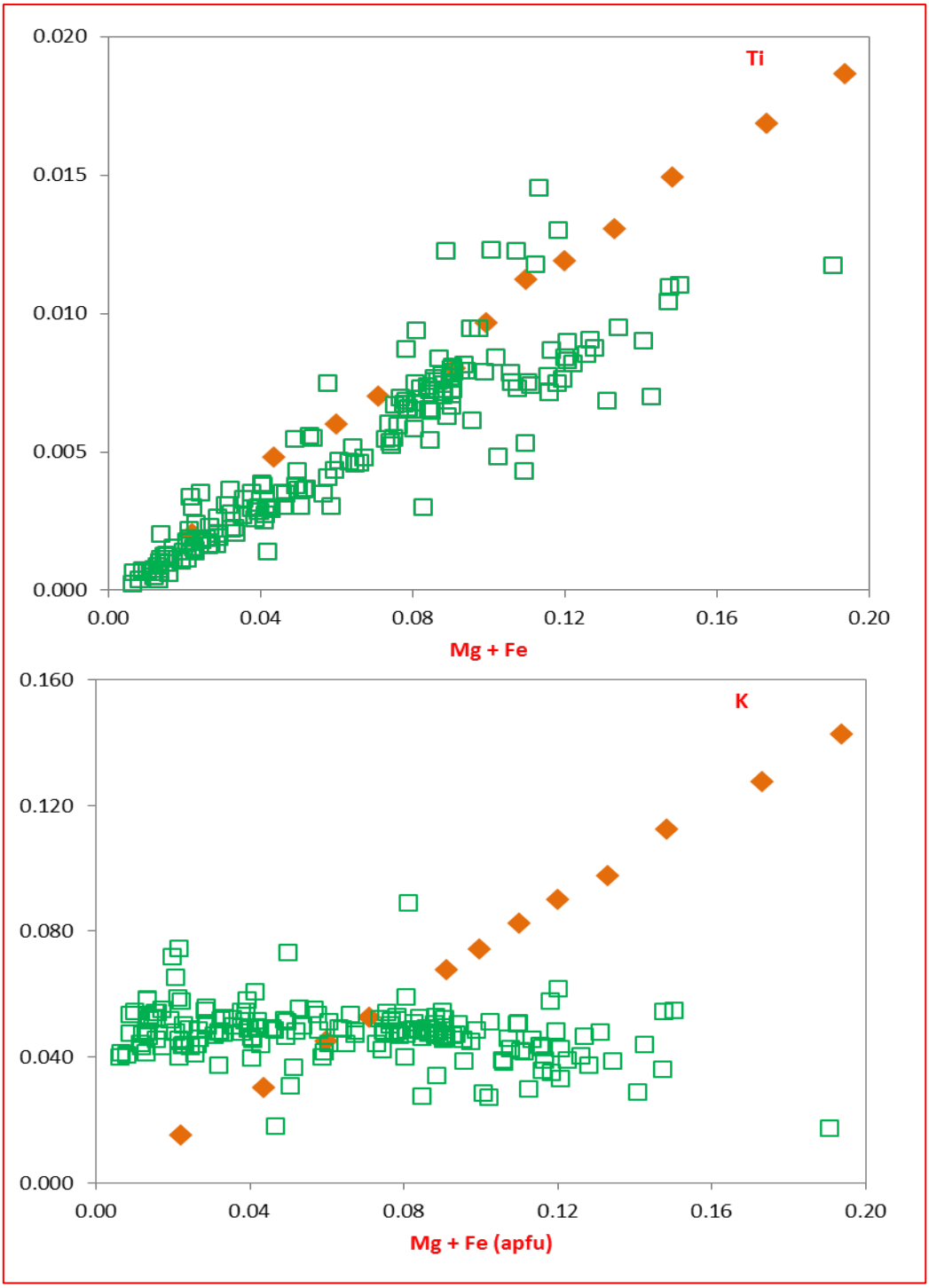

Figure 3: Ti and K values plotted against maficity for S-type granitic rocks comparing typical compositional trends displayed by S-type granites with model trends for granite magmas produced by the accumulation of biotite. S-type granite suites are denoted by green squares and the orange diamonds represent compositional trends produced by the accumulation of biotite.

3.3 Wall-rock assimilation

The wall rock assimilation model proposes that major- and trace-element compositional variations in granites are a consequence of contamination of the ascending granitic magma by assimilation of crustal wall rock material (Clarke, 2007). Proponents of this model have suggested that hot mantle-derived mafic magmas ascending through the continental crust, may melt the crust and assimilate crustal material into the magma (Beard et al., 2005; Huppert et al., 1984). Some studies suggest that wall rock assimilation occurs in conjunction with fractional crystallization, “traditionally” known as assimilation and fractional crystallization (AFC) models (Paolo, 1981). The AFC model suggests that the ascending magma is initially modified by assimilation of crustal material into the magma followed by the effective fractionation of crystals. Ideally, country rock material may be assimilated either as intact or mechanically disaggregated xenoliths or by dissolution of the xenoliths or partial melting of wall rocks (Beard et al., 2005; Clarke, 2007).

The AFC model has been criticized as a mechanism to generate the large-scale compositional variations displayed by granites. Glazner (2007) documented that the major pitfall of assimilation models is the lack of thermal energy in the ascending magma required to dissolve assimilated country rock material. Glazner suggested that an alternative way for effective assimilation of country rock material into the ascending magma would be by mechanical disaggregation. This reduces the requirement for thermal energy. However, the hybrid magmas would have very high crystal contents (50-70 vol. %). Consequently, the energy consumed in this process would most likely result in extensive cooling, crystallization and inevitable formation of highly viscous crystal-rich magma. Thus, the magma would be immobile and unable to undergo further evolution. Clemens et al.(2009, 2010), noted that assimilation models based on isotope and trace element data, fail to pass the test of agreeing with major-element chemistry of modelled hybrid rocks.

The common occurrence of metasedimentary xenoliths or enclaves in S-type granite has been used to support the notion that some degree of assimilation of crustal material occurs

(Chappell and White, 1988). However, preservation of low-grade xenoliths and the almost complete lack of anatectic evidence in xenoliths argue strongly that this interpretation is incorrect (Clemens, 2003; Clemens and Stevens, 2012). According to Clemens (2003) and Vernon (2007), the common occurrence of metasedimentary xenoliths in S-type granites serves as an indication that assimilation of crustal material into these magmas is not efficient enough to effect large-scale compositional changes to the magmas. Clemens and Mawer (1992) documented that for AFC to have been effective in producing the more mafic S-type granites, assimilation of very large amount of crustal material would be required to produce the observed maficity range. However, rapid evacuation of the magma from the source region and high ascent rates inhibit significant interaction between the magmas and wall rocks as they traverse through the upper crust (Clemens and Stevens, 2016). The above-mentioned authors proposed that the existence of compositionally diverse granites, that in the magmatic state would be out of chemical equilibrium with crustal rocks overlying their sources implies that felsic magmas separate efficiently from their anatectic sources and reach their emplacement regions with very little chemical interaction with the crust through which the magma must move.

3.4 Restite entrainment and restite unmixing (RU)

In combination, the restite entrainment model (Chappell et al., 1974) and restite unmixing model (Chappell et al., 1987), propose that the entire residual component of the source rock is entrained to the melt in the source region. The unmixing part of the model arises from the notion that during ascent progressive segregation of the entrained restite components from the melt produces the compositional variations observed in granites. The restite components may include unmelted fragments of the source rock, mineral phases that did not take part in the melting reactions, crystalline solids produced by the incongruent breakdown of hydrous silicates and residues of mineral phases partially consumed by the incongruent melting reaction (White et al., 1999; Chappell et al., 2000). Entrainment of restite as the origin of compositional variations in granites implies that granites “image” their source rocks in a

straightforward way i.e. compositions of the most mafic granites represents the composition of their source (Wall et al., 1987).

Amphibolite-facies enclaves found in some S-type granite rocks have been interpreted to represent entrained restite fragments, which subsequently led to the suggestion that these granite magmas were generated by relatively low-temperature fluid present melting reactions (Chappell et al., 2000). However, this view is at odds with the general view that most granitic magmas are products of high-temperature fluid-absent incongruent breakdown of biotite (Vielzeuf and Montel, 1994; Stevens et al., 1997). The adequacy of this model to account for compositional variations displayed by mafic S-type granites has been a subject of substantial debate. The most prominent concern involves identification of restitic phases in high-level granitic rocks. According to some scholars, identification of restitic components requires that, (i) the metasedimentary enclaves proposed to represent residuum must be melt-depleted in comparison to the source rocks (Clemens, 2003). (ii) The mineral and textural features must have characteristics of phases that formed in high-grade metamorphic environments, and (iii) compositions of the mineral phases must reflect equilibrium with granitic melts at P-T conditions of anatectic environment (Wall et al., 1987; Vernon, 2007).

The above-mentioned authors documented that most inferred “restite’ phases have euhedral grain shapes, are stable at low pressures under magmatic conditions and exhibit grain-size variations similar to crystals within the host rock that have definitely crystallized from the melt. Furthermore, Clemens (2001, 2003) documented that the metapelite enclaves inferred to as restites are normally biotite rich, whereas biotite would have broken down in most partial melting reactions that generate S-type magmas. The biotite should also have broken down if the metapelite enclaves were resistate (i.e. unmelted rocks fragments in the source region), from a high-temperature granulite-facies terrane (Vernon, 2007). Clemens (2003) reasoned that such enclaves are mid-crustal xenoliths rather than restite fragments.

Another limitation of this model is that mobilization of a crystal-rich magma preceding separation of crystals from the melt is at odds with the mechanisms proposed for the efficient

ascent of granite magmas to higher crustal levels. Firstly, magmas generated by fluid-present melting reactions at low temperatures would most likely be close to H_2O saturation and would likely remain near their source region because of the negative slope of the H_2O-saturated granite solidus (Cann, 1970). Secondly, the RU hypothesis require diapiric ascent of the granite magmas i.e. the magma must ascend to shallow crustal levels by heating and softening the wall rocks through which it passes (Clemens and Mawer, 1992; Clemens, 2012). Diapiric mobilization has been ruled out as an effective mechanism for significant transport of granite magmas through the crust, based on thermal limitations and the lack of field evidence (Clemens and Mawer, 1992). Furthermore, crystal-rich magmas have a high bulk density and become gravitationally stable, thus they would most likely not travel great distances from their source regions (Clemens and Droop, 1998). Additionally, the RU model assumes that most mafic granitic rocks represent compositions of their source rocks. However, this premise is not supported by geochemical evidence for example, unlike their source rocks S-type granites have a uniform and perfectly correlated Ti vs. maficity range (Stevens at al., 2007; Clemens et al., 2011). For the assumption that compositions of mafic granitic rocks emulate compositions of their source rocks to be valid, there ought to be evidence of large plutonic bodies with pelitic compositions exposed in high-level crystalline granite rocks. However, there is an apparent absence of such pelitic compositions high-level S-type granitic rocks (Clemens and Stevens, 2012).

3.5 Peritectic Assemblage Entrainment (PAE)

The PAE hypothesis was first proposed by Stevens et al. (2007) as a universally applicable model to explain compositional variations observed in S-type granitic rocks, using the Cape Granite Suite (CGS) in South Africa as an example. These authors noted that compositions of most S-type CGS rocks have mafic contents too high to represent pure melts. They suggested that compositions of mafic granites may be accomplished by addition of a Fe and Mg-rich component to the magma in the source. The major-element compositions of these rocks plotted against maficity (e.g. Ca vs. maficity and K vs. M) evolve along trends consistent with

the average to mafic compositions representing mixtures of melt and crystals and the leucogranitic compositions representing pure melts (Stevens et al., 2007; Villaros et al., 2009). It can be seen from Fig. 4 below, that a significant portion of the S-type granite rock compositions have much higher Fe + Mg values than average leucocratic S-type melt compositions; this alone indicates that the compositions of these rocks are unlikely to represent pure melts (Garcia-Arias and Stevens, 2016). Arguing from the major-element geochemistry viewpoint, the PAE hypothesis sees the compositional variations in mafic S-type granites as reflecting mixtures between leucocratic melts and the peritectic mineral assemblage produced by incongruent fluid-absent melting of biotite.

The peritectic mineral assemblage produced during partial melting of metapelitic rocks may consist of garnet, cordierite, plagioclase, sillimanite, kyanite, potassium feldspar, rutile, ilmenite, and orthopyroxene. However, for common source compositions undergoing anatexis near the base of the crust, garnet and ilmenite will dominate the peritectic assemblage (Stevens et al., 2007). The specific peritectic assemblage and the mineral proportions within this assemblage are dependent on the stoichiometry of the biotite melting reaction (Clemens and Stevens, 2012). The PAE model proposes that much of the compositional variations observed in granitic rocks are produced in the source and that two parameters control the composition of the magma; 1. The composition of the melt; 2. the amount of peritectic assemblage entrained to the magma. The peritectic minerals are proposed to be readily entrained into the melt because they are abundant at the sites of melting and have significantly smaller grain sizes than pre-anatectic metamorphic minerals (Stevens et al., 2007). PAE is proposed to explain the major-element correlations that exist in S-type granites as a function of maficity. That is, the positive correlation between Ti and M, the increase in Ca, Mg#, ASI, and the decrease in Si and K, with increasing maficity. Stevens et al., (2007) proposed that most mafic S-type granodiorites reflect mixtures of melt and ~30 mol. % of the peritectic assemblage produced by the biotite incongruent melting reaction in the source, whilst the most leucocratic granites represent pure melts. Co-entrainment of the accessory mineral suite,

which occurred as inclusions within reactant biotite and along pre-anatectic grain boundaries, is proposed to influence the trace element composition of the granites (Villaros et al., 2009b). From a geochemical perspective, the PAE hypothesis adequately explains the major and trace element compositional trends defined by granite rocks as a function of increasing maficity (Clemens and Stevens, 2012). As a result, PAE hypothesis is considered the most viable mechanism to date that explains the genesis of most compositional variations observed in crystalline granitic rocks.

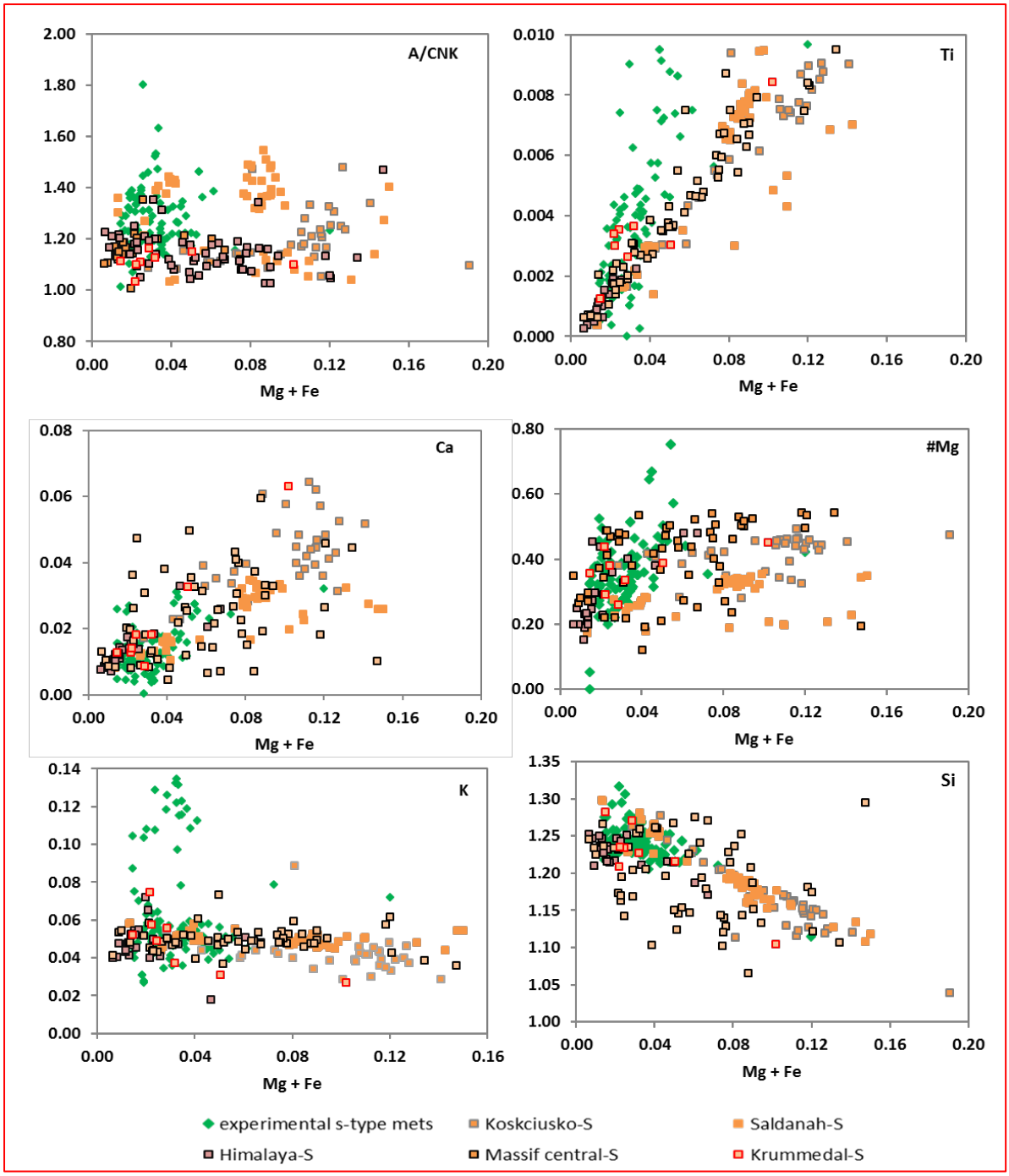

Figure 4: A comparison of major element compositions plotted against maficity for S-type granitic rock suites and experimental leucocratic S-type melts.

References for S-type granitic rock suites are the same as in Fig. 1. Compositions of experimental melts are taken from (Stevens et al., 1997; Montel and Vielzeuf, 1997; Vielzeuf and Holloway, 1988; Green, 1976; Pickering and Johnston, 1998; Patiño Douce and Johnston, 1991; Patiño Douce and Harris, 1998; Vielzeuf and Montel, 1994; Castro et al, 1999).

4 Predicted “fates” of entrained peritectic minerals

Different models of granite petrogenesis such as restite and peritectic assemblage entrainment stem from the idea that granitic magmas leave their source regions as crystal-melt mixtures. Another similarity between these models is the scarcity of physical evidence in crystalline granites to support any of the models. Hence, it is vital to look into what becomes of the high-P-T, entrained, peritectic phases when the magma reaches shallow levels in the crust. The sections below will document the known “fates” of high P-T minerals in high-level S-type granites.

4.1 Theoretical and natural rocks studies

Minerals that come into contact with a melt, with which they are out of equilibrium, will re-equilibrate to reduce the free energy of the system (Putins, 2009). The equilibration process occurs through a wide range of mechanisms and is ultimately responsible for most of the mineral assemblages we see in the Earth’s crust (Putins, 2009; Pichavant et al., 2007). The proposed reaction mechanisms include ion-exchange, congruent/incongruent melting or dissolution (Clarke, 2007; Putins 2002, 2009), coupled dissolution-precipitation (Villaros et al., 2009a; Taylor and Stevens, 2010), nucleation and growth of new phases and diffusive equilibration within crystals and melts (Tsuchiyama and Takahashi, 1983; Acosta-Vigil et al., 2006; Pichavant et al., 2007). Dissolution-driven equilibration is proposed to occur if the temperature of the magma is lower than the stability field of the mineral phase or if the phase is under-saturated in the silicate melt (Clarke, 2007). If a mineral dissolves congruently, physical evidence of the former existence of the phase will not be preserved (Putins, 2009; Clarke, 2007). In contrast, incongruent melting produces new crystals and if incomplete, leaves partially reacted crystal cores that are compositionally and texturally different from the original crystals, as well as reaction rims of new phases and/or precipitation of a new phase that is not in physical contact with the reactant (Putins, 2002; Clarke, 2007). The coupled dissolution-precipitation reaction mechanism involves brings crystals into equilibrium by dissolution of a phase and subsequent re-precipitation of that phase with compositions and

textures that are better equilibrated with the surrounding magmatic P-T conditions (Putins, 2002; Villaros et al., 2009b).

Recent petrogenic models that call for the assembly of large granitic plutons through small, pulsed, injection of magma batches (Glazner et al., 2007) paired with fast ascent rates of granitic magmas through fractures (Clemens and Mawer, 1992; Clemens and Stevens, 2016), might imply that granitic systems have relatively little opportunity to undergo chemical re-equilibration. The rate at which equilibrium between crystals and melt is approached in granitic systems depends on the kinetics of individual reaction mechanisms relative to the rates of pressure and temperature change (Piwinskii, 1967; Pichavant et al., 2007). Maas et al. (1997) suggested that early-formed-high-temperature-pressure magmatic silicates would most likely retain some of their original characteristics, due to sluggish reaction kinetics particularly where low magmatic temperatures prevail.

Clemens and Droop (1998) documented that the melt portion of a magma generated by fluid-absent melting reactions is proposed to have the ability to either dissolve or react with most of the entrained mineral phases as the magma ascends to shallow crustal levels. Similarly, proponents of the PAE model have reasoned that although the entrained peritectic crystals are abundant at the sites of melting, the survival of these crystals along the magma ascent path is unlikely due to continuous re-equilibration with the magma during ascent and cooling, by either dissolution or reaction with the melt (Clemens and Stevens, 2012). It is proposed that as the magma ascends, decreasing temperature and increased H_20 activity will cause peritectic feldspars to dissolve in the melt, whereas ferromagnesian peritectic minerals will react with the melt to form hydrous minerals such as biotite and hornblende. Where the entrained peritectic assemblage remains part of the magmatic assemblage, it may re-equilibrate with the magma through a coupled dissolution-precipitation mechanism (Clemens et al., 2011; Clemens and Stevens, 2012; Villaros et al., 2009a). Consequently, high-level crystalline rocks are generally devoid of high-P-T mineral assemblages and, where evidence of the latter phases exists, they typically show evidence of partial re-equilibration (Clemens

and Wall, 1988; Clemens et al., 2011; Clemens and Stevens, 2012; Taylor and Stevens, 2010).

For example, in S-type rocks, garnet crystals rimmed by cordierite, biotite and/or pseudomorphic replacement of garnet by either biotite or cordierite or both, serve as evidence of some degree of equilibration between peritectic or high-P-T garnets and granitic magmas (Clemens, 1981; Clemens and Wall, 1984; Villaros et al., 2009a). In some granitic rocks, garnet is rimmed by biotite and muscovite (Miller et al., 1981). In S-type felsic volcanic rocks, garnet crystals are commonly rimmed by orthopyroxene and cordierite (Clemens and Wall, 1988). In plutonic S-type granites orthopyroxene is not a common phase. However, evidence of its former existence is proposed to be indicated by aggregates of biotite and quartz and in some cases clear pseudomorphic replacement of orthopyroxene by biotite and quartz intergrowths have been documented (Clemens, 1981, Mass et al., 1997; White et al., 1999). In I-type granitic rocks, zoned plagioclase crystals along with pseudomorphic replacements of orthopyroxene by quartz and biotite intergrowths display evidence of partial re-equilibration of phases that were stable at high temperature and possible high pressure within the magma system (Maas et al., 1997; White et al., 1999; Clemens et al., 2011).

Evidence of the dissolution-precipitation mechanism has been observed in the S-type granites of the CGS in South Africa (Villaros et al., 2009a) and in migmatites from the Mkhondo Valley Metamorphic Suite in Swaziland (Taylor and Stevens, 2010). Villaros et al (2009a) studied garnet crystals in the S-type Peninsula pluton that showed very little evidence of replacement by cordierite or biotite and discovered that the major- and trace-element compositions of the garnet crystals are characterized by homogenous, unzoned cores, with relatively Mg-rich compositions surrounded by more Mn-rich rim zones. The authors noted that compositions of the core domains are identical, regardless of significant compositional differences of their host rocks. Villaros et al. (2009a) reasoned that this was an indication of equilibration via the dissolution-precipitation process between the garnet crystals and the magma at higher temperatures. These authors further proposed that, at some stage along the magma ascent

and cooling path, decreasing temperature and melt volume would impede on the efficiency of the dissolution-precipitation mechanism, preserving the higher temperature cores and rims that were re-equilibrated under lower pressure-temperature conditions. Thus, the rim zones of the garnet crystals may reflect the stage where the system no longer had the capability to facilitate the equilibration process. Similarly, Taylor and Stevens (2010) discovered that even in migmatites, entrained peritectic garnet crystals recrystallized and re-equilibrated with the surrounding magma through a dissolution-precipitation mechanism within structures in which melts had longer residence times. Thus, the crystals lost their peritectic character and adopted a more magmatic character. However, within structures that lost melt rapidly, the entrained garnet crystals retained their peritectic compositions.

Villaros et al. (2009a) proposed that compositional re-setting of garnets could not possibly have been achieved by self-diffusion, as this would require very much longer than the typical duration of granite magmatism. The author's used diffusivities published by Carlson (2006) for Fe, Ca, Mg and Mn to estimate the minimum time it would take garnet crystals to equilibrate with the magma through self-diffusion at ~850 ºC/ 10 kbar, i.e. the proposed conditions of magma generation for the S-type Peninsula pluton. They determined that the self-diffusion process would take approximately 3.95 x 10^6 years for garnets with 1mm radius and 3.95 x 10^8 years for garnet crystals with 1 cm radius. In contrast, it has been proposed that dissolution of a garnet crystal with a diameter of 1 cm could happen on a time scale of days (Skinner, 1956). Fast dissolution rates paired with rapid crystal growth rates, proposed to be on the orders of 10^{-10} to 10^{-11} cm/s (Hawkesworth et al., 2000), imply that the proposed dissolution-precipitation mechanism would reset the composition of a 1 cm garnet crystal in 10^2 to 10^3 years (Villaros et al., 2009). Granitic magmatism is proposed to operate on the time scales of ≤ 10^6 years (Petford et al., 2000). Therefore, Villaros et al. (2009) proposed that a coupled dissolution-precipitation mechanism is the most efficient process through which garnet crystals may possibly re-equilibrate with ascending granitic magmas. Low-density minerals (e.g. feldspars) or minerals with intra-crystalline channels (e.g. micas, cordierite) are thought

to re-equilibrate with granitic magmas within time spans of days to months, whereas dense minerals (e.g. garnet and spinels), are more refractory even when their compositions are far from equilibrium with the melt they coexist with (London et al., 2012).

4.2 Experimental studies

Experimental phase-equilibrium studies of Piwinskii (1967, 1968) conducted using a range of natural “granitic” rocks, revealed that re-equilibration of K-feldspar and plagioclase close to solidus conditions (2 kbar and < 800 ºC), was difficult to achieve, even with excess water in the system. The range of granitic rock compositions used as starting material for the experiments are quartz-monzonite, tonalite, granodiorite and granites obtained from Central Sierra Nevada Batholith, California, all natural rock powders. In both studies, the starting material was sealed in gold capsules and the experiments were carried-out in internally heated pressure vessels using the conventional quenching technique (Tuttle, 1949; Tuttle and Bowen, 1958). Piwinskii (1967), carried-out experiments at 2 kbar and temperature range of 690 to 800 ºC. The experimental duration ranged between 11 to 33 days. In this investigation, Piwinskii used natural granodiorite and quartz-monzonite as starting material for the experiments, the rocks were crushed into fine powders. The granodioritic rock had 15.6 wt% H_2O and the quartz-monzonite contained 17.8 wt% H_2O. The plagioclase crystals in both rock types had oscillatory zoning. Plagioclase from the quartz-monzonite had an average core composition of An_{29} and rim composition of An_{21} and plagioclase from the granodiorite had an average core composition An_{35} and rim An_{29}. Experiment using the quartz-monzonite was held at 690 ºC for 33 days and granodiorite was held at 800 ºC for 11 days. The results of Piwinskii (1967) revealed that the granodiorite produced 60 % melt and the quartz-monzonite 15 % melt. Furthermore, composition of the plagioclase crystals from the run using granodiorite had changed to average of An_{41} and the crystals were unzoned. Contrary, the crystals from the quartz-monzonite had homogeneous cores enclosed by 3 µm rims, the compositions of the individual grains ranged from An_{30} to An_{41}. Piwinskii (1967) concluded that the plagioclase

crystals in the granodiorite had attained equilibrium after 11 days and the crystals in the quartz-monzonite had failed to attain equilibrium with the melt after 33 days of experimental time.

Experiments of Piwinskii (1968) were carried-out using natural tonalite, granodiorite and granite rocks as starting material, with each batch containing 15 wt% H_2O. The experimental run duration was between 18 to 150 days. Experimental pressure ranged from 1 to 3 kbar. However, equilibrium tests were conducted only at 2 kbar pressure and temperature range of 640 to 760 ºC. The plagioclase crystals used in this study were zoned in a similar way to those in the study of Piwinskii (1967). The plagioclase crystals from the granodiorite had an average core composition of An_{36} and rim of An_{28}, crystals from the granite core composition of An_{16} and rim composition of $An_{8.0}$ and the tanolite had core of An_{49} and rim An_{41}. The experimental results (Piwinkii,1968) showed that the composition of plagioclase cores in all the different rock types did not change much even with increased run duration e.g. results from the runs using granodiorite show that the core composition changed from An_{36} in the starting material to An_{41} and An_{43} after 18 and 150 days, respectively. Texturally, the crystals remained zoned. However, the plagioclase cores were homogeneous, surrounded by thin rims, which differed from the oscillatory zoning in the starting material. Noteworthy, the crystal zoning became less prominent with increased experimental run duration. Furthermore, Piwinskii (1968) interpreted the rim zones as growth features resulting from the reaction between the melt and the plagioclase crystals. The author proposed that attainment of equilibrium between plagioclase and melt in runs held at T ≤ 725 ºC / 2 kbar pressure, requires run durations ranging between 4 to 6 months. Runs held at ≥ 760 ºC / 2 kbar equilibrium was attained after 2 months.

Recently, Zarrebini (2016) conducted an experimental investigation looking into the fates of entrained peritectic minerals in average I-type granodioritic magma. The experiments were conducted at P-T conditions equivalent to magma emplacement levels. Zarrebini used a synthetic I-type granodioritic powder as starting material for all experiments. The hypothetical peritectic fraction comprised of natural high-P-T minerals with a size range of 200 – 600 µm. The bulk composition had a net water content of 1.60 wt%, which was added as kaolinite.

Zarrebini (2016) carried-out all experiments in a cold-seal pressure vessel, at pressures of 1.9 and 1.4 kbar and a temperature range of 763 – 723 ºC. Contrary to the outcomes presented by Piwinskii (1967, 1968), the experimental results of Zarrebini (2016) revealed that reasonable equilibrium between entrained peritectic plagioclase and a granodioritic I-type magma could be attained within 10 days. A coupled dissolution-precipitation mechanism was proposed to be responsible for the efficient re-equilibration of “peritectic" plagioclase. Additionally, that study showed that entrained peritectic ferromagnesian phases such as garnet and orthopyroxene, re-equilibrated partially with the surrounding magma within 10 days’. Although these phases persisted in the lower temperature run products, their compositions and textures no longer resembled those of the high-P-T peritectic crystals. These crystals were also commonly rimmed by biotite or amphibole. Thus, during the experiment these crystals underwent compositional change due to the dissolution-precipitation process before or during reacting with the melt portion of the magma to produce the mica or amphibole rim.

4.3 Phase-equilibrium modelling

This section examines the predicted fate of an entrained peritectic mineral assemblage in monzogranitic S-type magma from a thermodynamic modelling perspective. Phase assemblages were calculated using Theriak/Domino software developed by De Capitani and Petrakakis (2010) and the database of Holland and Powell (1998), over a pressure range of 0.5 to 12 kbar and temperature range of 600 – 1000 ºC. The pseudosection diagram presented on Fig.5 was calculated using a biotite-quartz-plagioclase schist composition taken from Villaros et al. (2009a). This composition was chosen because it is believed to be potentially representative of the source rock of the S-type granites from the Peninsula Pluton, which forms part of the Cape Granite Suite in South Africa. The H_2O content of the schist was modified to be consistent with the proposition that large volumes of S-type granitic melts are produced through fluid-absent melting of their source rocks driven by incongruent breakdown of biotite (Vielzeuf and Montel, 1994; Stevens et al., 1997). A H_2O content of 0.89 wt% was chosen as

a reasonable estimate. This water content was calculated using a T-X_{H2O} pseudosection at 10 kbar, which is a pressure, proposed by Villaros et al. (2009a) for the source of Peninsula pluton and is the generally accepted pressure for the formation of granitic magmas (Montel and Vielzeuf, 1994). This H_2O content was the highest bulk rock water content that allowed for fluid-absent melting at 10 kbar. The reason for calculating the pseudosection using a composition representative of an S-type granite source rock was to constrain the peritectic minerals produced by incongruent biotite melting. The pseudosection in Fig.5, demonstrates that, at P-T conditions reasonable for partial melting in the source, incongruent breakdown of biotite yields an assemblage of melt coexisting with peritectic garnet, plagioclase, K-feldspar, sillimanite, Ilmenite and rutile. However, ilmenite is unstable slightly above 850 ºC.

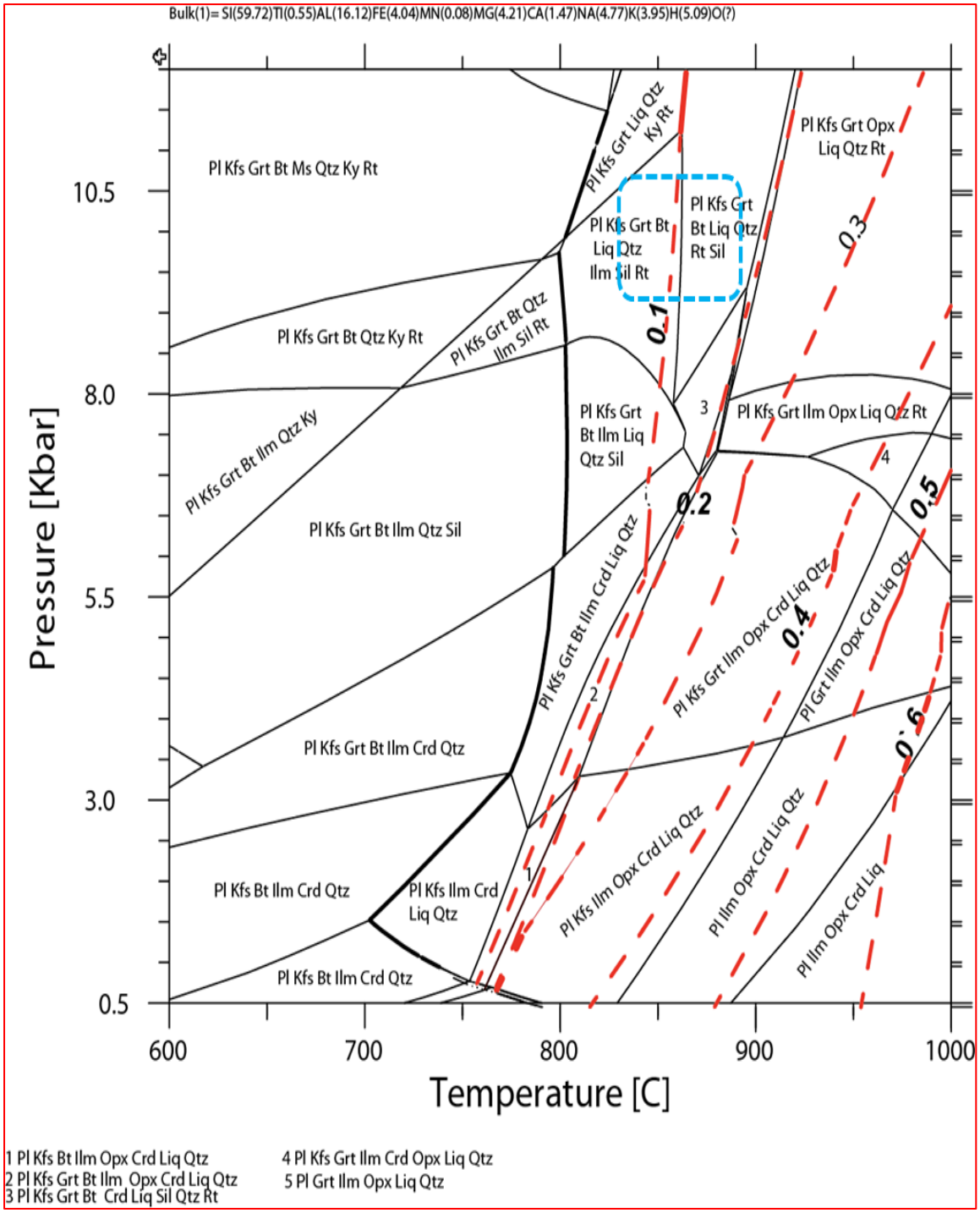

Figure 5: Pseudosection diagram calculated using a biotite-quartz-plagioclase schist composition intended to represent the composition of S-type granite source rock. The blue dashed square represents the proposed PT conditions for the Peninsula pluton and the red dashed line represent melt isopleths (vol %.). Mineral abbreviations are adopted from (Kretz, 1983). Garnet and rutile grow in mode along with melt.

To predict the “fates” of the entrained peritectic mineral assemblage, following entrainment to the magma in the source, and magma segregation and ascent, a pseudosection presented in

Fig. 6, was calculated using a synthetic monzogranitic composition or a quartz-monzonite according to a classification of (Middlemost, 1994). The composition used to construct the psuedosection is presented in Table 1. This composition is also used as the starting material for this study's experiments.

To predict the "fates" of the entrained peritectic mineral assemblage, following entrainment to the magma in the source, and magma segregation and ascent, a pseudosection presented in Fig. 6, was calculated using a synthetic monzogranitic composition or a quartz-monzonite according to a classification of (Middlemost, 1994). The composition used to construct the psuedosection is presented in Table 1. This composition is also used as the starting material for this study's experiments.

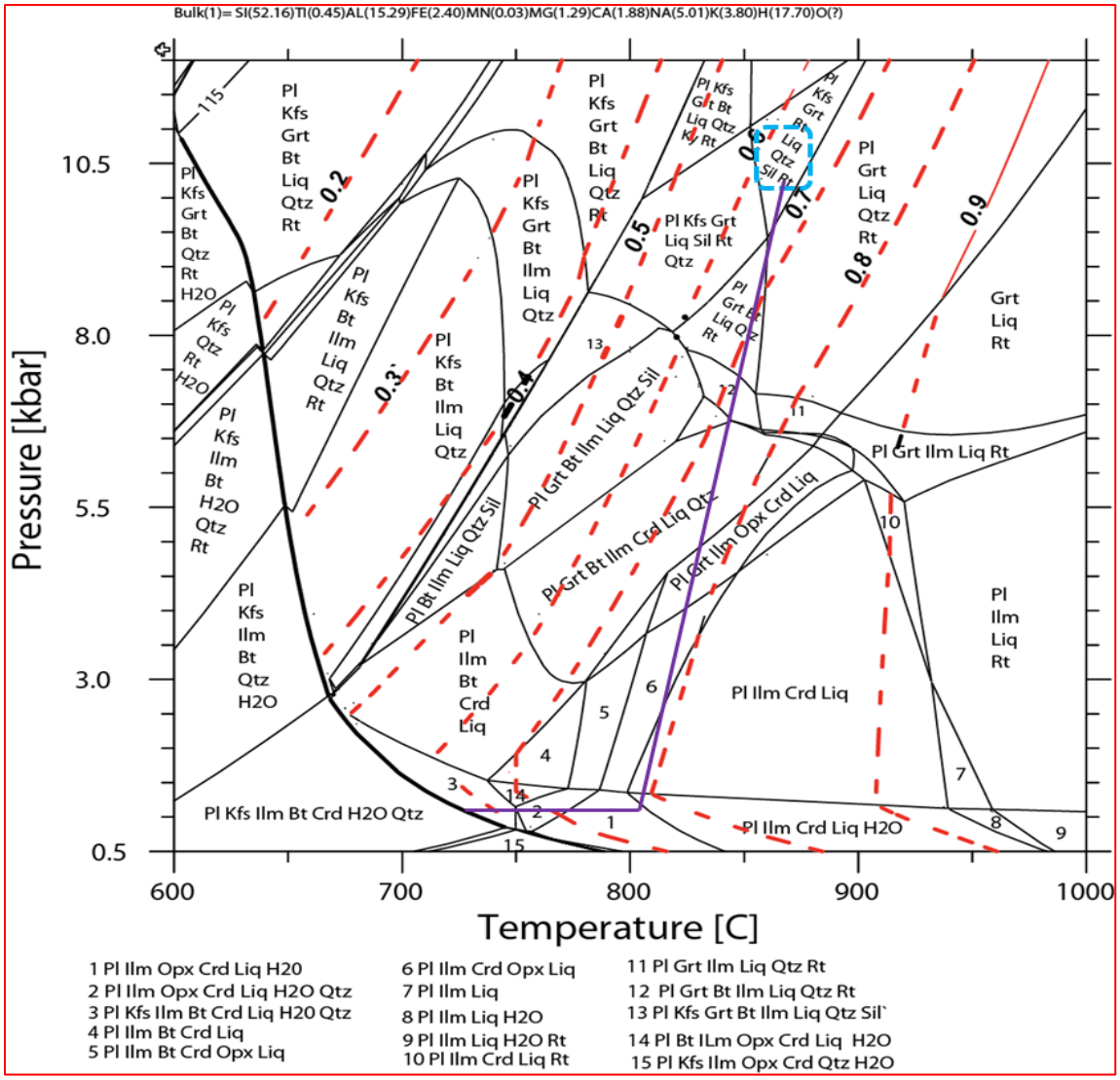

Figure 6: Pseudosection diagram calculated using a S-type monzogranitic magma composition.

The purple line illustrates a hypothetical adiabatic ascent and cooling path, the red dashed lines represent melt isopleths (vol %.) and the blue dashed square represents the S-type granite source region explored in Figure 5. Note that at all reasonable conditions of magma genesis, the magma consists of a significant fraction of crystals. Melt isopleths are sub-parallel to an adiabatic ascent path, thus, while melt volume grows as a consequence of ascent, the magma consists of in excess of 20% crystals throughout the hypothetical ascent and crystallization history investigated.

Mineral Assemblages

At the proposed P-T conditions of melting in the S-type granite source regions, the predicted stable mineral assemblage of the S-type monzogranitic magma composition (Fig. 6) is similar to that predicted for likely S-type granite source rock (Fig. 5). This indicates that the approach followed in this work is relevant to any hypothesis of granite magma formation that proposes that the magma composition is created in the deep crust. The important fact is that granite magmas contain a significant proportion of crystals under all plausible conditions of formation. Thus, the question as to what becomes of these crystals on ascent is equally relevant to all hypotheses of how the magma composition was generated. It is generally suggested that granitic magmas evacuate their source regions and ascend to higher crustal levels along steep adiabatic paths. The pseudosection predicts that the bulk assemblage that segregates from the source comprises of melt, biotite, quartz and a peritectic mineral assemblage made up of plagioclase, garnet, sillimanite, K-feldspar and rutile. The lower-pressure stability limit of this assemblage is ~9 kbar. Between 9 to 7.5 kbar pressure range and temperature of ~848 / 847 ºC, the melt coexists with a stable assemblage comprising of plagioclase, garnet, biotite, rutile and quartz. In a small region, between 7.5 to 6.9 kbar and 846 to 841 ºC, ilmenite joins the above mineral assemblage and coexists with rutile as a second Ti-Fe oxide phase. Below 6.9 kbar, rutile is unstable and ilmenite becomes the only Fe-Ti oxide phase for the rest of the ascent path. Between 6.9 and 4.5 kbar and 840 to 810 º C, garnet coexists with cordierite. In the pressure range of 4.5 and 3.8 kbar and temperature ~810 ºC, orthopyroxene coexists with cordierite and garnet. This region marks the lower-pressure stability zone of garnet in this magma composition. Below 3.8 kbar and between 810 and 750 ºC, cordierite and orthopyroxene are the dominant ferromagnesian minerals. However, below 750 ºC orthopyroxene is unstable. Below this temperature, biotite and cordierite are predicted to be the only ferromagnesian phases. Unlike garnet, plagioclase is predicted to be stable throughout the magma ascent path. The magma is predicted to cross the solidus at 733 ºC/ 1 kbar.

Phase Compositions

The compositions of different mineral phases coexisting with the melt are predicted by the pseudosection to change as the magma experiences decompression. The composition of garnet, at or near the source region, is predicted to be $Alm_{63.86}Py_{32.89}Grs_{2.19}Spss_{1.06}$. As the magma ascends, the pyrope (Mg) content of the garnet is predicted to decrease while the almandine (Fe) and spessartine (Mn) content increases such that, when the garnet reaches its lowermost stability limit, it has a composition of $Alm_{65.31}Py_{22.07}Grs_{1.87}Spss_{10.75}$. Although garnet is stable from the source to near-solidus regions in the magma, its composition changes to adapt to different conditions along the magma ascent path. Notably, the predicted composition of garnet differs significantly from the composition of hypothetical peritectic garnet added in the bulk composition used to calculate the pseudosection. Similarly, the composition of plagioclase also changes with decreasing pressure and temperature. At P-T conditions of the source region, the plagioclase has a compositional range of $An_{36.55}Ab_{57.99}Or_{5.46}$. At 733 ºC and 1 kbar, where the magma is predicted to cross the solidus, the composition of plagioclase is $An_{30.40}Ab_{64.57}Or_{5.03}$. Importantly, the predicted compositions of plagioclase differ significantly from the composition of the hypothetical peritectic plagioclase added in the bulk composition used to construct the pseudosection.

Concluding remarks

The theoretical and experimental studies cited above combined with phase-equilibrium modeling done in this study, have demonstrated that an entrained high P-T crystal load is likely to undergo continuous modification (i.e. re-equilibration) along the magma ascent path. Phase-equilibrium has demonstrated that the assemblage that crystallizes at shallow levels is different from the assemblage that segregates from the source. This agrees with findings of Clemens and Wall (1988).The abovementioned authors proposed that the diverse mineral assemblage contained within S-type granites is not exclusively determined by the chemistry of the initial melt but the P-T conditions of crystallization. During magma evolution, changes in P-T conditions and melt chemistry commonly lead to changes in stable phase assemblages.

Although phase-equilibrium modelling provides an understanding of how phase assemblages and mineral compositions change over a defined P-T range, this represents an over simplified view of natural systems. It does not take into account reaction kinetics, works on an “ideal” system, assumes attainment of equilibrium and it does not account for mineral impurities and heterogeneities that may exist in nature and within experimental products (Anderson, 2002). It has been shown that natural granitic or magmatic systems generally, do not attain compositional equilibrium for all involved phases. Disequilibrium features in granite rocks are commonly demonstrated by zoned high P-T phases and /or early-formed phases that are rimmed by lower-temperature magmatic hydrous phases (Maas et al., 1997; Villaros et al., 2009b; Clemens et al., 2011).

5 Experimental methods

5.1 Experimental philosophy

The reasoning applied in this experimental study is twofold. Firstly, it is possible to design experiments to simulate crystal entrainment into granitic magmas by knowing the mineralogy of their high-grade source rocks. This information can be obtained from phase-equilibrium modelling, as well as previous experimental works using appropriate compositions. In addition, the composition of the melt in the source can be estimated from phase equilibrium modelling, as well as from melt inclusions studies and from previous experimental works. Thus, the hypothetical magma that segregated from the source can be created by mixing an appropriate assemblage of crystals with a synthetic glass or oxide mixture designed to represent the melt. For example, the work of Stevens et al., 2007, has demonstrated granodioritic S-type granites are geochemically very similar to a 70:30 mol% mixture of melt produced by biotite incongruent melting in metasediments at 850 to 900 °C and 10 kbar and the peritectic assemblage produced in conjunction with the melt. Secondly, this study seeks to study the entrained minerals once the magma that has ascended to a magma chamber within the upper-crust, where these crystals are unlikely to be stable. It is known from phase-equilibrium modelling and general studies (e.g. Clemens and Wall, 1988; Villaros et al., 2009a) that high P-T minerals within S-type magmas, such as garnet are unlikely stable in shallow magma chambers. Phase-equilibrium modelling may be used to acquire insight, within the limitations of the modelling, into the phase proportions and compositions within the source rocks and within the resultant magmas at any point along the ascent and cooling path. However, this is an equilibrium view, with no opportunity to consider reaction kinetics. Experiments afford us the ability to examine rates of processes, which cannot be obtained from phase-equilibrium modelling. Unlike many experimental studies, which focus on attainment of equilibrium in granitic systems, this study seeks to examine how rapidly the reactions that break down out of equilibrium crystals occur and what the reaction pathways are. At this point, it is worth noting

that it is expected that experiments will depart from equilibrium because of kinetics effects and that the experiments are specifically designed to do that.

5.2 Starting Material

The bulk composition used in all experiments was composed of a synthetic “melt” fraction and a mixture of natural minerals designed to replicate the hypothetical “peritectic” assemblage. This starting material prepared to be compositionally identical to common S-type monzogranites from the Peninsula Pluton of the Cape Granite. Figure 7 provides an illustration of the process followed to synthesize the bulk composition.

Synthesizing the bulk composition involved two steps, first of which is the synthesis of the silicate gel and mineral additions to this to make up the “melt” component, followed by addition of the hypothetical peritectic assemblage. The synthetic silicate gel was prepared according to the method described by Hamilton and Henderson (1968), but with some variations. The composition of the melt was modelled after an experimental melt composition from (Stevens et al., 1997), which was produced from the partial melting of a metapelite at 1000 ºC and 1 GPa. This composition was chosen because it is believed to be a good representative of a typical silicic S-type granitic melt. To make “melt fraction”, firstly, an oxide mixture was synthesized from a gel prepared from alkali carbonates, Al_2O_3, TiO_2, MgO and tetraethyl orthosilicate (TEOS). Secondly, and as a departure from the Hamilton and Henderson (1968) technique, FeO was added as synthetic fayalite instead of Fe metal sponge and Fe2O3 powder, with the necessary correction to the amount of Si added via TEOS. Similarly, H2O was added as kaolinite instead of as liquid H_2O to the capsule, with the necessary corrections to the amount of Al_2O_3 and TEOS used in preparing the gel. The FeO component was added as fayalite to avoid possible iron oxidation on converting the gel to an oxide mixture, as a furnace with redox control was unavailable. H_2O was added as kaolinite to avoid possible water loss when welding the experimental capsules and to ensure that the water content in all experiments was exactly the same. The compositions of the different components to the

starting material are provided in Table 1. Full details of the silicate gel and fayalite synthesis techniques are provided in Appendix (1).

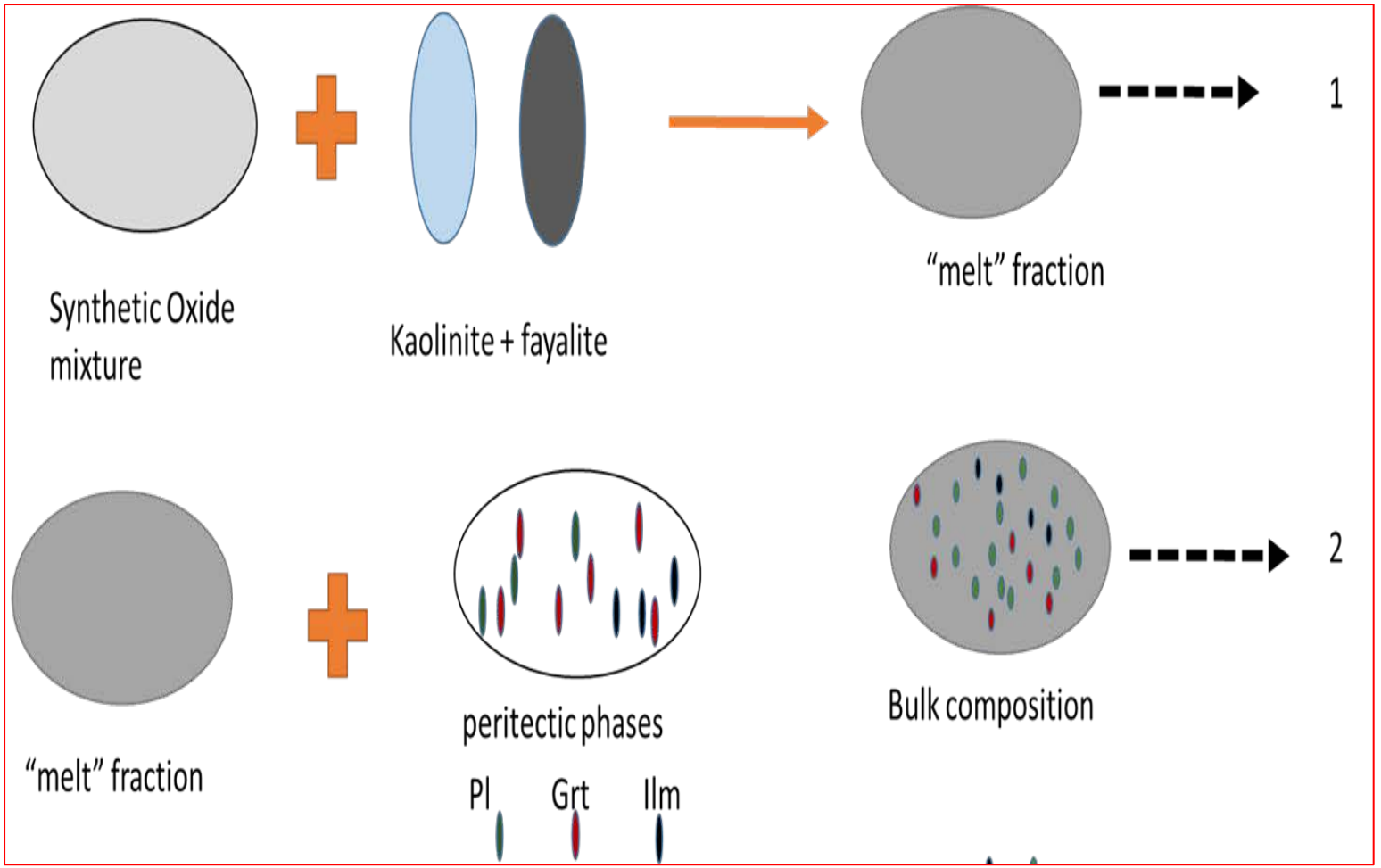

Figure 7: Schematic illustration of the components used to synthesize the starting material

The hypothetical peritectic assemblage was added to the “melt fraction” as coarse-grained crystals relative to the representative melt fraction. The chosen hypothetical peritectic assemblage in this study comprises of plagioclase, ilmenite and garnet. Dr Gautier Nicoli provided the sample from which the abovementioned minerals were obtained. The rock sample is a granulite-grade leucosome taken from the Limpopo Belt in South Africa. The hypothetical peritectic minerals were combined to form a hypothetical peritectic bulk composition consisting of 20 wt% plagioclase, 8 wt% garnet and 1 wt% ilmenite. This peritectic bulk was mixed with the synthetic gel in a 30:70 ratio to form a starting material for the experiments. The 30 wt% contribution of the peritectic mineral assemblage was chosen based on the proposal that it is the required amount to generate the most mafic granitic rock compositions (Stevens et al., 2007). The overall bulk composition was synthesized in such a way that, on reaching the experimental P-T conditions, it would replicate a partial melt generated at high-P-T condition through fluid-absent melting, coexisting with a peritectic mineral assemblage. Additionally, 0.05 wt% of natural cordierite powder was added into the starting bulk composition to give growing grounds for cordierite. The added amount of cordierite is considered negligible to have a significant effect on the overall bulk composition. Hence, it is not listed as one of the constituents of the starting bulk composition.

Table 1: Starting bulk composition and components.

	A			**B**	**C**	**D**
	Hypothetical peritectic assemblage			Peritectic	Synthetic	Bulk
	Pl	Grt	Ilm			
SiO_2	61.19	39.23		53.06	70.92	65.56
TiO_2	-	-	49.75	1.66	0.41	0.79
Al2O3	24.41	21.66	-	22.75	13.71	16.42
Fe_20_3	-	2.42	6.43	-	-	-
FeO	-	24.70	42.93	8.69	1.54	3.68
MnO	-	0.45	1.01	0.15	-	0.05
MgO	-	9.84	0.45	2.60	0.43	1.08
CaO	6.46	3.29	-	5.38	0.92	2.26
Na_2O	7.93	-	-	5.54	2.24	3.23
K_2O	0.25	-	-	0.17	5.05	3.59
H_2O	-	-	-	-	4.77	3.34
Total	100.25	101.58	100.58	100.00	100.00	100.00
xO2-	8	12	3			
Si	2.72	2.97	-			
Ti	-	-	0.94			
Al	1.28	1.93	0.00			
Fe^{3+}	-	0.14	0.12			
Fe^{2+}	-	1.56	0.90			
Mn^{2+}	-	0.03	0.02			
Mg	-	1.11	0.02			
Ca	0.31	0.27	-			
Na	0.68	-	-			
K	0.01	-	-			
Σcation	4.99	8.00	2.00			
Mg#		39.48	1.61			
XAlm		52.66				
XPyp		37.39				
XSpss		0.97				
XGrs		8.98				
XAn	30.60					
XAb	67.99					
XOr	1.41					

Fe_2O_3 (Fe^{3+}) calculated following the technique of Droop (1987)
Mg# = (Mg/(Mg + FeT))* 100
XAb = (Na/(Ca + Na + K)) * 100
XOr = (K/(Ca + Na + K)) * 100
XAn = (Ca/(Ca + Na + K)) * 100
XAlm = (FeT/(Ca + Mg + Mn + FeT)) * 100
XPyp = (Mg/(Ca + Mg + Mn + FeT)) * 100
XGrs = (Ca/(Ca + Mg + Mn + FeT)) * 100
XSpss =(Mn/(Ca + Mg + Mn + FeT)) * 100
FeT = Fe^{3+} + Fe^{2+}

5.3 Experimental Design

5.3.1 Experiential apparatus

All experiments were conducted using Inconel (Nickel-Chromium based) cold-seal pressure vessels. The experimental apparatus is illustrated in Fig. 8. The pressure vessels used in this study have an external diameter of 24 mm, internal diameter of 5 mm, and are 200 mm in length (external). The hotspot of the vessel was determined to be at a depth of ~185 mm, which coincides with the maximum internal depth of the vessel. Sealed gold capsules with a diameter of ~ 4 mm were kept in place by ~161 mm long steel filler rods inside the Inconel pressure vessel. Ab Inconel sheathed (type-K) thermocouple with a diameter of 1 mm and 350 mm length were used to measure temperature in an external thermocouple well in the hot zone of the vessel. The standard error limit of the thermocouple is ±2.2 ºC (http://www.thermometricscorp.com). The Inconel vessel was heated using a Marshall Furnace (series 1100) which has an internal length of ~ 292 mm, an internal diameter of ~ 42 mm and a maximum operating temperature of 1200 ºC. A RKC-REX-C100 temperature controller monitored and controlled the furnace temperature. The vessel temperature was monitored using a BI 60B Series digital temperature controller. The temperature within the furnace is generated by a series of nickel-chrome wires coiled around a ceramic tube. The ceramic tube is placed in a mullite tube that acts as an insulator and helps distribute temperature evenly across the furnace. An air-driven Haskel pump generated the water pressure used to pressurize the vessels and pressure was measured via a Heise Bourdon gauge with an accuracy of ± 0.1 % (http://www.heise.com).

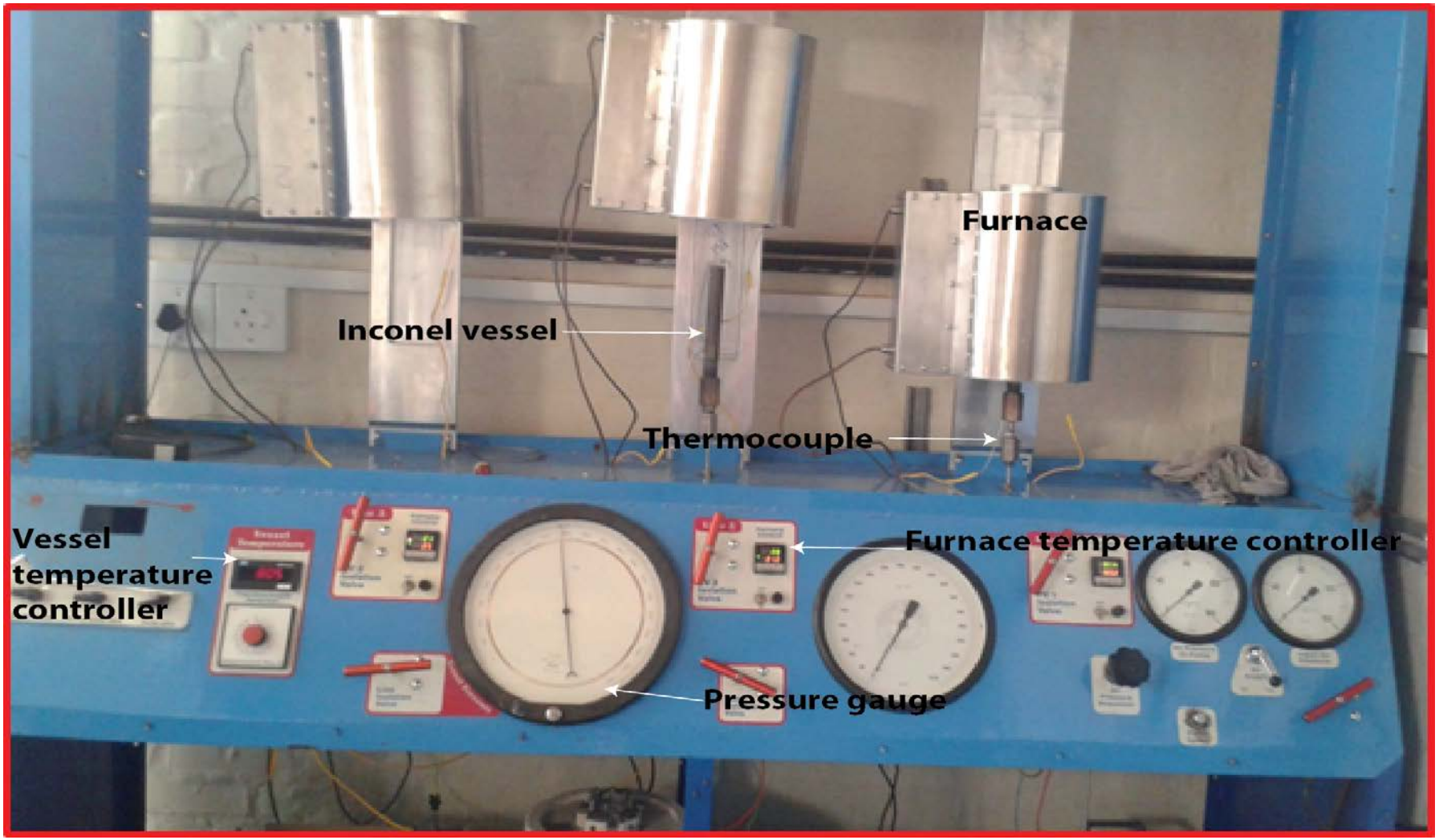

Figure 8: Image of the experimental apparatus.

5.3.2 Experimental procedure

For all experimental runs, gold capsules were loaded with about 0.2 - 0.3 g of starting material. The loaded capsules were kept in a furnace heated at 110 ºC for an hour to drive out any adsorbed water that may have accumulated while loading sample powder. Immediately after removal from the furnace, capsules were crimped and arc-welded shut. Weighing either side of a vacuum test in a water bath was conducted to check for leaks. Capsules were loaded into the Inconel vessel and held in the hot spot using the filler rod. Thereafter, the Inconel sheathed thermocouple was placed in the external thermocouple well located at the top of the vessel and the furnace was placed over the vessel, (see Fig. 9 a-c). Prior to heating, the experiments were pressurized to the experimental condition and maintained at this pressure during heating by bleading pressure off as temperature of the vessel increased. The run duration for all experiments was 20 days. Experiments were conducted at a constant pressure of 1 kbar at temperatures of 743, 754 and 804 °C. At the end of the runs, experiments were isobarically quenched to a temperature well below the boiling point of water (~ 80 ºC). The capsules were removed from the vessel, weighed, punctured and placed in a furnace heated at 110ºC and re-weighed an hour later to check for the presence of water in the run products.

5.3.3 Calibration experiment

The maximum temperature gradient between the capsule and the external thermocouple within the thermocouple well was estimated to an average of 21 ºC. This gradient was constrained by running a calibration experiment in which two Inconel sheathed (type-K) thermocouples. One thermocouple was placed inside the vessel via a modified elbow filling on the pressure line, ensuring that the tip was located at position of the bottom end of the capsule. Another thermocouple was placed in the external thermocouple well (see, Fig. 9 d-e). The calibration experiment was set at 800 ºC (external thermocouple reading) and 1.5 kbar. The calibration experiment was monitored for a day. The calibration experiment was set up at 1.5 kbar, as initially the experiments were conducted at 1.5 and 1 kbar. However, the run products of the experimental runs conducted at 1.5 kbar were lost in the analytical laboratory

and due to time constraints, these experiments could not be repeated. The set-up for the calibration experiment required the internal thermocouple wire to be placed through and braised to a steel cone. Once this was done, the assembled piece (steel cone and thermocouple wire) was inserted into the pressure line through a modified T-piece attachment. Thereafter, the T-piece was attached to the base of the experimental apparatus in a way that allowed the thermocouple wire to be exposed above the experiment platform. A capsule with a modified filler rod was placed inside the cold seal vessel. The last step of the equipment setup was placing the furnace over the vessel. For all experimental runs, the temperature was adjusted in a way that accounts for the temperature differences between the external well and the internal temperature at the capsule position. Thus, the recorded experimental temperatures are the inferred temperature readings at the capsule position.

Table 2: Calibration experiment

	Time	Control T (ºC)	External T (ºC)	Internal T (ºC)	Difference (ºC)
Day 1	12:35:00 PM	812	801	784	17
	2:36:00 PM	812	804	788	16
	2:37:00 PM	810	801	786	15
	4:19:00 PM	810	800	777	23
Day2	8:38:00 AM	809	801	777	24
	11:23:00 AM	814	805	780	25

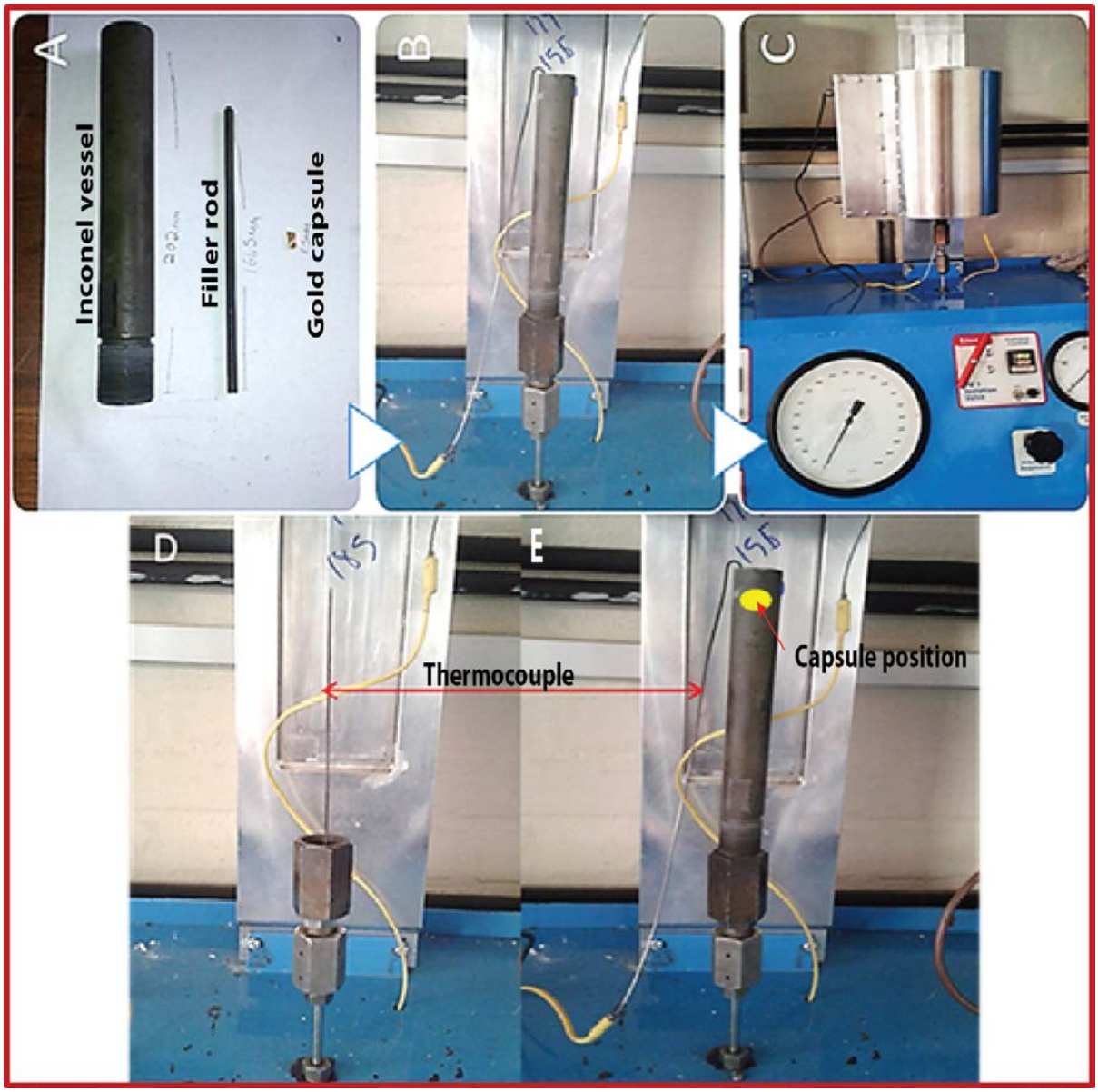

Figure 9: Images A - C show the set up for experimental runs. Image D - E show the set up for the calibration experiment.

5.4 Analytical techniques

Phase modelling methodology

Phase-equilibrium modelling has contributed greatly in aiding the understanding of natural systems. Different programs have been created for the purpose of conducting phase-equilibrium investigations and two different approaches are used by the three programs that currently receive widespread use. Perple_X (Connolly and Kerrick, 1987) and Theriak-Domino (de Capitani and Petrakakis, 2010) predict assemblages and phase compositions by minimization of Gibbs free energy of the system. THERMOCALC (Powell and Holland, 1988; Powell et al., 1998) uses simultaneous solution of non-linear equations. The pseudosection diagrams presented in this study were calculated using THERIAK-DOMINO Software (de Capitani and Petrakakis, 2010) and the internally consistent database of Holland and Powell (1998). The a-x solution models used for different minerals are GT07W2 and BI07 (White et al., 2007) for garnet and biotite, PLC1 (Holland & Powell, 2003) for plagioclase, OPX (White et al, 2002) for orthopyroxene, Crd (Holland & Powell, 1998) for cordierite, ILM05 (White et al., 2000) for ilmenite and LIQtc2 (White et al., 2007) for the melt. The pseudosection diagrams were edited and labeled using Adobe Illustrator® CS5.

Although thermodynamic modelling has a lot of benefits such as demonstrating how phase assemblages, phase compositions and phase proportions within a specified composition change over a defined P-T space, they are not without limitations. Generally, positions of predicted stability fields are not dependent on the solution models but on end member properties of the different phases, whereas the predicted compositions are dependent on solution models (de Capitani and Petrakakis, 2010). Thus, it is important that the solution models must incorporate the complete compositional range of the minerals. However, in some instances, the solution models used by the software may be unsuitable for certain bulk compositions to be modelled or have some inaccuracies (de Capitani and Petrakakis, 2010; White et al., 2011). For example, currently there is no suitable or accurate model for Ti in most silicates, Fe^{3+} in most minerals, and Cl & F in most hydrous minerals (de Capitani and

Petrakakis, 2010). Another significant shortfall of thermodynamic modelling is that it cannot constrain reaction pathways and kinetic parameters i.e. equilibration rates, rates of reactions, mineral impurities etc. What phase-equilibrium modelling does is provide relevant but oversimplified approximations of how natural systems are likely to behave (de Capitani and Petrakakis, 2010). Because of this, mismatches may exist between the behavior of natural systems and/or experiments and the predictions of phase-equilibrium modelling.

Tropper and Hauzenberger (2015) compared outcomes of Theriak-Domino phase-equilibrium modelling and the results of an experimental study conducted using granulite facies rocks from the Bohemian Massif by Tropper et al. (2005). The findings of Tropper and Hauzenberger (2015) revealed that there is generally a good agreement between experimental and calculated phase assemblages. However, they noted that the stability of biotite is over-estimated in the modelling and the melt proportions generated in the experiments are larger than what the modelling calculates. They reasoned that the discrepancies resulted from: (i) high F-contents of micas, which are not accounted for in the relevant biotite solution models, and (ii) lack of attainment of equilibrium in the experimental run products, which is responsible for the production of abnormally high melt volumes. As it stands, the combination of phase-equilibrium modelling and experimental studies, and the ultimate comparison of the outcomes to natural systems is a powerful tool that can be used to plan experiments and gain a better understanding of the P-T evolution of granitic systems.

Scanning Electron Microscopy

The rock sample, from which the hypothetical peritectic minerals were obtained, was crushed to fine grain size. The individual grains of the various minerals were handpicked using tweezers under a WILD M400 Photomicroscope. The various minerals were sieved to ensure that all the crystals added to the bulk composition fell within a size range of 100 - 200 µm. The hypothetical peritectic crystals and successful experimental run products were mounted in epoxy and left overnight to set. The samples were subsequently ground flat, polished and carbon coated with 15 µm of carbon. Major element compositions and textures of the minerals included in the starting material and experimental run products were analyzed using a Zeiss EVO MA15VP Scanning Electron Microscope (SEM) at Stellenbosch University. The used SEM is equipped with Energy Dispersive X-ray Spectrometry (EDS or EDX) Silicon Drift Detector (SDD), Backscattered Electron Detector (BSD) and uses Oxford INCA software.

The analyses were performed using a beam current in the range of -19 to -20 nA, an accelerating voltage of 20 kV and a working distance of 8.5 mm. However, for imaging no specific working distance was maintained. The beam current was at times controlled by adjusting the spot size. Cobalt standard was used to optimize quantification once beam had stabilized. Each spectrum produced was processed by ZAF corrections and quantified data was standardized using natural scientific mineral standards (Astimex Scientific limited, MINM25-53 #05-010) (Appendix 2). To verify the quality of the analytical data, almandine garnet and plagioclase standards of known compositions were analyzed as unknowns. The compositions of both standards were then compared to their actual published compositions (Astimex Scientific limited, MINM25-53 #05-010) the results are presented in Table 2.

Analyses of quenched melts produced in all run products were performed via SEM. However, to analyze the quenched melts, a Gatan cryogenic stage was introduced to the SEM to cool the samples. Liquid nitrogen was utilized to ensure that the analyzed samples were cooled to a temperatures ≤ -180°C.

Table 3: Standard verification for Garnet and plagioclase.

Almandine Garnet			
	Published Standard	Measured (n=4)	σ
SiO_2	39.19	39.46	0.19
Al_2O_3	22.05	22.16	0.08
FeO	23.27	23.08	0.13
MnO	0.59	0.60	0.00
MgO	10.70	10.80	0.07
CaO	4.20	4.11	0.07
Na_2O	0.00	0.00	0.00
K_2O	0.00	0.00	0.00
total	100.00	100.00	0.00
Plagioclase			
	Published Standard	Measured (n=4)	Std
SiO_2	54.21	54.28	0.05
TiO_2	0.07	0.00	0.05
Al_2O_3	28.53	28.52	0.01
FeO	0.37	0.53	0.11
MgO	0.13	0.00	0.09
CaO	11.80	11.68	0.09
Na_2O	4.35	4.42	0.05
K_2O	0.41	0.37	0.03
total	99.87	99.79	0.06
n = number of analyzed points, σ = standard deviation 1			

Mineral formulae were calculated using a technique outlined by Deer et al. (1992). The resultant mineral formulae were used to evaluate the quality of the analytical data. Where necessary, the Fe^{3+} content was calculated following technique of Droop (1987).

X-ray Fluorescence

Major element composition for starting synthetic gel (melt) was determined by X-Ray Fluorescence Spectrometry (XRF) on a PANalytical Axios Wavelength Dispersive spectrometer. The spectrometer is fitted with an Rh tube at 3kWatt.Standards used in the calibration procedures and quality control for major element analyses was NIST® and SARM®. Standards used in calibration procedures for the major elements were BE-N, JB-1 (basalt reference values), JG-1 (granodiorite reference value), and NIM-G & WITS-G (granite reference values).

X-ray Diffraction

The composition of the fayalite powder used in the synthesis of the experimental starting bulk composition was determined using a Bruker D8 X-ray Powder Diffractometer (XRD) with a Cu sealed tube.

Thermogravimetric Analysis (TGA)

To prepare the synthetic gel for analysis, a small fraction of the powder was dried for an hour in a furnace heated at 110°C. The H_2O content of the fraction of the starting material meant to replicate the melt was determined by TGA in flowing argon. The H_2O content measured by TGA was within a 0.001 % error if the calculated water content.

5.5 Predicted experimental outcomes

Fig.10 below illustrates a low-pressure section of (Fig. 6) and illustrates the chosen experimental P-T conditions. The psuedosection shows that across all chosen experimental P-T conditions, the stable assemblages are devoid of garnet. Cordierite, biotite and orthopyroxene are predicted to be the stable ferromagnesian phases. However, biotite is predicted to be unstable at 804 ºC. Ilmenite is predicted to be the only Fe-Ti oxide mineral at these low P-T conditions. The pseudosection model predicts that plagioclase is stable across all investigated P-T conditions.

The modal proportions of the different minerals and the melt mode are predicted to vary as a function of changing temperature. Modal proportions of plagioclase, quartz and biotite increase with decreasing temperature, the melt mode decreases with decreasing temperature, whilst Ilmenite and cordierite proportions remain steady across all temperatures. Likewise, compositions of the individual mineral phases are predicted to vary along the hypothetical isobaric cooling path. The composition of plagioclase is predicted to become more albitic with decreasing temperature. The calculated compositions range from $An_{50.73}Ab_{47.09}Or_{2.18}$ to $An_{37.55}Ab_{58.72}Or_{3.73}$ at 804 and 743 ºC, respectively. The composition of plagioclase is predicted to differ from the composition of the hypothetical entrained plagioclase in the starting material. The modelling predicts that change in temperature over the experimental range will have little effect on the compositions of ilmenite, cordierite and biotite. A detailed discussion of predicted mineral phases, modal proportions and compositions will be presented in sections to follow.

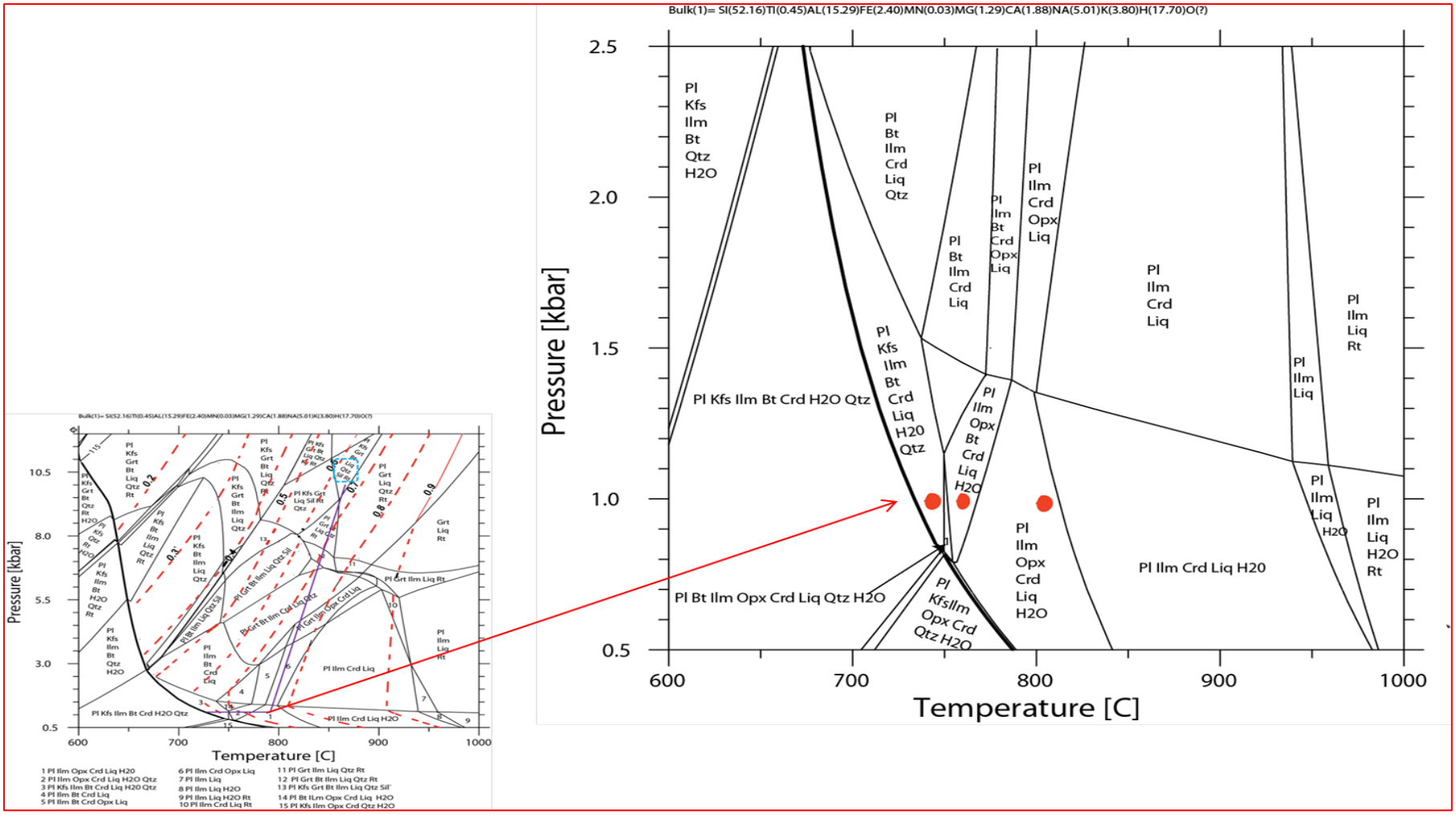

Figure 10: Pseudosection displaying predicted experimental outcomes. The orange circles represent the chosen P-T conditions for this study's experiments.

6 Results

6.1 Phase assemblages

Phase assemblages produced in all successful experimental runs are listed in Table (3) below. The averaged mineral compositions of the phases produced in experimental run products are summarized in Tables 4 to Table 8; supplementary data is provided in Appendix 3 to Appendix 9.

Table 4: A summary of phase assemblages produced in the experimetal run products.

Experiment	P(kbar)	T(°C)	Experimental assemblage
1	1	804	Pl Bt Ilm Crd Hc Liq *Grt*
2	1	754	Pl Bt Qtz Crd Ilm Liq H_2O *Grt*
3	1	743	Pl Kfs Qtz Ilm Crd Bt Liq H_2O *Grt*
metastable phases : blue text in italics			

6.2 Textural characteristics

This section provides a detailed textural description of the minerals produced in the experimental run products. Visual display of the textures produced in the various experimental run products is demonstrated in figure 11 to 13 below.

6.2.1 Experiment 1: 804 ºC / 1 kbar

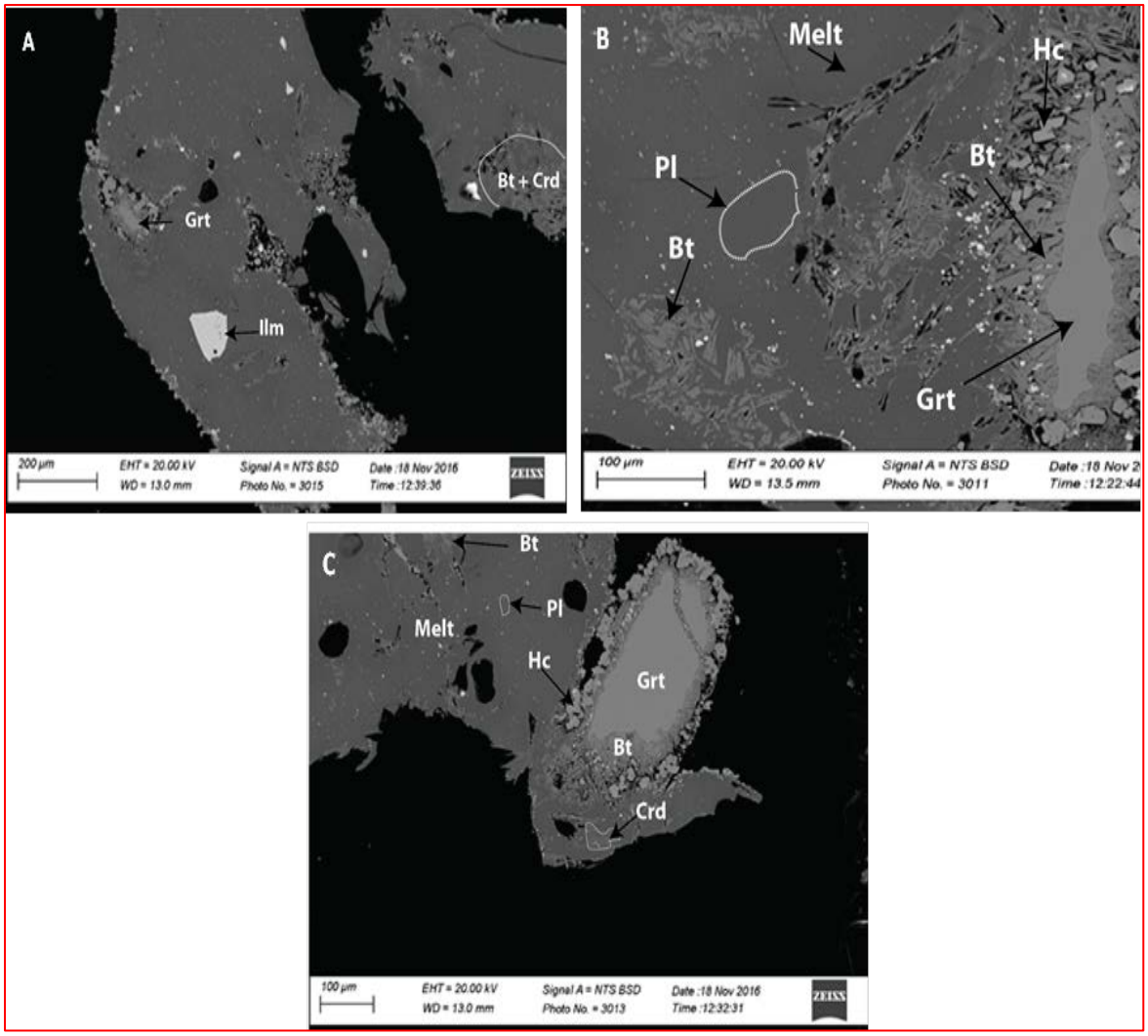

Figure 11: Back-Scattered Electron (BSE) images for experiment 1 (804 ºC / 1 kbar).

A: shows an overview of the run product. From this image, interlocking biotite and cordierite crystals are located on the far right appearing to be pseudomporphing a garnet crystal. The quenched melt portion in this run product appears to be significantly higher than the crystal fraction. B: illustrates plagioclase crystal, prominent accumulation of randomly oriented biotite crystals and resorbed garnet crystal surrounded by biotite-hercynite reaction front. C: Demonstrates garnet crystal surrounded by a smaller biotite-hercynite reaction front and cordierite crystals growing from the matrix adjacent to the reaction front.

Plagioclase

The plagioclase crystals in this run product display two distinct crystal shapes (Fig.11b - c). The first type appears as medium-sized anhedral (50 µm) found in close proximity to aggregates of biotite, generally surrounded by the quenched melt. The second type appears as aggregates of ~5 µm crystals dispersed across the run product. These crystals are significantly smaller than plagioclase crystals in the starting material.

Ilmenite

The size of the ilmenite crystals ranges from ~1 – 50 µm and they have round or subhedral crystal shapes (Fig. 11). They are randomly distributed across the run product. They are characteristically surrounded by quenched melt. However, they also occur as inclusions within plagioclase crystals. These crystals are significantly smaller than the (100 – 200 µm) crystals added in the starting material.

Garnet

The garnet crystals have resorbed edges. They are surrounded by a reaction front of biotite and hercynite (Fig. 11). The preserved cores are smaller than the garnet crystals in the starting material.

Biotite

The biotite crystals appear as reaction rims around garnet crystals where they share grain boundaries with hercynite. They also occur as domains of randomly oriented biotite crystals appearing to be pseudomporphing pieces of garnet. The individual crystal sizes range from 5 – 10 µm. These “pseudomorphs” have an overall length of 100 – 120 µm (Fig. 11).

Cordierite

The cordierite crystals within this run product appear as elongated interlocked pseudomorphs of garnet. They also appear interlocked with biotite crystals displaying pseudomorphs of garnet. These crystals have a size range of 100 – 200 µm. This size range is the same as the

size range of the garnet crystals of the starting material. They also occur as 50 µm elongated crystals in the matrix of the run product adjacent to garnet crystals that are surrounded by biotite and hercynite reaction front (Fig. 11c).

Hercynite

It is present as one of the replacement products of the garnet crystals. It appears as euhedral crystals with a size range of 5 – 10 µm. These crystals occur exclusively around and in between the biotite, reaction rims armoring the refractory garnet crystals (Fig.11 b - c).

6.2.2 Experiment 2: 754 ºC / 1 kbar

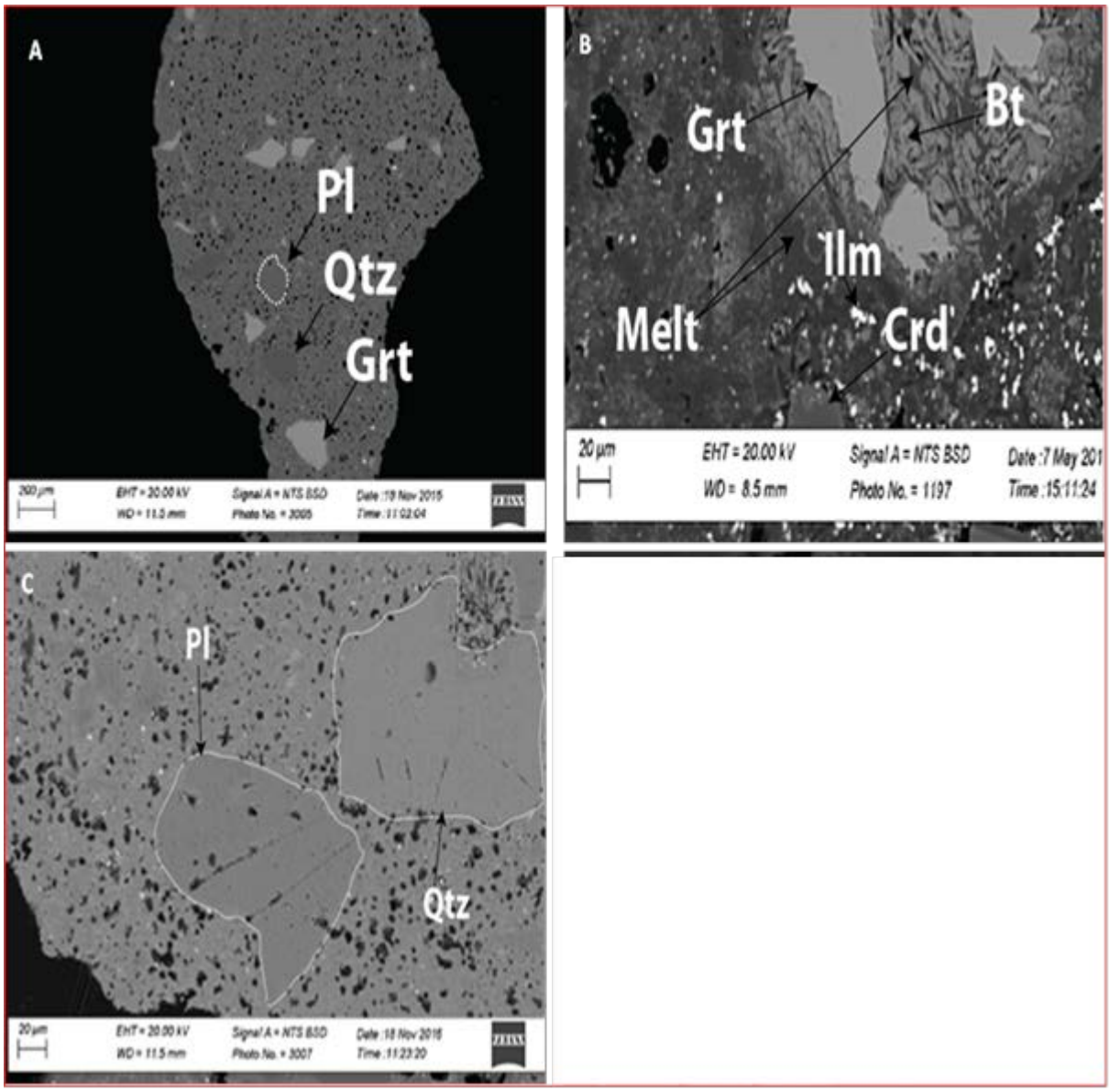

Figure 12: BSE images for Experiment 2: 754 ºC / 1 kbar.

A: Shows the size and spatial distribution of the larger quartz, plagioclase and garnet crystals and vesicles. The melt volume in this run product appears to be smaller than in the higher temperature experiment. B: Shows various remnant garnet nuclei surrounded by biotite reaction rims. C: Displays subhedral plagioclase and quartz crystals embedded in the melt.

Plagioclase

The plagioclase crystals in this run product are found in close proximity to quartz (Fig.12 a & c). The crystals have semi-oval and anhedral shapes. Their sizes range between 60 – 90 µm.

Ilmenite

The ilmenite crystals are widely spread across the run product. The crystal sizes range from < 2 to 5 µm (Fig. 12 a - c).

Garnet

In this run product, the garnet crystals are fractured and biotite crystals rim the various “nuclei” (Fig. 12 b). A big portion of the garnet crystal appears to have reacted with the melt to produce biotie..

Biotite

The biotite crystals appear as reaction rims around garnet crystals (Fig. 12 b).These crystals have small sizes <5 µm and they are randomly oriented between and around different garnet nuclei.

Cordierite

The crystals exhibit euhedral shapes and a size range of 30 – 100 µm. These crystals are surrounded by the melt. The crystals in this run product, are bigger than those in the higher temperature experiment.

Quartz

The quartz crystals are evenly distributed across the run product. However, they commonly occur in close proximity to plagioclase crystals. The crystals exhibit round and subhedral shapes. The crystal sizes range between 10 – 100 µm. They have subhedral to euhedral crystal shapes see (Fig. 12 a & c).

6.2.3 Experiment 3: 743 ºC / 1 kbar

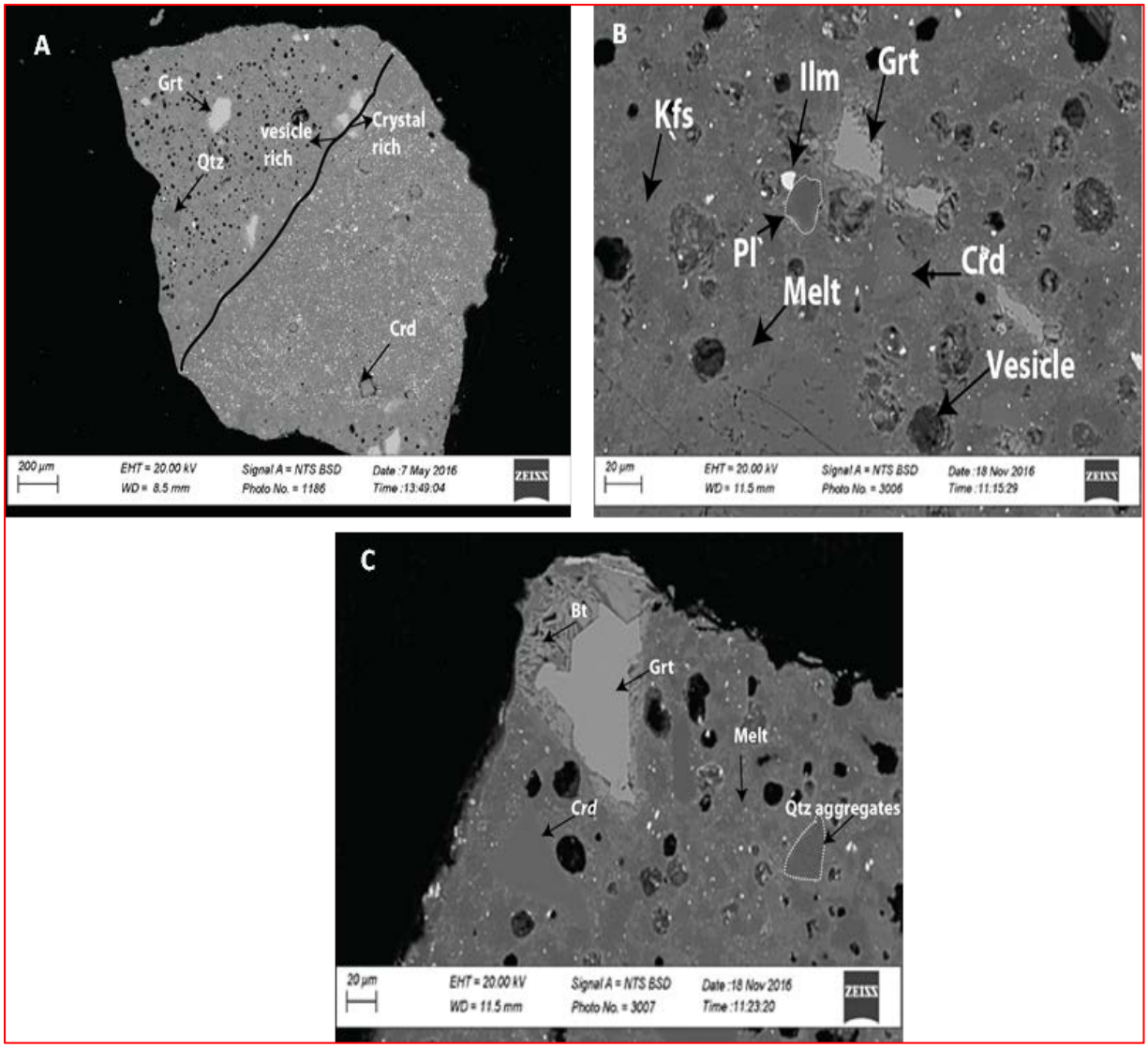

Figure 13: BSE images for experiment 3: 743 ºC / 1 kbar.

A: An overview image of the run product, showing two distinct zones, a vesicle rich and crystal rich zone. The black line marks the boundary between the two zones. The image shows that the crystal fraction in this run product exceeds the melt fraction. B: Shows garnet crystals surrounded by thin biotite crystals (<< 2 µm) with cordierite growing from the melt adjacent to the garnet crystals and some vesicles filled with quenched melt and crystals. Quartz and k-feldspar make up the matrix of this run product. C: shows garnet crystal surrounded by a larger biotite reaction front.

Plagioclase

The plagioclase in this run product occurs as 30 – 70 µm surrounded crystals. They occur on a matrix of quartz, quenched melt, and K-feldspar (Fig. 13 b). Similar to the crystals found in

the higher temperature experiments, the size of the plagioclase crystals differs significantly from that of plagioclase in the starting material.

Ilmenite

Similar to the plagioclase crystals, ilmenite crystals produced across all experimental run products are significantly smaller than the ilmenite crystals in the starting material. They are evenly distributed across the run product (Fig. 13). The size of the crystals ranges between ~ 5-10 µm.

Garnet

The garnet crystals are significantly smaller than those in the starting material. It appears as if they are remnants of the original crystals. Similar to the run product at 754 ºC, the reaction products that have partly replaced the garnet crystals psuedomorph the original crystal shapes in the starting material. The edges of the crystals look like the might be some re-crystallization process involved (Fig. 13b - c).

Biotite

In this run product, the biotite crystals occur exclusively as reaction rims surrounding garnet crystals. They have thin elongated crystal shape, the size of the crystal ranges from 2 – 10 µm.

Cordierite

In this run product, cordierite crystals have subhedral to euhedral crystal shapes. They are scattered across the run product, but they also occur adjacent to remnant garnet crystals. The size of the crystals range between 30 -100 µm, see Fig. 13b-c.

Quartz

The quartz crystals together with K-feldspar make up the matrix of the run product. They appear as small aggregates with an average size of ~5µm and as big 100 µm sub-rounded or oval shaped crystals (Fig. 13b - c).

K-Feldspar

It is only present in this experiment. The K-feldspar crystals occur between small quenched melt pools and they share grain boundaries with quartz crystals. The size of the k-feldspar crystals is ~5 – 10 µm (Fig.13).

6.3 Phase Chemistry

This section provides a comprehensive description of the experimental mineral compositions. Where necessary, a comparison between compositions of the phases in the starting material and the experimental compositions are provided. The averaged compositions of the phases produced are presented in Tables 5 to 9 and graphical presentation of the analyses is presented in figures14 to 19.

6.3.1 Ilmenite

The compositions of ilmenite produced in the experiments differ significantly from the composition of the original ilmenite crystals in the starting material. The compositions of ilmenite in the experimental run products are more magnesian than the ilmenite crystals in the starting material. In all run products, the Si^{2+} content remains very low (≤ 0.02 atoms per formula unit (apfu) indicating that the analyses are most likely not contaminated by either quartz or quenched melt. The ilmenite crystals show variable Mg# (Mg / (Mg + Fe_T) values ranging between an average of 7.84 and 4.88, and these values are significantly higher than the 1.61 Mg# value of the ilmenite in the starting material. The Fe_T (Fe^{2+} + Fe^{3+}) and MgO (Mg) decrease with decreasing temperature. The Fe_T and Mg contents decrease from an average of 1.04 to 0.92 and 0.09 to 0.05 apfu, respectively. The ilmenite in the starting composition has an average Fe_T content of 1.02 (Fe^{3+} 0.12 and Fe^{2+} 0.90), Mg 0.02, Ti 0.94, Mn 0.02 apfu. Compared to the ilmenite produced in the experimental runs, the Mn content of ilmenite in the starting is 0.01 apfu higher across all investigated temperatures. Additionally, compositions of experimental ilmenite and the crystals in the starting material, have a deficiency in both Fe and Ti, compared to the contents of these elements in an “ideal” ilmenite composition, see Fig. 14.

In the 804 ºC experimental run, the ilmenite crystals have 6.24 Mg#, 0.02 Fe_T and 0.07 Mg apfu more and 0.13 apfu Ti less than the ilmenite in the starting material. The greatest Mg# variation between the experimental ilmenite and ilmenite in the starting material is seen in this run product. Ilmenite crystals produced in the 754 ºC and 743 ºC experiments have 4.62 and

3.27 Mg#; 0.04 and 0.03 apfu Mg more and 0.04 and 0.10 Fe_T apfu less than those in starting material, respectively. Furthermore, the Ti content in the 754 ºC run is 0.03 apfu less than that of ilmenite crystals in the starting material, whilst in the 743 ºC run product, the Ti content is 0.04 apfu more than that of ilmenite in the starting material. Unlike in the starting material, the ilmenite crystals produced in the 804 ºC and 754 ºC experiments have trace amounts of Na_2O and $K_2O \leq 0.01$. In these run products, the Si^{2+} content is low (0.02 apfu, $SiO_2 << 1$ wt%) indicating that the analyses are most likely not contaminated by either quartz or melt inclusions.

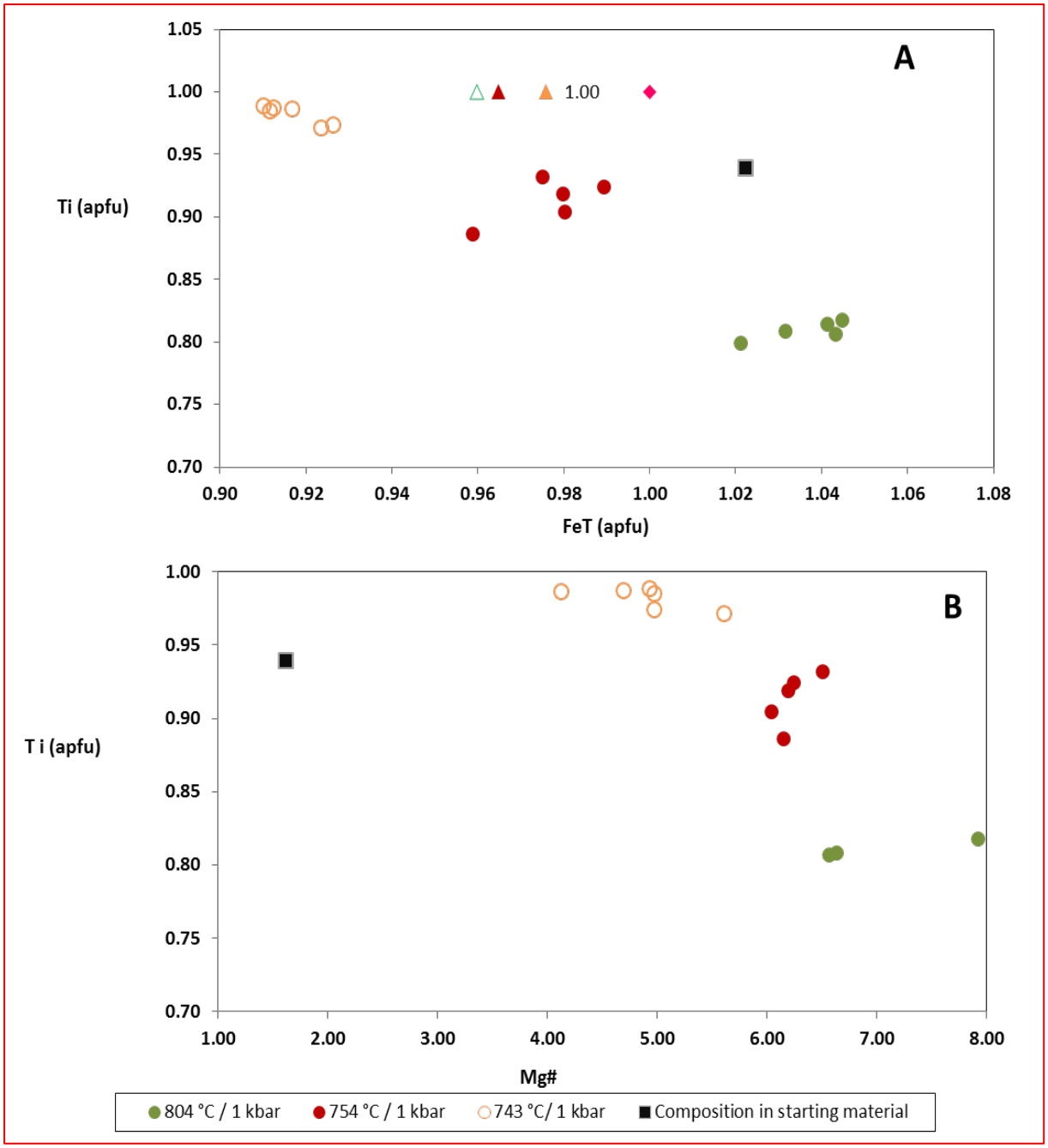

Figure 14: Compositions of ilmenite produced in the experiments compared with the composition of ilmenite crystals in the starting material and compositions predicted by phase equilibrium modelling.

The predicted compositions are denoted by triangles. The colours of the triangles corresponds to the colours of the experiments, i.e. open green triangle- 804 ºC/ 1 kbar, red– 754 ºC/ 1 kbar and orange- 743 ºC/ 1 kbar. The pink diamond represents composition of "ideal" ilmenite with 1:1 Fe and Ti contents.

6.3.2 Plagioclase

The compositions of plagioclase crystals in the different run products are homogeneous and no longer resemble the composition of the original plagioclase in starting the starting material. Compared to the plagioclase crystals in the starting material, the experimental crystals have lower albite (Ab) content. The plagioclase crystals in the starting material have an average Ab content of 67.99 and the average An content of plagioclase produced over the three experiments range between 44.33 and 62.16. Furthermore, the analyses demonstrate that the Ab content of the experimental plagioclase crystals increase with decreasing temperature (see Fig. 15). The plagioclase crystals produced in the 804 ºC run, show the most significant compositional change when compared to the plagioclase crystals in the starting material crystals. The average composition of the crystals in the starting material is $An_{30.60}Ab_{67.99}Or_{1.41}$ and that of plagioclase produced in this experiment is $An_{50.13}Ab_{44.33}Or_{5.54.}$ The Ab content of the plagioclase crystals produced in the 754 ºC is 9.49 less than that of the crystals in the starting material and 14.17 more than the plagioclase produced in the 804 ºC experimental run. The overall average composition of the plagioclase crystals is $An_{39.50}Ab_{58.50}Or_{2.01}$. Compared to plagioclase crystals produced in the other experiments, the composition of plagioclase crystals in the 743ºC experiment is more similar to the composition of the plagioclase crystals in the starting material. However, the Ab content of the plagioclase crystals in this experiment is 5.8% lower than the content of the crystals in the starting material. The average composition of the plagioclase crystals in the 743 ºC experiment is $An_{35.15}Ab_{62.16}Or_{2.69.}$

K-feldspar

K-feldspar was only present in the run product at 743 ºC and has an average composition of $An_{4.56}Ab_{28.40}Or_{67.04}$. No K-feldspar was added to the starting composition; it grew from the melt and it was stabilized by the low experimental temperature.

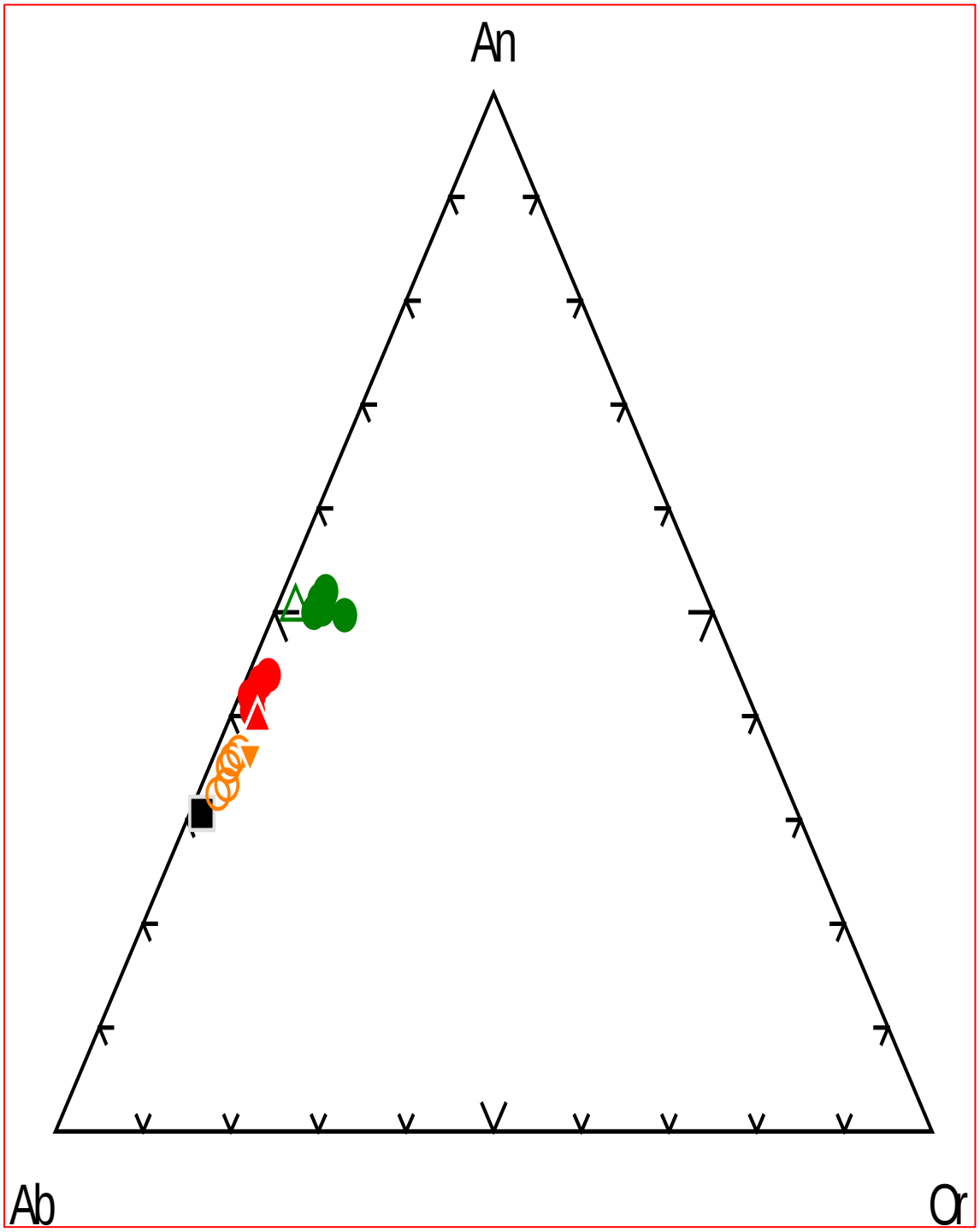

Figure 15: Compositions of plagioclase produced in this study compared with the composition of plagioclase crystals in the starting material and compositions predicted by phase equilibrium modelling.

The legend is the same as in Fig. 14.

6.3.3 Garnet

Refractory garnet crystals are present across all investigated P-T conditions. The garnets are almandine (Alm) – pyrope (Pyp) solid solution, with small amounts of grossular (Grs) and spessartine (Spss). The Grs and Spss contents range between 5.96 and 8.56 %, and 0.97 and 1.01 %, respectively. The composition of remaining garnet crystals differs slightly from the composition of the garnet in the starting material. The Ca content of the experimental garnet crystals is lower than that of garnet in the starting material and it increases with decreasing temperature. Whilst the Mg content of the experimental garnet crystals is higher than that of the starting material. Noteworthy, garnet crystals in all the run products did not show any obvious degree of zoning. Where zoning was “suspected”, the rims were too small with diameters much smaller than a micron.

The total iron content of the garnet produced in the 804 ºC run is higher than that of the original garnet in the starting bulk compositions, whilst the garnet crystals in the lower-temperature runs have lower iron contents than the original garnet crystals. The Mn and Mg# contents of the experimental garnets are very similar to those in the starting material. The Fe and Mg contents in the experiments below 804 ºC show a negative correlation with temperature i.e. garnet in the 743 ºC run has higher Fe and Mg contents than garnet produced in the 754 ºC run product.

The garnet crystals in the 804 ºC run have an average composition of $Alm_{53.31}Pyp_{39.72}Spss_{1.01}Grs_{5.96}$ and the average composition of garnet in the starting material is $Alm_{52.66}Pyp_{37.39}Spss_{0.97}Grs_{8.98}$. It can be seen from the above mineral formulae that the experimental garnet has lower Grs content and slightly higher Alm and Pyp contents than original garnet in the starting material. The Ca content of the experimental garnet is 0.09 apfu less than that in the starting material. The Fe^{3+} content is the same as in the starting material and the Mg and Fe^{2+} contents are 0.07 and 0.02 apfu respectively, higher than those of garnet crystals in the starting material. The Mg# content of garnet in the starting material is 0.85 less than the average content of the experimental garnet. The garnet crystals in the 754 ºC run

product have 0.04 and 0.11 apfu Ca and Fe^{3+} respectively, less than garnet crystals in the staring material. The Fe^{2+} and Mg contents are respectively 0.04 and 0.03 apfu higher than garnet in the starting material. The average Mg# value of the garnet in this run product is 0.17 and 1.02 higher than the garnet in the 804 ºC run product and original garnet in the starting material, respectively. The average composition of the garnet in this run product is $Alm_{53.45}Pyp_{38.07}Spss_{0.92}Grs_{7.56}$. From the mineral formula it can be seen than the garnet in this run product has and increase of 0.79% Alm and 0.68% Pyp, over the garnet in the starting material. In contrast, there is a decrease in 1.42% Grs relative to garnet in the starting material. Compared to the compositions of garnet in the higher-temperature experiments, the composition of garnet in the 743 ºC run product is more similar to the composition of the garnet in the starting. However, the garnet in this run product has 0.04 Ca and 0.10 Fe^{3+} apfu less than garnet in the starting material. The Fe^{2+} and Mg contents are 0.03 apfu higher than original garnet and the Mg# value is 1.19 higher than the garnet in the starting material. The average composition of garnet in this run product is $Alm_{53.18}Pyp_{38.12}Spss_{0.91}Grs_{7.79}$.

Hercynite

Hercynite spinel only formed part of the mineral assemblage in the 804 ºC run product. It has Al content of 56.79 wt% Al_2O_3, Fe_T content of 34.88 wt% and Mg content of 7.75 wt% MgO.

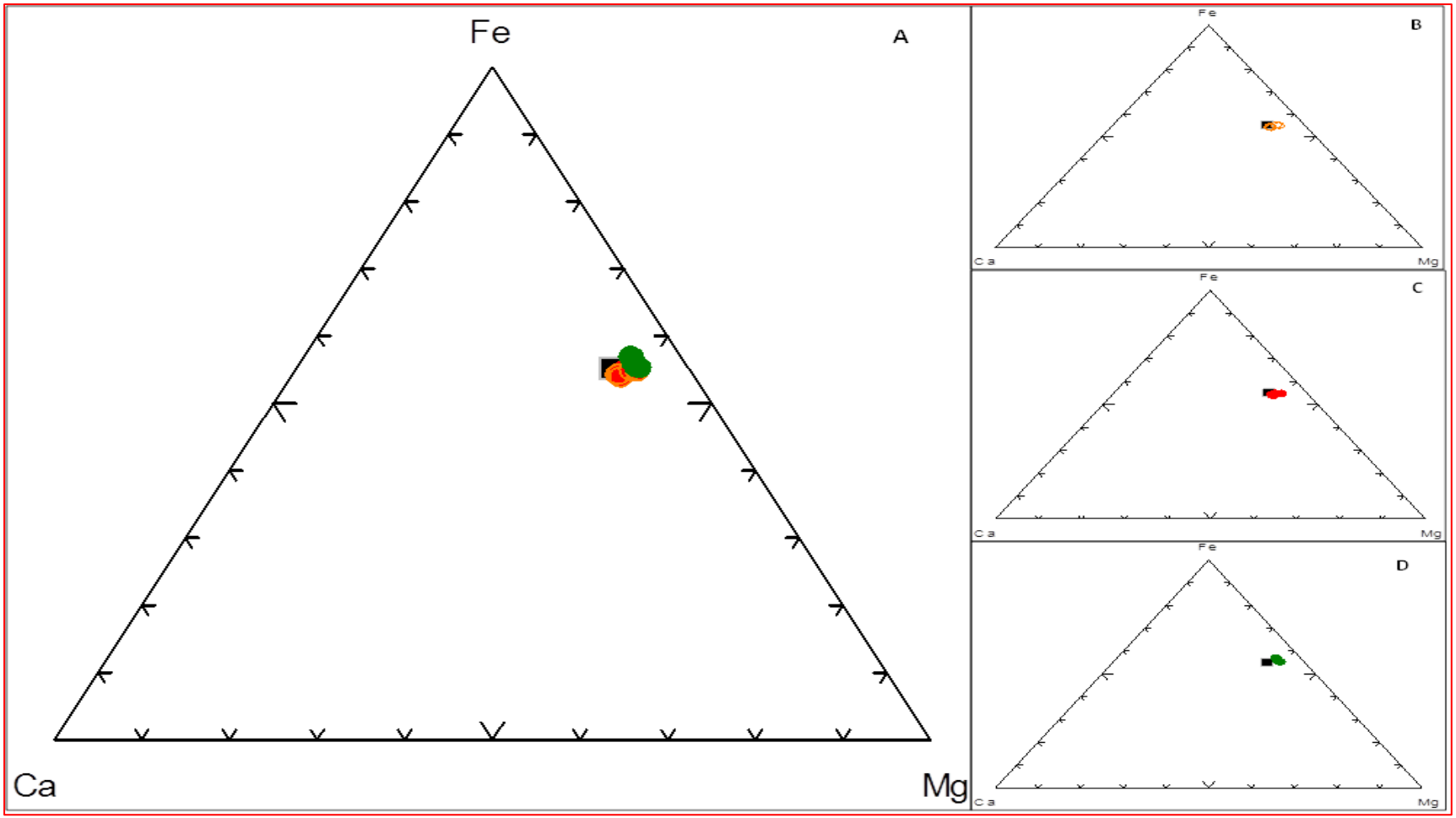

Figure 16: Compositions of remnant garnet crystals compared with the compositions of garnet crystals in the starting material.

The legend is the same as in Fig. 14.

6.3.4 Cordierite

The cation totals of the cordierite crystals are above the ideal of 11 based on 18 oxygen atoms. The Mg# of the cordierite crystals is variable and it decreases with decreasing temperature. It varies between 71.8 at 804 ºC and 56.3 in the 743 ºC experimental run. In the 804 ºC experiment, cordierite crystals have an average of 0.58 Fe^{2+}, 1.48 Mg and 4.00 Al apfu. The Mg# content of the crystals produced in the 754 ºC run; are on average 1.83 less than those produced in the 804 ºC experiment, and the Al and Fe^{2+} contents are 0.04 apfu more than those in the 804 ºC run product. The cordierite produced in the 743 ºC experimental run product, has 0.87 Fe^{2+}, 1.13 Mg and 4.04 Al apfu. The crystals produced in this run product have XFe (Fe^{2+}/ (Fe^{2+}/ Mg) value of 43.39. Furthermore, the Mg# value of cordierite is significantly higher than that of the remnant garnet crystals. All analyzed compositions have some quantity of alkalis (Na_2O + K_2O). The amounts range from 0.06 to 0.17 apfu and do not show any systematic variations with temperature, see Fig. 17.

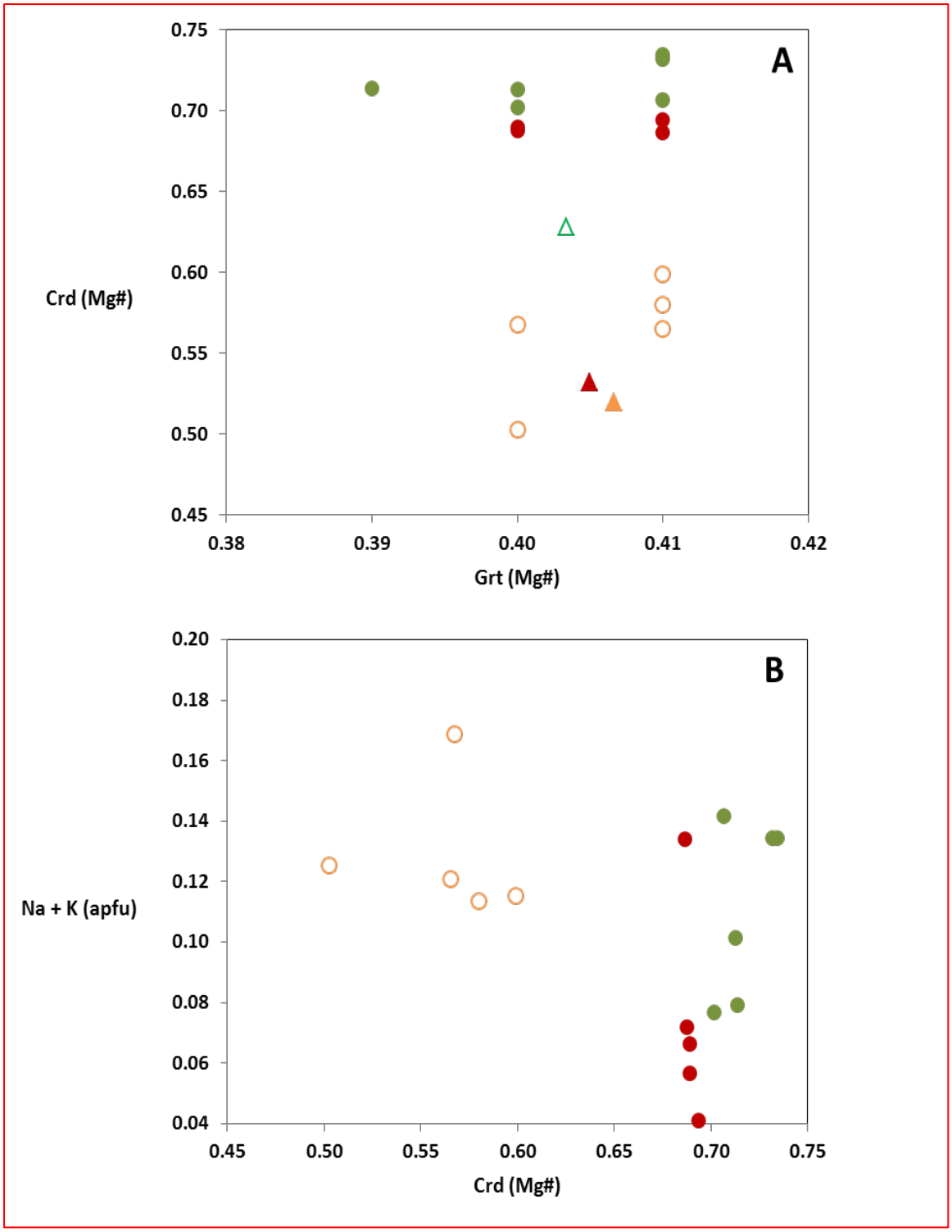

Figure 17: Compositions of cordierite produced in this study.

Figure A compares Mg# contents of experimental and predicted cordierite with that of the remnant garnet crystals. The legend is the same as in Fig. 14.

6.3.5 Biotite

Biotite crystals are present in all experimental runs as products of the garnet-melt reaction. Different biotite crystals in each run product do not show any discernible zoning. According to the classification of Deer et al. (1992), the compositions of biotite produced in this study represent a solid solution between phlogopite-annite-eastonite-siderophyllite. The biotite crystals in the 804 ºC run product have an average Mg# value of 57.28 and the average contents of $Al^{(IV)}$ and $Al^{(VI)}$ are 2.14 and 1.24 apfu, respectively. The overall mineral formula of the biotite produced in this run product is $K_{1.58}\ Na_{0.25}Ca_{0.05}Fe_{1.70}Mg_{2.28}Ti_{0.13}Al^{(VI)}_{1.24}Si_{5.86}\ Al^{(IV)}_{2.14}H_2O_{12}$. In 754 ºC run product, the biotite crystals were too small to obtain accurate analyses. However, identification of the mineral was possible by comparing the spectrum of the crystals to those of biotite produced in the other experimental run products. Therefore, there is no doubt about the presence of biotite in this experimental run product. In the 743 ºC the most significant feature of the biotite in this run product is that it has no Ti was detected in the analyses. The average Mg# value and $Al^{(VI)}$ content of the biotite crystals is 4.04 and 0.11 respectively less than the average values in the 804 ºC run product. Contrary, the average Mg, Fe and $Al^{(IV)}$ contents are respectively 0.23, 0.50 and 0.49 apfu higher than the contents produced in the 804 ºC run. The overall average mineral formula of biotite in this run product is $K_{1.72}\ Na_{0.12}\ Ca_{0.05}\ Fe_{2.21}\ Mg_{2.51}\ Ti_{0.00}\ Al^{(VI)}_{1.12}\ Si_{5.37}\ Al^{(IV)}_{2.63}H_2O_{12}$. Furthermore, the Mg# value of biotite is higher than that of garnet, See Fig. 18.

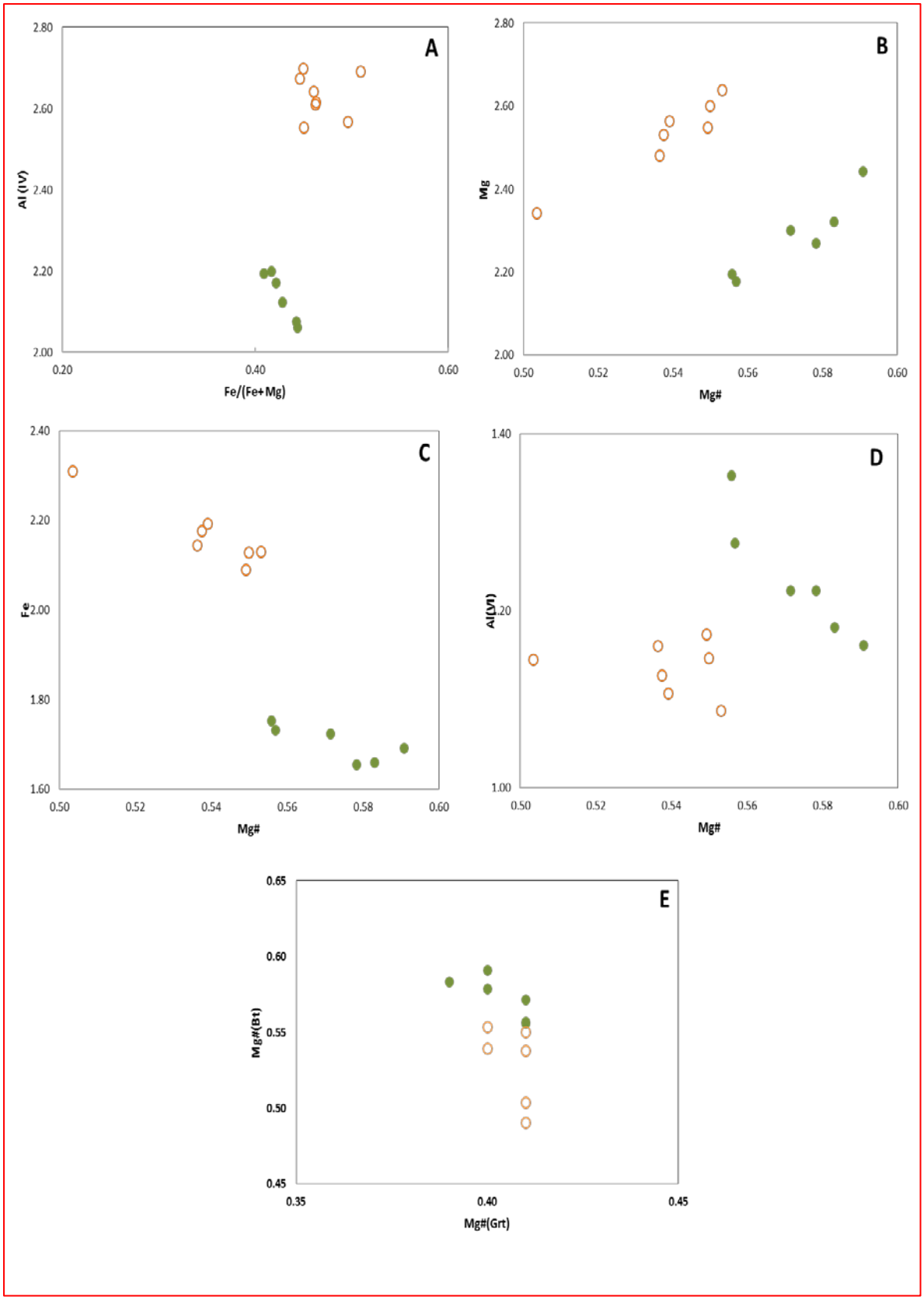

Figure 18: Compositions of biotite.

Table 5: Averaged compositions of Ilmenite.

P(Kbar)	1		1		1	
T(°C)	804		754		743	
Duration(days)	20		20		20	
n	5	σ	5	σ	6	σ
SiO_2	0.66	0.21	0.96	1.22	0.80	0.08
TiO_2	42.92	0.71	48.63	0.83	52.75	0.46
Al_2O_3	0.64	0.10	0.37	0.08	0.61	0.07
Fe_2O_3	19.92	1.59	6.43	1.99	-	-
FeO	32.68	1.55	41.01	1.39	44.29	0.28
MnO	0.64	0.10	0.18	0.13	0.27	0.06
MgO	2.42	0.42	1.74	0.05	1.28	0.13
Na_2O	0.24	0.23	0.10	0.13	-	-
K_2O	0.21	0.05	0.04	0.06	-	-
Total	100.34	0.43	99.45	0.46	99.99	0.04
xO2	3		3		3	
Si	0.02	0.01	0.02	0.03	0.02	0.00
Ti	0.81	0.01	0.91	0.02	0.98	0.01
Al	0.02	0.00	0.01	0.00	0.02	0.00
Fe^{3+}	0.35	0.02	0.12	0.04	-	-
Fe^{2+}	0.69	0.03	0.86	0.03	0.92	0.01
Mn	0.01	0.00	0.01	0.00	0.01	0.00
Mg	0.09	0.01	0.06	0.00	0.05	0.01
Na	0.01	0.01	0.00	0.01	-	-
K	0.01	0.00	0.00	0.00	-	-
Σ cation	2.00	0.00	2.00	0.00	1.99	0.01
Mg#	7.84		6.23		4.88	

n = number of analyzed points, σ = standard deviation 1

Fe_2O_3 (Fe^{3+}) calculated using the technique of Droop (1987)

Mg# = (Mg/(Mg + FeT))*100

FeT = Fe^{3+} + Fe^{2+}

Table 6:Average plagioclase and alkali feldspar compositions.

	Pl		Pl		Pl		Kfs	
Exp	1		2		3		3	
P(kbar)	1		1		1		1	
T(°C)	804		754		743		743	
duration(days)	20		20		20		20	
n	6	σ	7	σ	5	σ	7	σ
SiO_2	56.95	0.55	58.50	0.66	60.43	0.57	65.11	0.12
TiO_2	0.28	0.26			0.12	0.08	0.28	0.06
Al_2O_3	25.98	0.52	25.32	0.43	22.54	1.47	18.47	0.26
FeO	0.28	0.06	0.86	0.07	3.45	0.11	0.68	0.12
MgO	-	-	-	-	0.37	0.24	0.12	0.12
CaO	10.61	0.35	8.25	0.77	6.92	0.46	0.92	0.07
Na_2O	5.18	0.25	6.75	0.45	6.76	0.17	3.17	0.30
K_2O	0.98	0.25	0.35	0.07	0.45	0.05	11.36	0.39
Total	100.26	0.20	99.67	0.34	100.34	0.18	100.11	0.23
xO2- a	8		8		8		8	
Si	2.57	0.02	2.63	0.02	2.72	0.03	2.97	0.01
Ti	0.01	0.01	-	-	0.00	0.00	0.01	0.00
Al	1.38	0.03	1.34	0.02	1.19	0.07	0.99	0.01
Fe^{2+}	0.01	0.00	0.02	0.02	0.10	0.06	0.03	0.00
Mg	-	-	-	-	0.02	0.02	0.01	0.01
Ca	0.51	0.02	0.40	0.04	0.33	0.02	0.04	0.00
Na	0.45	0.02	0.59	0.04	0.59	0.01	0.28	0.03
K	0.06	0.01	0.02	0.00	0.03	0.00	0.66	0.02
∑Cations	4.99	0.01	5.00	0.00	4.99	0.01	4.99	0.01
An	50.13		39.49		35.15		4.56	
Ab	44.33		58.50		62.16		28.40	
Or	5.54		2.00		2.69		67.04	

n = number of analyzed points, σ = standard deviation 1

An = (Ca/(Ca + Na + K)) * 100

Ab = (Na/(Ca + Na + K)) * 100

Or = (K/(Ca + Na + K)) * 100

Table 7: Experimental garnet and hercynite average compositions.

	Grt		Grt		Grt		Hc	
Exp	1		2		3		1	
P(Kbar)	1		1		1		1	
T(°C)	804		754		743		804	
Duration(days)	20		20		20		20	
n	6	σ	4	σ	6	σ	12	σ
SiO_2	39.63	0.21	39.26	0.47	40.02	0.15	0.20	0.10
Al_2O_3	21.95	0.39	22.31	0.23	22.57	0.12	56.79	1.14
Cr_2O_3	0.06	0.10	0.03	0.06	0.16	0.10	-	-
Fe_2O_3	2.41	1.09	0.85	0.63	0.74	0.53	7.19	1.67
FeO	25.27	0.91	25.34	0.94	25.46	0.38	27.69	0.89
MnO	0.47	0.09	0.45	0.06	0.43	0.04	0.34	0.05
MgO	10.56	0.34	10.09	0.39	10.21	0.18	7.75	0.32
CaO	2.20	0.10	2.48	0.12	2.98	0.34	-	-
Na2O	-	-	-	-	-	-	0.32	0.20
Total	102.56	0.27	100.79	0.77	102.58	0.25	99.96	0.35
x02	12		12		12		4	
Si	2.96	0.02	2.99	0.01	2.98	0.01	0.01	0.00
Al	1.93	0.04	1.98	0.01	1.98	0.01	1.86	0.03
Cr	0.00	0.01	0.01	0.01	0.01	0.01	-	-
Fe^{3+}	0.14	0.06	0.03	0.03	0.04	0.03	0.15	0.03
Fe^{2+}	1.58	0.06	1.60	0.03	1.59	0.02	0.64	0.02
Mn	0.03	0.01	0.03	0.01	0.03	0.01	0.01	0.00
Mg	1.18	0.04	1.14	0.02	1.14	0.02	0.32	0.01
Ca	0.18	0.01	0.23	0.03	0.23	0.03	-	-
Na	-	-	-	-	-	-	0.02	0.03
Σcation	8.00	0.00	8.00	0.00	8.00	0.00	3.00	0.00
Mg#	40.33		40.50		40.67		28.81	

XAlm	53.31	53.45	53.18
XPyp	39.72	38.07	38.12
XSpss	1.01	0.92	0.91
XGrs	5.96	7.56	7.79

n = number of analyzed points, σ = standard deviation 1

Fe_2O_3 (Fe^{3+}) calculated using the technique of Droop (1987)

Mg# = (Mg/(Mg + FeT))*100

XAlm = (FeT/(Ca + Mg + Mn + FeT)) * 100

XPrp = (Mg/(Ca + Mg + Mn + FeT)) * 100

XGrs = (Ca/(Ca + Mg + Mn + FeT)) * 100

XSpss =(Mn/(Ca + Mg + Mn + FeT)) * 100

FeT = Fe^{3+} + Fe^{2+}

Table 8: Average cordierite compositions.

Exp	1		2		3	
P(Kbar)	1		1		1	
T(°C)	804		754		743	
Duration(days)	20		20		20	
n	6	σ	5	σ	5	σ
SiO_2	47.92	0.29	48.17	1.40	46.99	1.47
Al_2O_3	33.02	0.42	33.45	0.47	32.71	0.59
FeO	6.77	0.37	7.22	0.08	9.88	0.62
MnO	0.03	0.06	0.09	0.08	0.18	0.00
MgO	9.64	0.12	9.10	0.17	7.22	0.72
CaO	0.19	0.08	0.13	0.08	0.31	0.11
Na_2O	0.34	0.13	0.27	0.13	0.39	0.05
K_2O	0.33	0.04	0.16	0.06	0.37	0.12
Total	98.24	0.63	98.59	1.97	97.76	0.45
XO^2	18		18		18	
Si	4.93	0.02	4.94	0.05	4.93	0.12
Al	4.00	0.00	4.04	0.00	4.04	0.00
Fe^{2+}	0.58	0.03	0.62	0.04	0.87	0.08
Mn	0.00	0.04	0.01	0.01	0.01	0.06
Mg	1.48	0.00	1.39	0.01	1.13	0.01
Ca	0.02	0.01	0.01	0.01	0.03	0.12
Na	0.07	0.01	0.05	0.01	0.08	0.01
K	0.04	0.03	0.02	0.03	0.05	0.01
Σcation	11.13	0.01	11.08	0.01	11.12	0.02
Mg#	71.75		68.92		56.30	
Xfe	28.25		30.69		43.39	

n = number of analyzed points, σ = standard deviation 1

Mg# = (Mg/(Mg + FeT))* 100

XFe= 100* (Fe^{2+}/(Fe^{2+}+ Mg))

FeT = Fe^{3+} + Fe $^{2+}$

Table 9: Average biotite compositions.

Exp	1		2	
P(Kbar)	1		1	
T(°C)	804		743	
duration(days)	20		20	
n	6	σ	8	σ
SiO_2	40.67	0.50	36.25	0.99
TiO_2	1.21	0.35		
Al_2O_3	19.85	0.31	21.51	0.68
FeO	14.12	0.32	17.79	0.84
MnO	0.05	0.07		
MgO	10.63	0.52	11.37	0.65
CaO	0.30	0.13		
Na_2O	0.90	0.11	0.41	0.04
K_2O	8.58	0.29	9.08	0.11
Total	96.30	1.33	96.41	2.27
xO2	11		11	
Si	5.86	0.05	5.37	0.05
$Al^{(IV)}$	2.14	0.05	2.63	0.05
Ti	0.13	0.04	0.00	0.00
$Al^{(VI)}$	1.24	0.06	1.12	0.04
Fe^{2+}	1.70	0.04	2.21	0.12
Mn	0.01	0.01	0.00	0.00
Mg	2.28	0.09	2.51	0.10
Ca	0.05	0.02	0.00	0.00
Na	0.25	0.03	0.12	0.01
K	1.58	0.05	1.72	0.04
Σcation	15.23	0.06	15.67	0.06
Mg#	57.28		53.24	
Xfe	42.72		46.76	

n = number of analyzed points, σ = standard deviation 1

Mg# = 100 * (Mg/(Mg + Fe^{2+}))

Xfe= 100* (Fe^{2+}/(Fe^{2+}+ Mg))

6.3.6 Quenched Melts

The compositions of quenched melts formed within experimental run products are presented in Table 10 below, additional data is provided in (Appendix 10). The analyses of the quenched melt compositions are normalized to 100% anhydrous. Figure (19) shows plots of various major elements and element ratios (atomic) plotted against maficity for the experimental glasses produced in this study.

Table 10: Average compositions of quenched melts. Analyses normalized to 100% anhydrous.

Exp	1		2		3	
P(Kbar)	1		1		1	
T(°C)	804		754		743	
Duration(days)	20		20		20	
n	9	σ	8	σ	7	σ
SiO_2	76.56	0.32	76.13	0.53	77.62	0.35
TiO_2	0.32	0.06	0.30	0.02	0.16	0.02
Al_2O_3	14.98	0.41	14.52	0.16	13.48	0.24
FeO	0.84	0.04	0.87	0.05	0.99	0.03
MgO	0.53	0.06	0.49	0.09	0.40	0.06
CaO	0.60	0.05	0.58	0.04	0.51	0.07
Na_2O	1.37	0.15	1.45	0.21	1.64	0.26
K_2O	4.81	0.30	5.66	0.42	5.19	0.11
Total	100.00		100.00		100.00	
Si	1.27	0.00	1.27	0.09	1.29	0.00
Ti	0.00	0.01	0.00	0.00	0.00	0.01
Al	0.15	0.00	0.14	0.00	0.13	0.00
Fe	0.01	0.00	0.01	0.00	0.01	0.00
Mg	0.01	0.00	0.01	0.00	0.01	0.00
Ca	0.01	0.00	0.01	0.00	0.01	0.00
Na	0.02	0.00	0.02	0.00	0.03	0.00
K	0.05	0.00	0.06	0.00	0.06	0.00
Mg#	0.53	0.00	0.50	0.05	0.42	0.00
ASI	1.75	0.26	1.52	0.13	1.45	0.41
Mg+ Fe	0.02	0.13	0.02	0.00	0.02	0.08

n = number of analyzed points, σ = standard deviation 1

Mg# = (Mg/ (Mg +Fe)

A/ CNK = mol. (Al_2O_3/ (CaO+Na_2O + K_20))

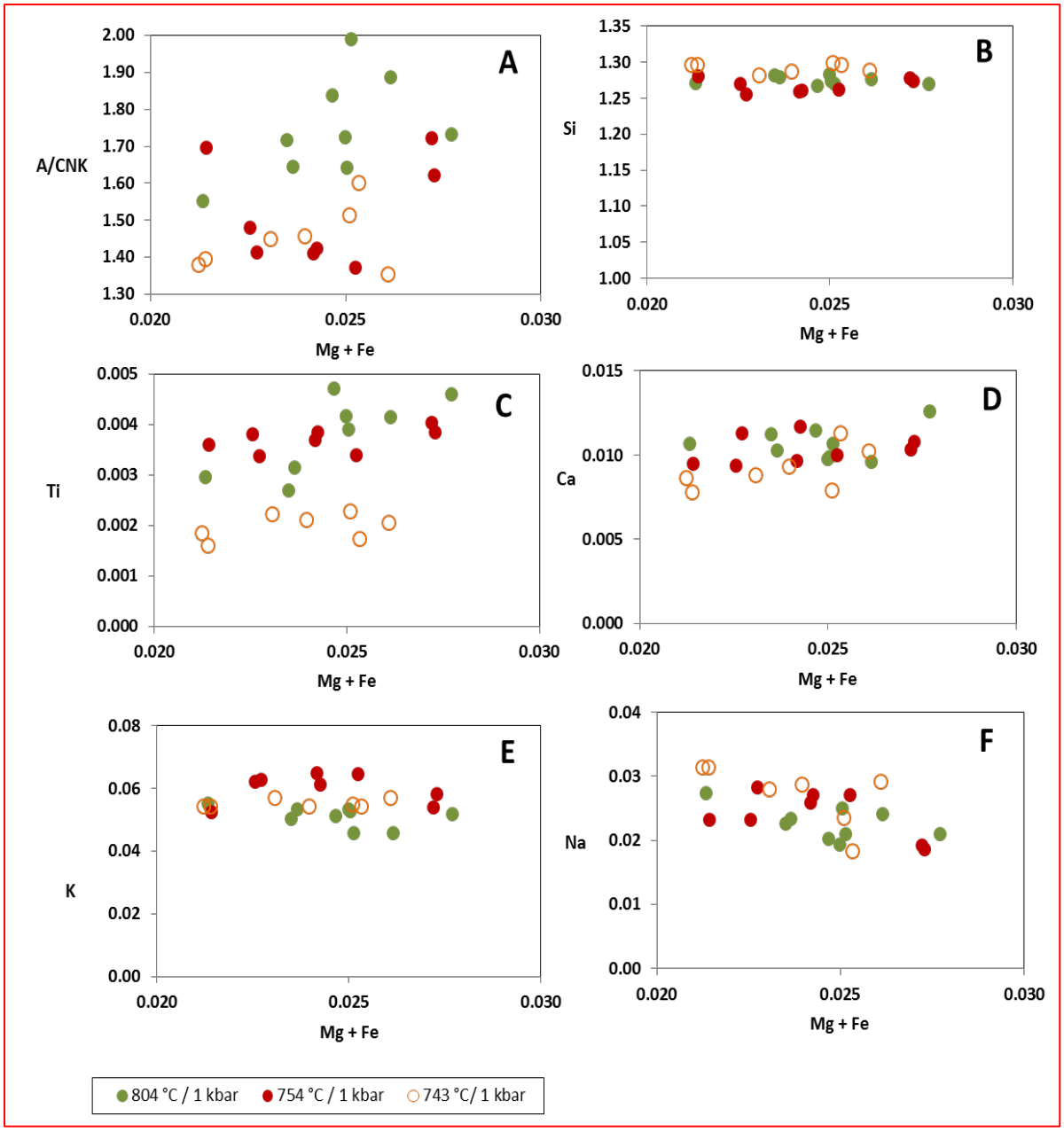

Figure 19: Compositions of quenched melts.

The diagrams illustrate major-element compositions and element ratios plotted against maficity.

The compositions of the experimental quenched melts in each run product are silicic and strongly peraluminous. The compositions of these quenched melts are similar to compositions of S-type granite melts from the literature (Montel and Vielzeuf, 1997; Stevens et al., 1997; Stevens et al., 2007). The most notable compositional variations between quenched melts produced in different run products area portrayed by the ASI and Mg# contents (Fig. 19 a & g). The variables decrease with decreasing temperature, the highest average ASI value is 1.75 and the lowest is 1.45 recorded at 804 and 743 ºC respectively. Similarly, Mg# decreases from an average 0.53 at 804 ºC to 0.42 at 743 ºC.

The low Fe and Mg contents of the quenched melts indicate that the garnet in the starting composition did not dissolve in the melt to liberate Mg and Fe components enriching the melt in these components. Instead, it appears that the portion of the garnet that reacted with the melt produced new Fe, Mg-rich phases such as biotite, cordierite and hercynite. The quenched melts also have low-Ti and Ca contents as it can be seen from figure 19 c-d. This is compatible with findings of Stevens et al., (2007) that propose that the Ti and Ca budget of granite magmas is concentrated within the peritectic mineral assemblage.

7 Experimental vs. Predicted outcomes

This section documents a comparison between outcomes predicted by phase-equilibrium modeling and the experimental results. Phase-equilibrium modeling provides an understanding of what happens in geological systems over a chosen P-T range, assuming attainment of equilibrium. Experiments seek to examine rates of equilibration in magmatic systems. The subsections below will document a detailed comparison between mineral assemblages, mineral compositions, and proportions produced in experimental runs and those predicted for by phase-equilibrium modelling.

7.1 Mineral Assemblages

Table 11 below provides mineral assemblages predicted by Theriak Domino phase-equilibrium modelling and assemblages produced by experiments. Generally, the mineral assemblages produced in experimental runs are in good agreement with what is predicted by phase-equilibrium modelling, particularly, concerning phases such as plagioclase, ilmenite, and cordierite. The latter phases are present in experimental run products across all investigated P-T conditions as predicted by phase-equilibrium modelling. However, there are some discrepancies between what is observed in the experiments and what is predicted by the modelling. The most significant discrepancy is the presence of metastable garnet in all the run products. Additional differences involve the absence of orthopyroxene at 804 ºC and 754 ºC, presence of hercynite and biotite at 804 ºC and the presence of K-feldspar in the 743 ºC experiment. The presence of biotite across all experimental run products is due to a reaction between garnet and the melt. This accounts for the presence of biotite in experiment 1 (804 ºC/ 1 kbar) outside its predicted stability field. The presence of refractory garnet in the run products, far below its predicted stability field, is a consequence of slow reaction rate between garnet and the melt. Details of the involved reaction(s) will be documented in the discussion section. In the case of K-feldspar, phase-equilibrium modelling underestimated its stability field. Therefore, the presence of biotite, K-feldspar and garnet outside their predicted stability fields and presence of hercynite at 804 ºC attest to the fact that phase-equilibrium modelling

does not take into account reaction kinetics. That is, it neglects rates of reactions or rates at which equilibrium is attained between magma and crystals with which it is out of equilibrium.

Table 11: A comparison of experimental vs. predicted mineral assemblages.

Experiment	P(kbar)	T(°C)	Experimental assemblages	Predicted Assemblages
1	1	804	Pl Bt Ilm Crd Hc Liq *Grt*	Pl Crd Ilm Opx Liq H_2O
2	1	754	Pl Bt Qtz Crd Ilm Liq H_2O *Grt*	Pl Bt Crd Ilm Opx Liq H_2O
3	1	743	Pl Kfs Qtz Ilm Crd Bt Liq H_2O *Grt*	Pl Qtz Ilm Crd Bt Liq H_2O
metastable phases are indicated by blue text in italics				

7.2 Phase proportions

Table (12) below compares and contrasts the wt% abundances between mineral phases produced in experimental run products and those predicted by phase-equilibrium modelling. Least-squares mixing calculation using mineral compositions and melt data presented in tables 4 to 9 was used to calculate proportions of phases produced in the experimental runs, using the solver function in Microsoft Excel. Comparison between experiments and modelling reveals a mismatch between predicted and experimental mineral abundances. The significant mismatches between modelling and experimental abundances are the presence of refractory garnet across all experimental runs, the absence of orthopyroxene in experiments 1 and 2 (804 & 754 ºC / 1 kbar). Furthermore, the solver calculated that there should be no cordierite in any of the run products, although it is a prominent phase in the experiments. Additionally, the solver predicts that the proportions of ilmenite, biotite and quartz decrease as the melt crystallizes, which is incorrect (see Table 12A). To correct the error in the solver calculations,

the least-squares mixing calculations were modified by restricting the abundance of garnet to values that seem reasonable, based on visual estimates from SEM images of the run products. The estimated garnet abundances are 0.5 wt%, 0.99 wt% and 1.32 wt% for experiment 1 (804 ºC / 1 kbar), experiment 2 (754 ºC / 1 kbar) and experiment 3 (743 ºC / 1 kbar), respectively.

As a fraction of the original garnet crystals in added in the starting material remains unreacted and out of equilibrium, it introduces an error in the modelling. The bulk composition used to calculate the phase-equilibrium model does not recognize the refractory garnet. Consequently, the bulk composition used to calculate the phase-equilibrium model differs slightly from the effective bulk composition that applies to the individual experiments. To correct this, the unreacted garnet fraction for each experiment was removed from the original bulk composition and a new bulk composition was calculated using the composition and proportions of experimental garnet. Subsequently, phase-equilibrium modelling was re-calculated using the newly calculated effective bulk composition. For example, in the starting bulk composition, the garnet fraction is 8 wt%, in experiment at 754 ºC/ 1 kbar the effective bulk composition has 7.01 wt% garnet. The resultant experimental and modelling mineral abundances are displayed in Table (12B) below, and the calculated pseudosections are presented in Fig. 20-22.

Table 12: Experimental vs. Predicted mineral abundances (wt%).

The predicted values in table A were calculated using the original bulk composition and those in table B were calculated using the effective bulk compositions of the respective P-T conditions.

A						
	Experimental proportions			**Predicted proportions**		
Exp	1	2	3	1	2	3
P(kbar)	1	1	1	1	1	1
T°C	804	754	743	804	754	743
Melt	77.06	70.04	64.20	73.08	63.25	53.96
Pl	9.96	14.84	17.52	18.25	24.21	27.09
Qtz	-	4.05	1.33	-	-	4.50
Bt	5.28	1.89	1.31	-	2.75	6.49
Ilm	1.73	1.53	1.34	1.44	1.34	1.21
Crd	-	-	-	6.72	7.04	6.74
Hc	2.39	-	-	-	-	-
Grt	3.09	7.30	7.14	-	-	-
Opx	-	-	-	0.51	1.42	-
Kfs	-	-	7.38	-	-	-
B						
	Experimental proportions			**Predicted proportions**		
Exp	1	2	3	1	2	3
P(kbar)	1	1	1	1	1	1
T°C	804	754	743	804	754	743
Melt	74.93	68.42	37.98	73.77	65.00	61.16
Pl	11.87	14.83	18.58	17.51	23.50	25.69
Qtz	-	1.66	13.90	-	-	1.84
Bt	2.60	4.50	6.68	-	2.42	3.57
Ilm	1.71	1.62	1.19	1.44	1.35	1.35
Crd	8.01	7.96	6.99	7.06	7.12	6.38
Hc	0.38	-	-	-	-	-
Grt	0.50	0.99	1.32	-	-	-
Opx	-	-	-	0.22	0.61	-
Kfs	-	-	13.41	-	-	-

The observed (experimental) and predicted mineral abundance trends predicted by modelling, using the relevant effective bulk compositions, for all phases that are predicted and are also produced in the experiments are in good agreement. For example, both techniques display that the abundance of melt decreases with decreasing temperature, whilst the abundances of biotite and plagioclase increase with decreasing temperature. Although the predicted and experimental modal trends are well matched, the absolute modal amounts differ. In the case of biotite, the estimated experimental proportions are higher than what phase-equilibrium modelling predicts, especially in experiment 3-743 ºC/ 1 kbar, which produced 3.11 wt% biotite more than the phase-equilibrium modelling predicts. Contrary to this, the observed proportions of plagioclase at 804, 754 and 743 ºC, are 5.64, 8.67 and 7.11 wt%, less than those predicted by phase-equilibrium modelling, respectively. The predicted and observed proportions of cordierite and ilmenite are very similar. In case of the melt, the predicted and observed proportions in the 804 and 754 ºC experimental runs are very similar. However, in the 743 ºC experiment, the observed proportions are 23.18 wt% lower than the predicted proportions. Phase-equilibrium modelling predicted a much higher melt volume at 743 °C possibly because the predicted crystalline phases are fewer than what is produced in the experiment.

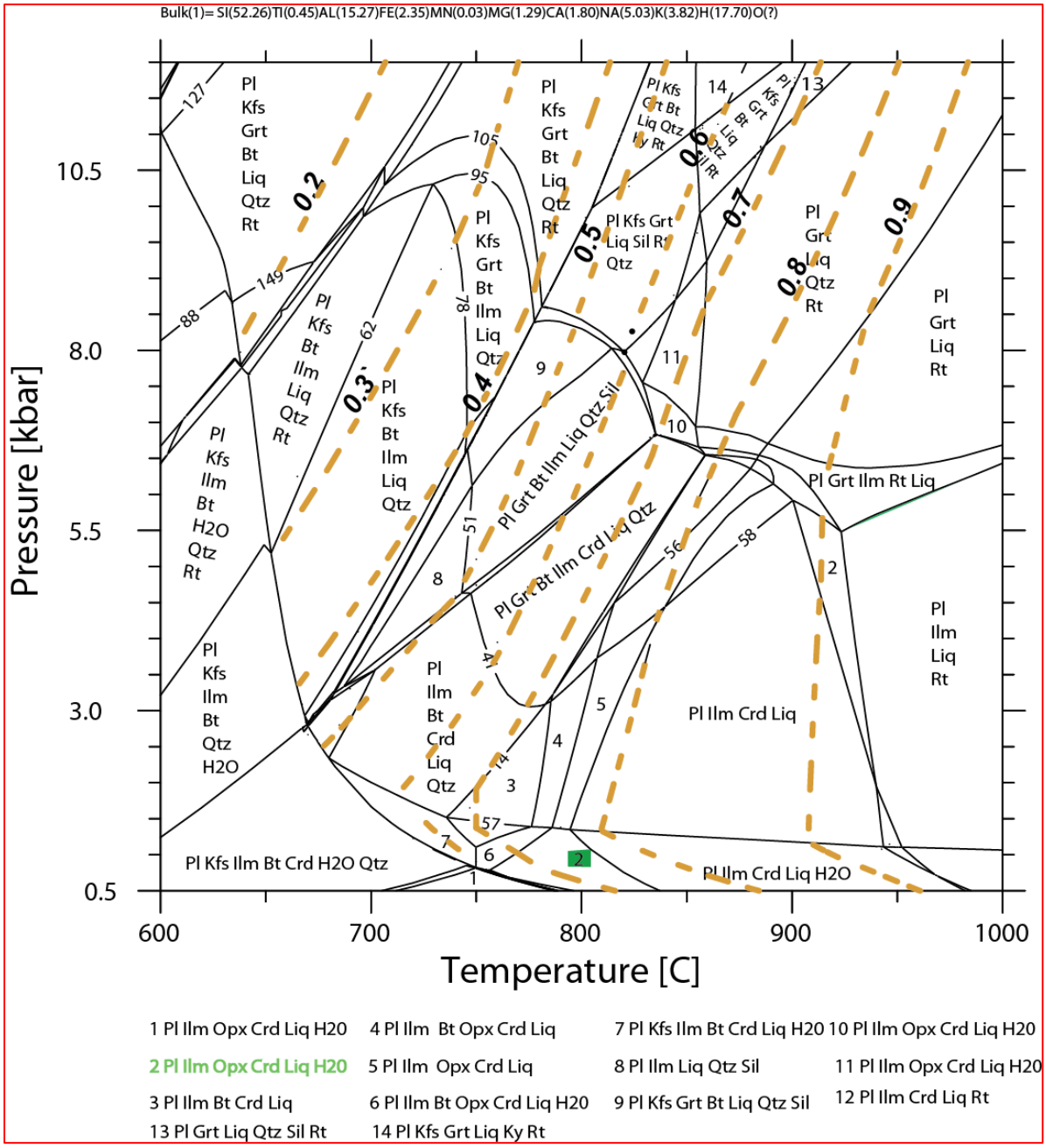

Figure 20: Pseudosection calculated using the effective bulk composition of experiment 1 (804 °C/ 1 kbar).

The green square illustrates the experimental P-T conditions. The yellow dashed lines illustrate melt Isopleths.

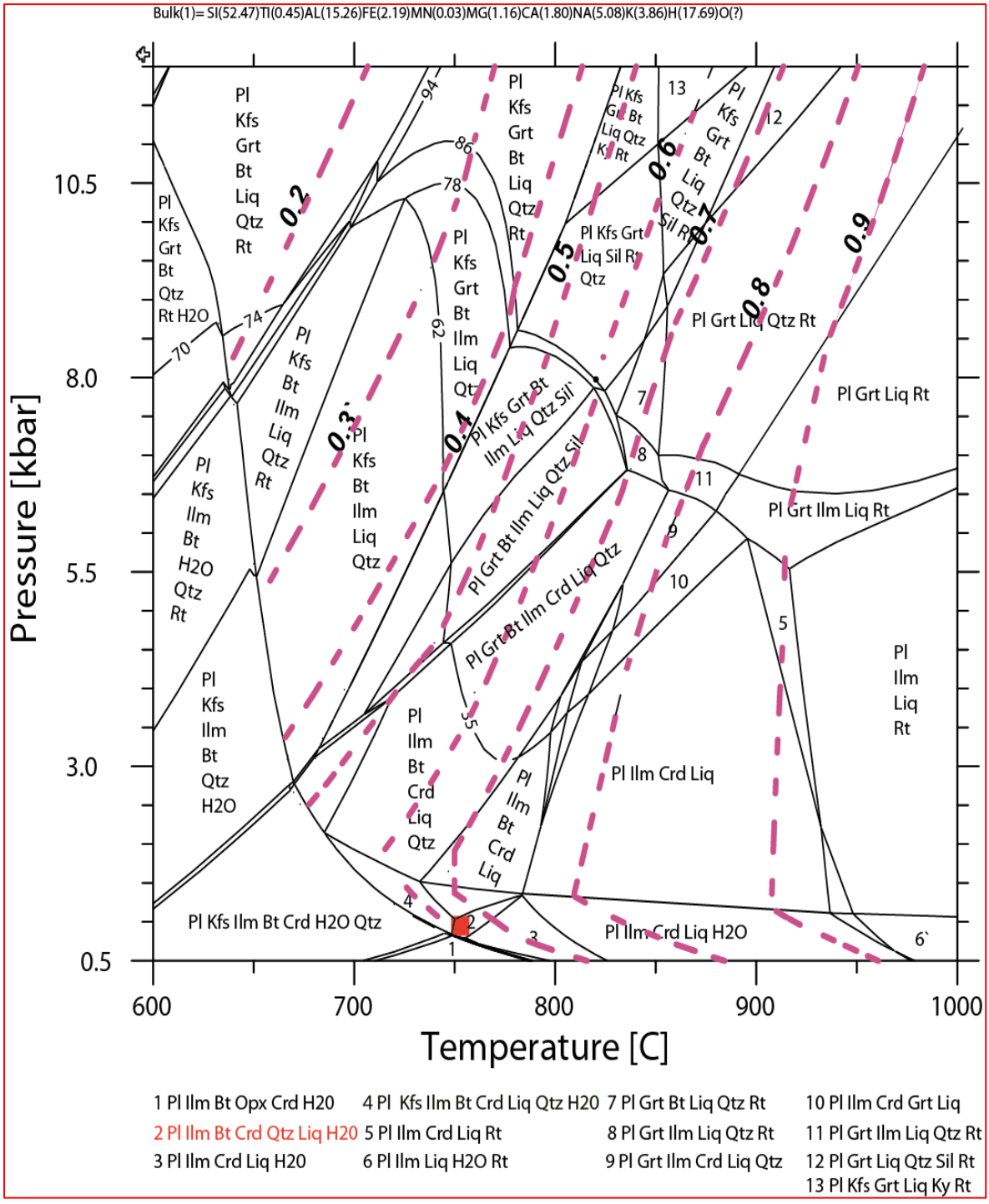

Figure 21: Pseudosection calculated with the effective bulk composition of experiment 2 (754 °C/ 1 kbar).

The red square illustrates the experimental P-T conditions. The purple dashed lines illustrate melt isopleths

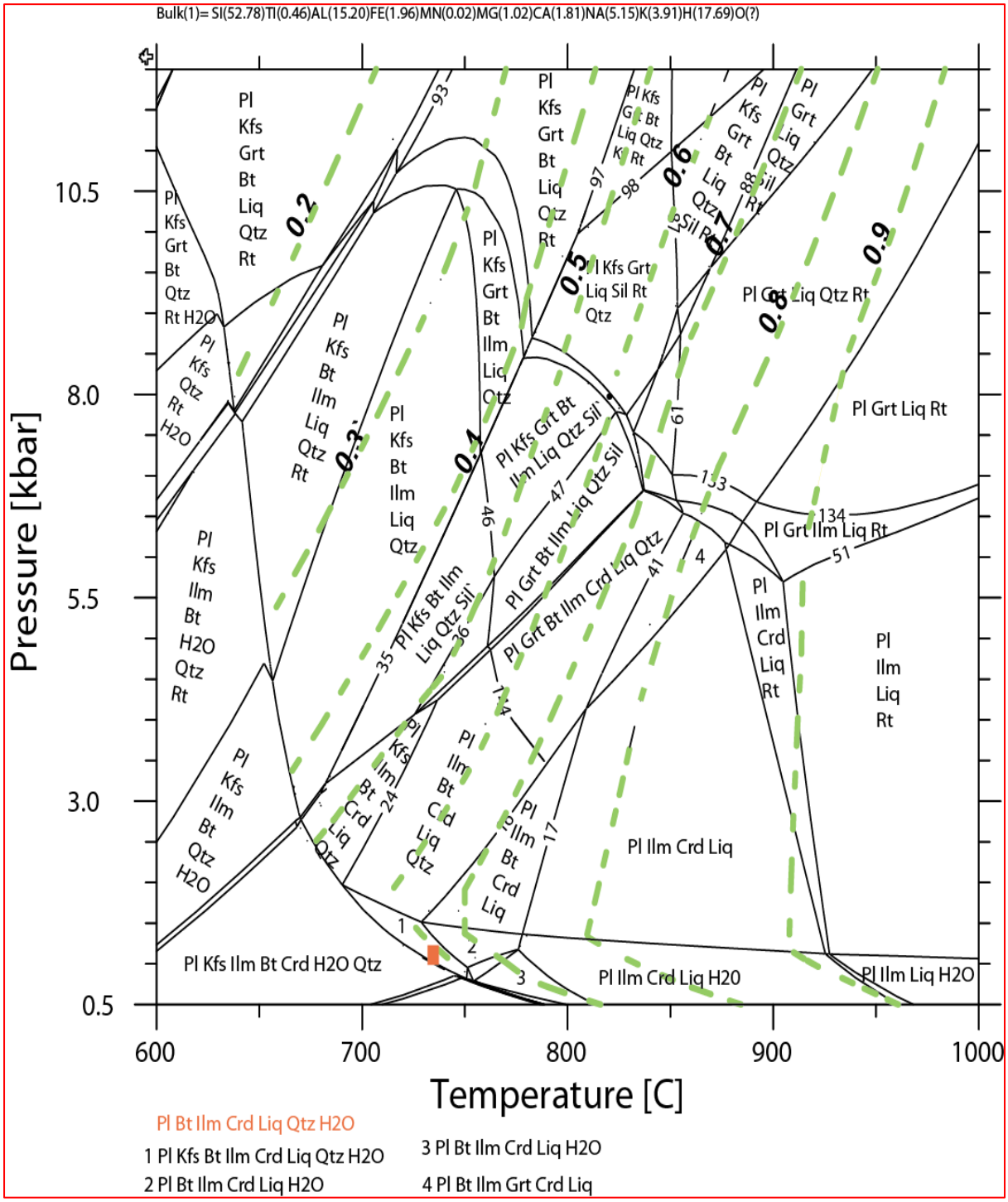

Figure 22: Pseudosection calculated with the effective bulk composition of experiment 3 (743°C/1kbar).

The orange square illustrates the experimental P-T conditions. The green dashed lines illustrate melt isopleths. The stable assemblage at 743 ºC is indicated by the orange text.

7.3 Phase Compositions

Table 13 below compares and contrasts experimental mineral compositions and compositions predicted by phase-equilibrium modelling. The table below includes only the mineral phases that appear on both the pseudosection and in the experimental products. The experimental composition of biotite produced in experiment 2 could not be obtained due to the very small sizes of the biotite crystals.

Generally, mineral compositions predicted for by modelling and those observed in experimental run products are similar. In the case of plagioclase, both techniques predict that the composition of plagioclase becomes more sodic with decreasing temperature. The absolute mol % proportions of Ab and An do not show significant variations, see Fig. 15. The predicted and experimental compositions of cordierite show minor variations. The predicted compositions have higher Fe and lower Mg contents than those of cordierite produced in the experiments. Additionally, the experimental compositions contain minor amounts of alkalis, which are not in the predicted compositions. In case of ilmenite, the most significant discrepancy between the experimental and predicted compositions is that the predicted compositions are a solid solution between ilmenite ($FeTiO_3$) - pyrophanite ($MnTiO_3$) - hematite (Fe_2O_3). The experimental compositions represent a solid solution between ilmenite ($FeTiO_3$) - pyrophanite ($MnTiO_3$) - geikielite ($MgTiO_3$) - hematite (Fe_2O_3). Furthermore, both predicted and experimental compositions have a slight Fe deficiency, with the exception of the ilmenite produced in the 804 ºC experiment that has an excess of 0.04 apfu Fe. However, the predicted compositions have the ideal Ti content of 1 whereas the experimental compositions have a slight deficiency of Ti, see Fig. 14 A.

Table 13: A comparison between predicted and experimental mineral compositions.

Experiment 1: 804 /1kbar		
	Predicted	Experimental
Pl	$An_{50.73}Ab_{47.09}Or_{2.18}$	$An_{50.13}Ab_{44.33}Or_{5.54}$
Ilm	$Fe_{0.96}Mn_{0.04}Ti_{1.00}O_3$	$Fe_{1.04}Mg0.09\ Mn_{0.01}Ti_{0.81}O_3$
Crd	$Mg_{0.86}Fe_{1.12}Mn_{0.01}Al_{4.00}Si_{5.00}O_{18}$	$Mg_{1.48}Fe_{0.58}Ca_{0.02}Na_{0.07}K_{0.04}Al_{4.00}Si_{4.93}O_{18}$
Experiment 2: 754 / 1kbar		
Pl	$An_{40.27}Ab_{56.49}Or_{3.24}$	$An_{39.49}Ab_{58.50}Or_{2.00}$
Ilm	$Fe_{0.96}Mn_{0.04}Ti_{1.00}O_3$	$Fe_{0.98}Mg0.06\ Mn_{0.01}Ti_{0.98}O_3$
Crd	$Mg_{0.81}Fe_{1.18}Mn_{0.01}Al_{4.00}Si_{5.00}O_{18}$	$Mg_{1.39}Fe_{0.62}Mn_{0.01}Ca_{0.01}Na_{0.05}K_{0.02}Al_{4.04}Si_{4.94}O_{18}$
Experiment 3: 743 /1kbar		
Pl	$An_{37.55}Ab_{58.72}Or_{3.73}$	$An_{35.15}Ab_{62.16}Or_{2.69}$
Ilm	$Fe_{0.98}Mn_{0.02}Ti_{1.00}O_3$	$Fe_{0.92}Mg_{0.05}\ Mn_{0.01}Ti_{0.92}O_3$
Crd	$Mg_{0.80}Fe_{1.19}Mn_{0.01}Al_{4.00}Si_{5.00}O_{18}$	$Mg_{1.39}Fe_{0.62}Mn_{0.01}Ca_{0.01}Na_{0.05}K_{0.02}Al_{4.04}Si_{4.94}O_{18}$
Kfs	$An_{1.33}Ab_{28.34}Or_{70.34}$	$An_{4.56}Ab_{28.40}Or_{67.04}$
Bt	$KFe_3Mg_2Ti_{0.01}Si_3AlH_2O_{12}$	$K_{1.72}Na_{0.12}Ca_{0.05}Fe_{2.21}Mg_{2.51}Ti_{0.00}Si_{5.37}Al_{3.75}H_2O_{12}$

Although K-feldspar is part of the stable assemblage in the field labeled 1 in Fig. 21, it is predicted to stabilize at 735 ºC. In this case, the composition of experimental K-feldspar is compared with the predicted composition at 735 ºC / 1 kbar. These compositions are very similar. The composition of biotite produced in experiment 3 is very similar to composition predicted by phase-equilibrium modelling.

Concluding Remarks

Generally, the experimental outcomes are compatible with thermodynamic model predictions. However, there are some discrepancies, namely the persistence of garnet in all experimental run products, the presence of biotite above its predicted stability field and the apparent absence of the predicted minor amounts of orthopyroxene in experimental run products. The discrepancies are consistent with the fact that phase-equilibrium modelling neglects reaction kinetics. One of the prominent discrepancies is the under-estimation of the stability for K-feldspar. The presence of refractory metastable garnet crystals creates an error in the modelling and amplifies the differences between observed and predicted outcomes. For instance, in this study, orthopyroxene was supposed to form as a potential replacement of garnet. However, the sluggish garnet-melt reactions may have hindered the formation of orthopyroxene. This underlines the need to distinguish between the bulk-rock composition and the effective bulk composition at a specific P-T point along the magma evolution path.

8 Discussion

The P-T conditions of this study's experiments equates to depths shallower than 5 km within the continental crust. It is worth mentioning that this study assumed instantaneous emplacement of the magma from deeper crustal to shallow crustal levels. Therefore, the fates of an entrained "peritectic" mineral assemblage in ascending monzogranitic S-type magma were not experimentally constrained at various P-T points along the magma ascent path. The chosen experimental conditions are intended to represent different steps in the cooling of the magma at the level of emplacement. Therefore, the experiments conducted in this study only provide a snapshot of what becomes of the entrained peritectic mineral assemblage at P-T conditions equivalent to emplacement levels of S-type granitic magmas.

8.1 Attainment of equilibrium

At the beginning of each experimental run, the crystals in the starting material were out of equilibrium with the melt. Minerals that encounter a melt, with which they are out of equilibrium, will re-equilibrate to reduce the free energy of the system (Putins, 2009). The proposed rapid evacuation and ascent rates of granitic magmas from their source regions fosters disequilibrium behavior in granitic systems, thereby allowing preservation of some refractory metastable phases (Clemens and Stevens, 2016). In many natural rocks, disequilibrium features between melt and crystals are typically displayed by compositional zoning in minerals and reaction rims (Muncill and Lasaga, 1987). The experimental run products of this study show that equilibrium was approached reasonably well, based on observed systematic changes of mineral assemblages, mineral compositions and proportions, with changing temperature. The outcomes of this study demonstrate that the different crystal phases that are intentionally out of equilibrium at the start of the experiments follow different equilibration pathways. Compositional and textural features of experimental plagioclase and ilmenite indicate that they are well equilibrated with the magma. On the other hand, the preservation of garnet "cores" surrounded by biotite reaction rims indicates poor equilibration between the surrounding magma and garnet crystals across all investigated P-T conditions. A detailed

discussion of the fates of a hypothetical, entrained peritectic assemblage in a monzogranitic S-type magma subjected to this study's experimental P-T conditions will be outlined below.

8.2 Fates of entrained "peritectic" mineral assemblage

8.2.1 Garnet

The pseudosection in Fig. 6 shows that garnet is a stable phase for the greater part of the magma's ascent journey but is unstable across all P-T conditions investigated in this study. However, the composition of garnet at various points along the ascent path differs significantly from that of the original garnet in the starting material. The modelling predicts that, as the magma decompresses, the composition of garnet will continuously re-equilibrate with the surrounding magmatic conditions until it reaches its lower pressure stability limit. Within the garnet stability fields, the magma will bring out-of-equilibrium garnet into equilibrium through a rapid, coupled, dissolution-precipitation mechanism (Villaros et al., 2009a).

Unlike the outcomes of phase-equilibrium modelling, garnet crystals are preserved in all experimental run products. The preservation of garnet cores rimmed by biotite suggests that the garnet is metastable. The outcomes of this study demonstrate that the entrained garnet crystals in the starting material reacted with the melt to produce biotite, hercynite, and cordierite. Phase-equilibrium modelling illustrates that both cordierite and biotite are stable phases across all investigated P-T conditions. Thus, the compositions of these minerals are most likely in equilibrium with the surrounding "magmatic" conditions. The reaction between the garnet crystals and melt resulted in either partial or complete (grain-scale) replacement of the garnet by the above-mentioned phases. The garnet-melt reaction that resulted in either partial or complete replacement of garnet crystals by biotite-hercynite, biotite and cordierite-biotite pseudomorphs occurred along the reaction interface (Putins, 2002; Ruiz-Agudo et al., 2014). The interaction between the melt and garnet at the reaction interface induces dissolution of garnet by liberating major cations (Mg, Fe, Al and Ca) from the garnet into the interfacial melt phase. The melt in the interfacial boundary layer becomes supersaturated with the cations in a matter of seconds (Zhang et al., 1989). Unfortunately, these cations are

incompatible in the melt. As a result, the insoluble components of the garnet manifest as hydrous Fe-Mg-Al-rich phases, stable under investigated P-T conditions, in this case biotite, cordierite, and Ca-rich plagioclase. This process allows biotite reaction rims to form along the edges of the garnet (Ruiz-Agudo et al., 2014). The rate at which garnet is replaced by biotite and/or cordierite appears to be controlled by the dissolution rate of garnet and transport of ions in the interfacial melt. Putins (2007) and Ruiz-Agudo et al. (2014) found that complete dissolution of a “parent” mineral, in this case garnet, requires that reaction products (biotite) must develop a porosity network that will allow interaction between the parent crystals and melt. Dissolution of garnet at the reaction interface in this study’s experiments is sluggish, so not all garnet crystals were replaced by biotite and cordierite within the 20-day experimental run time. Based on the experimental results, it is proposed that preservation of the garnet cores may be attributed to a number of factors. i) The duration of the experiments was most likely not long enough to allow the reaction to run to completion under the investigated P-T conditions. ii) The apparent fast growth rates of biotite, cordierite and hercynite crystals along the edges of the garnet crystals limited the interaction between garnet and the melt, thus decelerated the rate of garnet dissolution.

In the 804 ºC run product, interlocking biotite and hercynite spinel crystals rim the garnet crystals. There is also development of prominent pseudomorphic replacement textures indicating replacement of garnet by cordierite-biotite-hercynite intergrowths. The cordierite-biotite and biotite-hercynite intergrowths indicate simultaneous precipitation during the dissolution of garnet in the melt at the reaction interface. Although it is not predicted by phase-equilibrium modeling, hercynite formed as one of the prominent reaction product of garnet breakdown. The precipitation of hercynite in close proximity to the garnet crystals indicates zonation in the activity of aluminum oxide within the run product. The alumina content is likely to be higher around the dissolving garnet crystals and it stabilizes hercynite. A schematic illustration of the mineral textures and garnet-melt reaction is displayed in Fig. 23. The cordierite-biotite and biotite-hercynite intergrowths indicate simultaneous precipitation during the dissolution of garnet in the melt at the reaction interface. The garnet-melt reaction is demonstrated below.

$$Grt1 + melt\ components\ (K\text{-}feldspar + H_2O) \rightleftharpoons Bt + Hc + Grt2 + Crd \qquad (2a)$$

$$Grt1 + melt\ components\ (K\text{-}feldspar + H_2O) \rightleftharpoons Bt + Crd + Grt2 \qquad (2b)$$

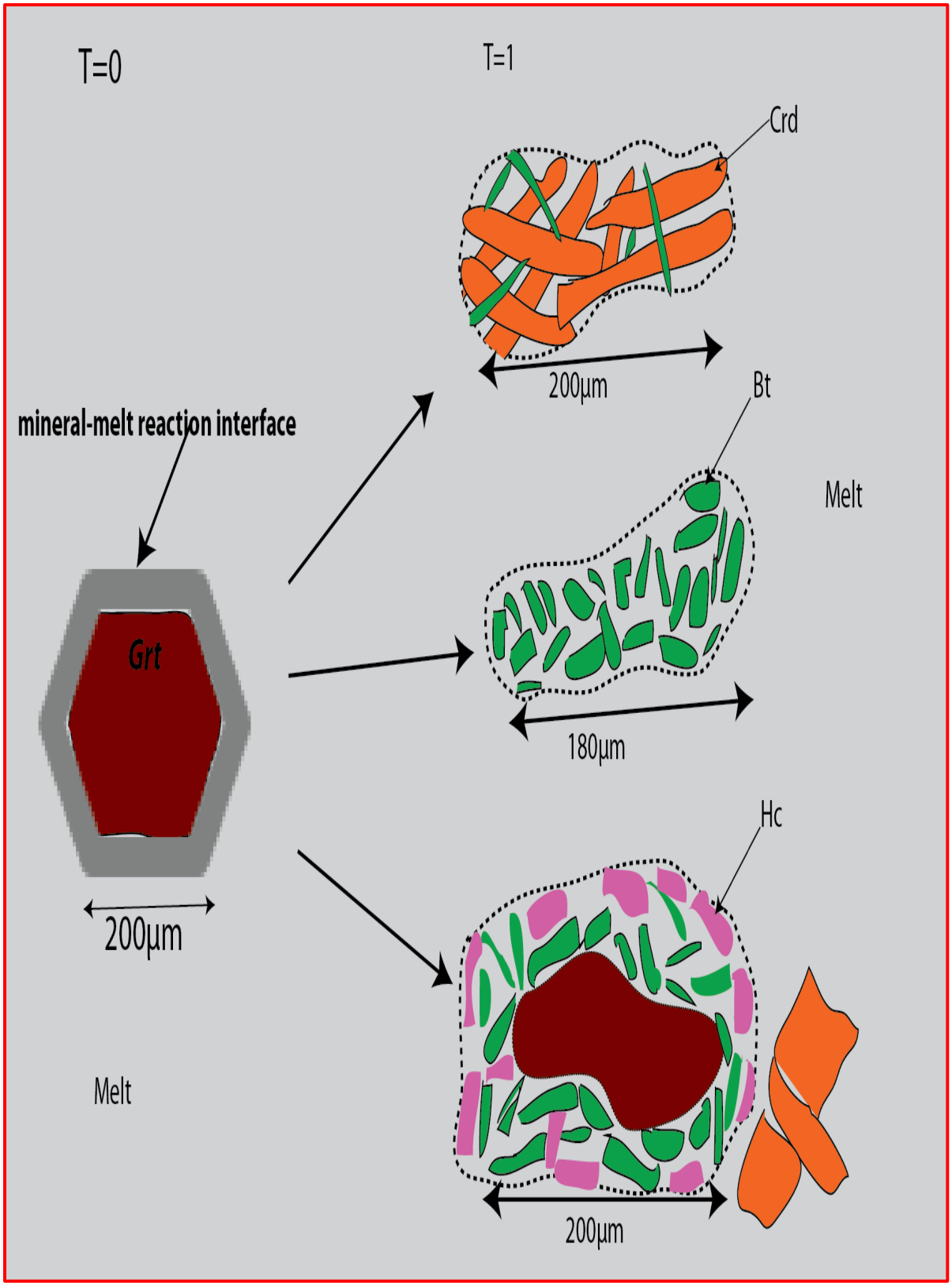

Figure 23: An illustration of the garnet-melt reaction at 804 ºC.

In the 754 and 743 ºC run products, cordierite and biotite are the only products of the garnet-melt reaction, see Fig. 24 below for schematic of the garnet-melt reaction. A simplified model of the garnet-melt reaction that produced biotite and cordierite these experiments is illustrated below. The Cordierite crystals have euhedral shapes, are surrounded by the melt whilst, thin biotite reaction rims share boundaries with remnant garnet crystals and melt. These textural features are interpreted to indicate that cordierite most likely did not crystallize simultaneously with the biotite reaction rims as a direct consequence of the garnet-melt reaction. Therefore, it can be reasoned that cordierite crystallized from the melt to buffer the Al_2O_3 component in the system.

Grt + melt components⇌Bt +Crd + Si0₂ (3)

3(Mg, Fe)₃Al₂Si₃O₁₂ + Melt components (2KAlSi₃O₈ + 2H₂O) ⇌ 2K (Mg, Fe)₃AlSi₃O₁₀ (OH)₂ + 1.5(Mg, Fe)₂Al₄Si₅O₁₈ + 1.5SiO₂

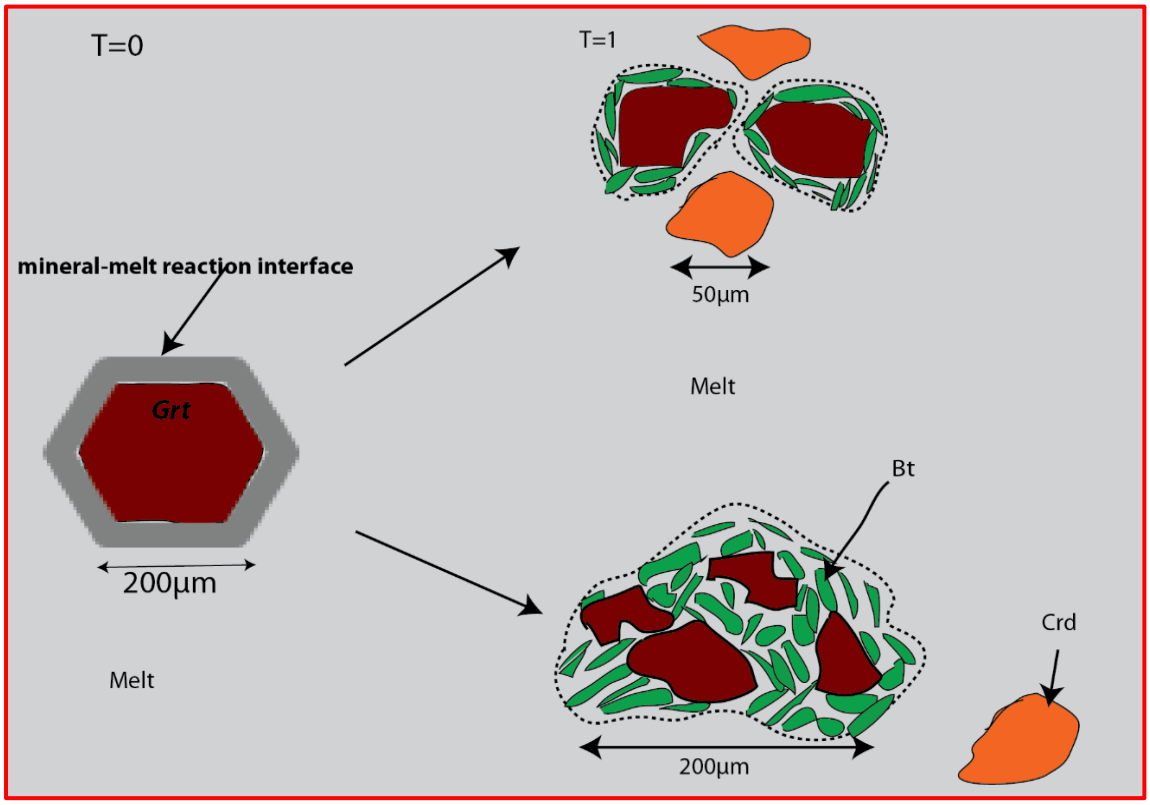

Figure 24: An illustration of the garnet-melt reaction for experimental runs below 804ºC.

The preservation of the external shape of the garnet crystals in all run products imply that the rates of dissolution of the reactant phase “garnet” must equal the rates of precipitation of product phases i.e. biotite and cordierite (hercynite) (Maliva and Siever, 1988). The resorbed crystal form and the lack of inclusions (e.g. melt) within the remnant, garnet crystals in the run products argue against re-equilibration of the garnet compositions by a coupled dissolution-precipitation mechanism. It is proposed that, the garnet crystals undergone some degree of re-equilibration through mineral-melt reactions that may have involved low degree ion exchange between the garnet crystals and the biotite reaction rims. Stevens et al (2007), documented that at low pressures, components such as Fe, Ca, Mg (Al), that are released during breakdown of peritectic garnet will be taken up by stable phases that incorporate them. In this case, the Ca content released during dissolution of garnet was taken up by plagioclase. The plagioclase in the 804 ºC experiment has the highest An content compared to plagioclase crystals that precipitated in the lower temperature experiments. This is in agreement with phase equilibrium modelling, which predicts that in the investigated P-T range, Ca-rich plagioclase is stable at highest investigated temperature. The Fe, Mg and Al components of the “peritectic” garnet manifest as biotite, cordierite and hercynite.

The rimming of garnet crystals by biotite reaction rims seen in this study’s run products has been observed to be a characteristic textural feature of rare garnet crystals in high-level S-type granite rocks (see Clemens and Wall, 1984; Maas et al., 1997; Villaros et al, 2009). In this regard, the experimental outcomes relate well with characteristics of natural S-type granitic rocks. The enclosure of garnet by biotite is interpreted to display disequilibrium between the garnet crystals and the bulk rock.

8.2.2 Plagioclase

Plagioclase is present and stable under all investigated P-T conditions as predicted by phase-equilibrium modelling. However, the compositions and textures of plagioclase crystals in the run products do not resemble those of the originally “entrained” peritectic plagioclase in starting composition. During experimental runs, compositions of the plagioclase crystals appear to have attained reasonable equilibrium with the surrounding magma across all investigated P-T conditions. Equilibration between the entrained plagioclase and the magma is proposed to occur either by diffusive transport of components between melt and crystals (Tsuchiyama and Takahashi, 1983) or through re-crystallization of new equilibrium crystals facilitated by a rapid dissolution-precipitation mechanism (Villaros et al., 2007; Zarrebini, 2016). During diffusion-controlled equilibration, diffusion profiles are expected to occur within crystals and intracrystalline diffusion would be the rate limiting process (Tsuchiyama and Takahashi, 1983; Acosta-Vigil et al., 2006). However, in cases where equilibration is facilitated by the dissolution-precipitation process, the slowest process between the rate of dissolution, the rate of diffusion of the slowest components in the melt and the rate of crystallization (Acosta-Vigil et al., 2006) determines the equilibration rate.

A number of observed features in the various experimental run products suggest that the original plagioclase crystals in the starting material have undergone significant compositional and textural modification. Such features include changes in crystals morphology e.g. plagioclase crystals in the run products are made up of randomly orientated small crystal clusters and they contain melt and in some cases ilmenite inclusions. The crystals in the starting material had euhedral shapes with a diameter of 100 to 200 µm. The clustered nature of the experimental plagioclase crystals indicates that during experimental runs a two-part process modified the peritectic crystals. The first part involves a mineral-melt reaction where the melt dissolves plagioclase crystals at the reaction interface liberating components such as Si, Al, Ca and Na. The resultant interfacial melts become saturated in these elements. The high silica content of the melts combined with the liberated components from the plagioclase

permits re-precipitation of new plagioclase crystals with compositions and textures that are well equilibrated with the surrounding magmatic conditions. Although the various nucleated plagioclase crystals are scattered across the run products, their compositions are similar (in each run product) and they are compositionally unzoned. The equilibration process between melt and plagioclase in this study is proposed to have been facilitated by a rapid coupled dissolution-precipitation mechanism. Figure 25 below provides an illustration of the precipitation-dissolution mechanism that re-equilibrated compositions of plagioclase.

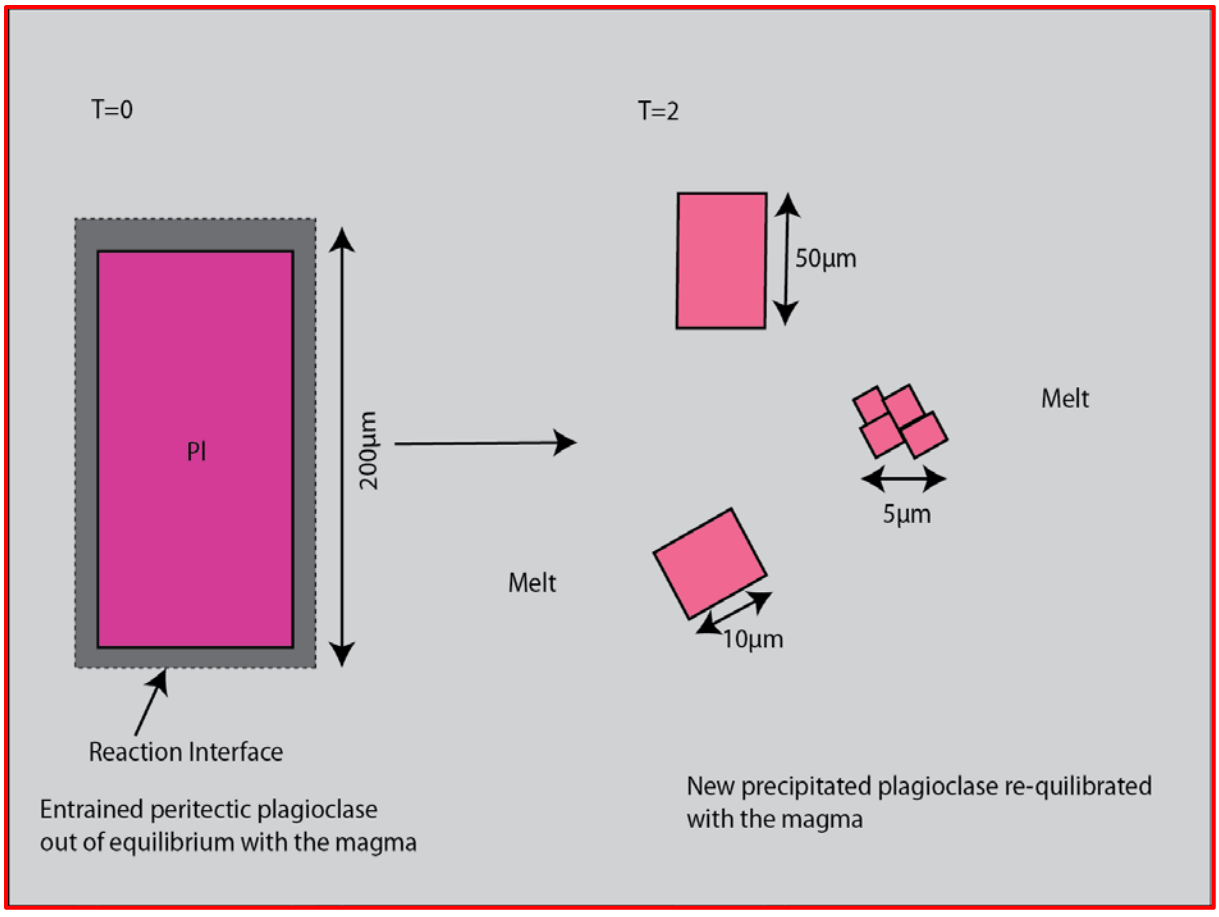

Figure 25: An illustration of the plagioclase precipitation-dissolution mechanism.

8.2.3 Ilmenite

Similar to the plagioclase crystals added in the starting material, the ilmenite in the starting material is predicted to be stable but out of compositional equilibrium with the surrounding melt under investigated P-T conditions. During the course of the experiments, compositions and textures of the crystals in the starting material were modified by a coupled dissolution-precipitation mechanism. The dissolution-precipitation process allowed crystallization of new ilmenite crystals that are compositionally and texturally better equilibrated with the surrounding magmatic conditions (see Fig. 26 below). This equilibration process is efficient and rapid enough to have run to completion within or in less than 20 days. The new ilmenite crystals are significantly smaller compared with the ilmenite crystals in the starting material. Furthermore, these small rounded ilmenite crystals are highly dispersed in all run products. Irrespective of the fact that the ilmenite crystals are far apart, they retained similar homogeneous compositions across all investigated P-T conditions.

The low-Ti and Fe content of the experimental melts confirm that the ilmenite crystals in the starting material did not “disappear” from the system by dissolving into the melt portion of the magma. Consequently, during experimental runs the peritectic ilmenite crystals lost their peritectic character and adopted a “magmatic” one due to the equilibration process between the melt and the entrained crystals at low P-T magmatic conditions.

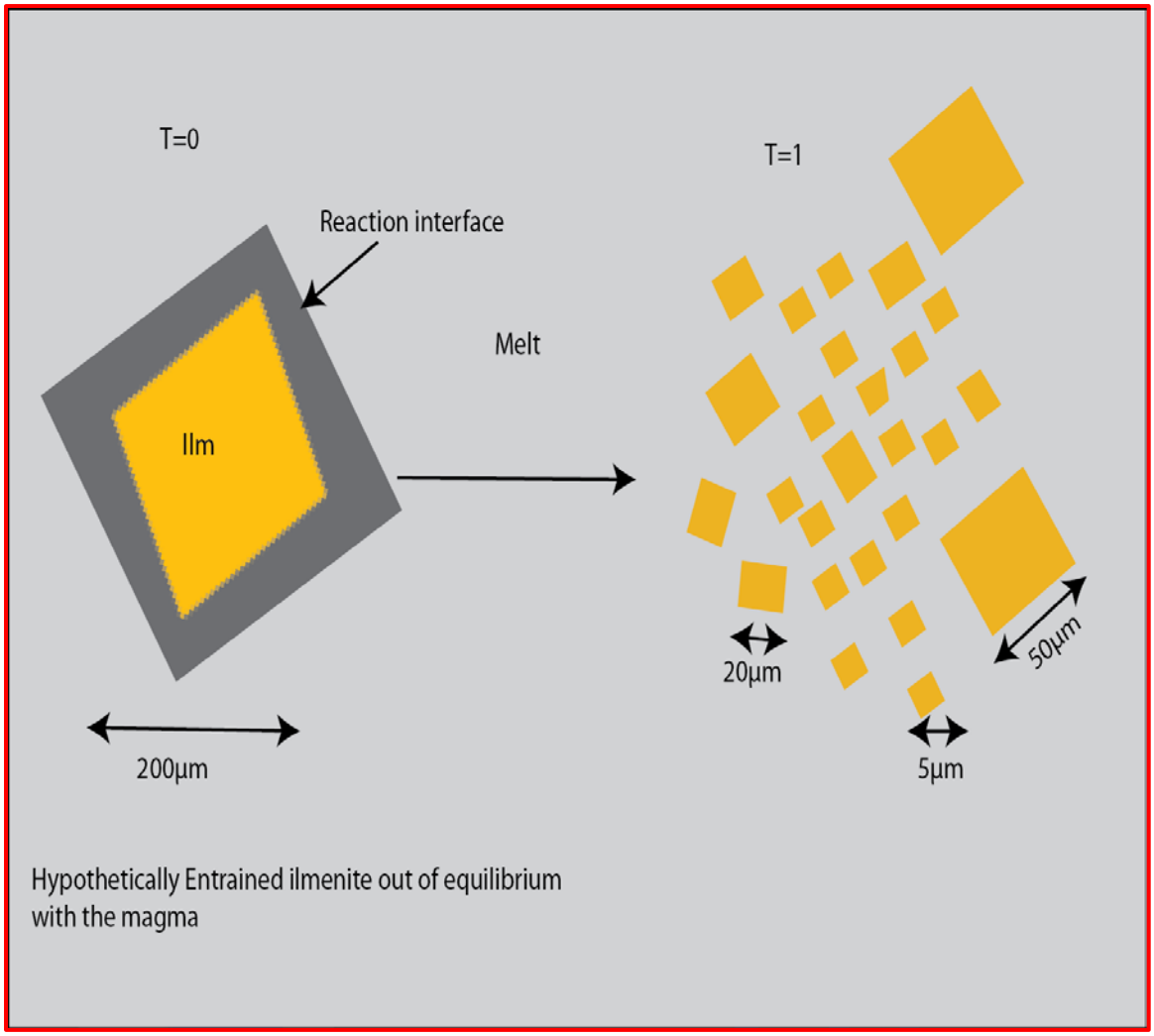

Figure 26: An illustration of the ilmenite dissolution-precipitation mechanism.

8.3 Equilibration rates

Mineral-Melt reaction rates

Rates of equilibration of garnet crystals in granitic systems are known to be very slow. It has been documented that diffusion rates of major cations (Mg, Ca, Fe and Mn) within garnet crystals are generally very slow (Carlson, 2006; Vielzeuf et al., 2007). The time required to reset compositions of garnet by self-diffusion is determined by the time required to re-equilibrate the slowest diffusing cation i.e. Ca (Villaros et al., 2009a). Experimental studies of Vielzeuf et al. (2007) have demonstrated that it takes a minimum of 36 days to re-equilibrate the Ca, Mg and Fe components of a 1 µm wide garnet rim, by self-diffusion over a temperature range of 1050 to 1250 ºC at 1.3 GPa pressure.

The outcomes of this research have demonstrated that the rate of reaction at the mineral-melt interface may be temperature dependent. This is evident by the observed increase of the proportions of refractory garnet cores with decreasing temperature. The garnet-melt reaction at 804 ºC although it appears to have been faster than in the lower temperature experiments, still failed to eradicate all the “entrained” garnet crystals. However, in this run product, the refractory garnet makes up about 0.5 wt% of the bulk-rock assemblage. The seemingly fast dissolution rate of garnet observed in the run product at 804 ºC is compatible with findings of Skinner (1956), who determined that, at 800 ºC dissolution of a garnet crystal with a 1 cm diameter would occur within the time scale of days. In the run products at 754 and 743 ºC, the metastable garnet proportions of the remnant garnet crystals are estimated to be 0.99 and 1.32 wt% respectively. These estimates are based on visual examination of SEM images and mass-balance calculations using the Solver function in excel.

The garnet crystals were partially digested by the melt through reactions at the garnet- melt interface. The garnet crystals reacted with the melt via an incongruent “dissolution-precipitation” mechanism. In this case peripheral regions of the garnet crystals reacted with the melt via dissolution reaction. Because the garnet is unstable at the investigated P-T

conditions, post its dissolution it was replaced by biotite (and hercynite) and cordierite crystallized from the melt to take-up the Al-content released by dissolution of garnet. The above-mentioned minerals took up the Fe and Mg (and Al) components of the garnet. This is attested by the fact that the Fe and Mg contents of the experimental melts remained low and the Al content of the melts remained relatively unchanged.

Dissolution-precipitation mechanism

Pichavant et al. (2007) showed that equilibration scales in magmatic systems are controlled by the kinetics of individual reaction mechanisms. The rates of equilibration processes are dependent on P-T conditions of the system (Acosta-Vigil et al., 2006; Villaros et al, 2009; Agostini et al., 2012) and H_2O contents of the melts (Lofgren, 1974a; Fenn, 1973). There is a general lack of dissolution and equilibration data for plagioclase in granitic systems at low P-T conditions similar to those of this study.

Previous experimental studies by Piwinskii (1967, 1968) utilizing range of granitic compositions determined that the rates of equilibration in granitic systems are very slow at temperatures just above the solidus, details in section 4.2 above. Noteworthy, the plagioclase crystals used by Piwinskii were zoned. Piwinskii (1967) utilized a natural quartz-monzonite with 17.8 wt% H_2O content as starting material for experiments at 690 ºC / 2 kbar and a granodiorite with 15.6 wt% H_2O for experiment at 800 ºC / 2 kbar. The results showed that the run at 800 ºC had 60 % melt whilst the one at 690ºC only had 15 % melt volume. Furthermore, the plagioclase in the 800 ºC run appeared to have attained equilibrium after 11 days and it was no longer zoned, but in the 690 ºC run the crystals still possessed prominent zoning, thus they failed to equilibrate with the granitic melt after 33-days experimental run time (Piwinskii, 1967).

Piwinskii (1968) conducted equilibration tests using natural granodioritic, granitic and tonalitic rock compositions; each had 15 wt% H_2O, over a temperature range of 760 – 690 ºC and a 2

kbar pressure. The experimental duration ranged from 21 to 150 days. In all the experiments held at temperatures ≤ 725 ºC, compositions of the plagioclase crystals did not change much even with increased run duration. However, Piwinskii (1968) noted that after 150 days although composition wise the crystals did not show much change, the zoning became less prominent. The author also noted that in runs held at ≥ 760 ºC, plagioclase crystals required shorter experimental durations compared to experiments held at lower temperatures to equilibrate with the melt. Piwinskii (1968) concluded that experimental runs at 760 ºC or more requires durations of approximately 2 months to reach equilibrium. However, to reach equilibrium between melt and plagioclase crystals in runs below 760 ºC requires experimental run times of 4 to 6 months. Noteworthy, this period may be a lengthy experimental durations, however it is quite rapid in geological times.

Experimental studies of Zarrebini (2016) also detailed in section 4.2 above, used a synthetic I-type granodioritic composition as starting material with 1.60 wt% H_2O and experiments were carried-out at temperatures of 736 – 723 ºC and at pressures of 1.90 and 1.40 kbar over a 10-day period. The experiments of Zarrebini demonstrated that equilibrium was attained between plagioclase (0.04 µm) and granitic melt in 10 days i.e. composition and texture of post experimental plagioclase crystals no longer resembled that of original crystals in the starting material and all crystals were unzoned. The experimental runs produced melt fractions ranging between 32.7 to 63.5 %. Because Zarrebini (2016) ran experiments at constant 10-day duration, ascertaining the dissolution time and/ or dissolution rate was not possible. Consequently, Zarrebini (2016) adopted the minimum dissolution rate determined for plagioclase in basaltic melts at 1 bar and 1 kbar, T > 1000 ºC proposed by (Agostini, et al., 2013; Donaldson, 1985) as an appropriate dissolution rate for plagioclase in an I-type granodioritic magma. Thereafter, Zarrebini (2016) estimated that at a constant rate of $1x10^{-7}$ cm/s a plagioclase crystal with 0.04 cm diameter would take 4.62 days to dissolve in an I-type melt and 1 cm crystal would dissolve in the melt after 116 days.

The results of the present study demonstrate that, in each of the experimental runs, the plagioclase crystals are compositionally and texturally different from the original plagioclase crystal added in the starting material. The compositional and textural modifications were achieved in 20 days, which is the duration for each experimental run. It is therefore proposed that equilibration between the melt and the crystals was attained in or under 20 days. In this case it is not easy to determine the rate of dissolution, because the experiments where all held at a constant duration. The exact minimum time needed to dissolve plagioclase crystals with size range of 100 – 200 µm cannot be determined. However, there is certainty that the original plagioclase crystals added in the starting material dissolved in the melt completely, but it was never all in solution as it precipitated simultaneously with dissolution to form new crystal that are equilibrated with the melt.

The results of this study for the experiment held at 804 ºC are in agreement with experimental results of Piwinskii (1967) for the experiment held at 800 ºC. In both studies the plagioclase are inferred to have equilibrated with the melts in a similar period. However, for runs held at temperatures below 804 ºC, the results of this study shows different observations from those of Piwinskii (1967, 1968), but they are in agreement with results of Zarrebini (2016). The experimental technique followed in this study is similar to that used by Zarrebini (2016), hence the similarity in the experimental outcomes. The discrepancy in equilibration times between this study and study by Piwinskii (1967; 1968) is probably due to various reasons. (i) Differences in melt volumes produced in the experiments. In the present experimental study, the melt volumes produced are on average higher those produced in studies of Piwinskii (1967; 1968) at similar P-T. For instance, the average melt fraction produced in this study at T < 760 ºC is 53.20 wt% and the average of Zarrebini (2016) is 47.08 wt% whilst Piwinskii (1967; 1968) recorded average melt volumes of 15.00 and 33.33 wt % , respectively. (ii) The plagioclase crystals used by Piwinskii were zoned whilst those used in this study were unzoned. (iii) Additionally, in this study a synthetic bulk starting material was used whilst in investigations by Piwinskii natural rock powders were used as starting materials for

experiments. It is possible that the use of “synthetic gel” in this study lead to faster reaction rates compared to the studies by Piwinskii.

It is proposed that the equilibration process was facilitated by a fast-coupled dissolution-precipitation mechanism. In 20 days, the plagioclase or ilmenite crystals were able to dissolve and re-precipitate new phases that are in equilibrium with the melt under investigated magmatic P-T conditions. This process has proven to be a very efficient process through which out-of-equilibrium plagioclase crystals are brought into equilibrium with the melt. Although the dissolution rate cannot be quantified in this study, the results do reveal that dissolution of plagioclase crystals in granitic magmas at P-T conditions close to the solidus is very fast. The fact that new plagioclase crystals also formed rapidly or rather simultaneously with dissolution shows that crystal growth rates are also quite fast. This is evident by the growth of 50 – 100 µm (0.005 – 0.01 cm) plagioclase crystals in 20 days and the crystallization of 30 – 200 µm (0.003 – 0.02 cm) in 10 days (Zarrebini, 2016). The findings of this study and that of Zarrebini (2016) challenges that assumption that the presence of large crystals e.g. K-feldspar in high-level granite bodies relates to slow growth over long periods of time (Luth, 1976).

Crystal growth rates in magmatic systems have been determined to be fast and are proposed to be on the order of 10^{-10} to 10^{-11} cm/s (Hawkesworth et al., 2000). Similarly, Lofgren (1974a) performed crystallization experiments in the system $NaAlSi_3O_8$-$CaAl_2Si_3O_8$-H_2O at a pressure range of 4 – 6 kbar. The latter author estimated that average growth rates of plagioclase may vary from 0.3 - 0.6 µ/h~ 1µ/h = $2.8x10^{-10}$ cm/s. Swanson (1974,1977) studied nucleation and growth of crystals using synthetic granodiorite and granite compositions in the system $KAlSi_3O_8$-$NaAlSi_3O_8$-$CaAlSi_3O_8$ –SiO_2 under H_2O-saturated and under-saturated conditions. Crystal growth rates of plagioclase, K-feldspar and quartz were found by Swanson (1977) to vary from $3x10^{-6}$ cm/s (3 mm/day) to $1x10^{-9}$ cm/s (1 mm/ yr) depending on the H_2O content of the system and the degree of undercooling. Swanson (1974) determined that growth rates ranged from $1.4x10^{-6}$ to $1x10^{-10}$ cm/s for plagioclase and maximum of $2x10^{-7}$ cm/s for potassium feldspar and quartz. The abovementioned author noted that the highest growth

rates were observed in experiments with H_2O under-saturated composition and smaller undercooling. Similarly, mineral phases produced by mineral-melt reactions and the dissolution-precipitation mechanism within this study displayed rapid growth rates. For instance, in 20 days, cordierite and biotite crystals grew rapidly following the incongruent dissolution of garnet. Likewise, plagioclase and ilmenite crystals dissolved and re-precipitated compositions and textures well equilibrated with the surrounding magmatic conditions.

9 Implications for S-type granite petrogenesis

S-type granites generally display a wide major and trace element compositional range. Analysis of experimental melt compositions by Stevens et al. (2007) have indicated that only the compositions of leucogranitic S-type rocks overlap with those of pure melts. The above-mentioned authors suggested that the average to mafic end-members represents mixtures of melt and crystals. Stevens et al. (2007) reasoned that compositional trends displayed by S-type granites (e.g. increasing Ca with mafic content and the very strong positive correlation between Ti and mafic content) may be explained by entrainment a peritectic mineral assemblage into the melt. However, a complication arises as these peritectic phases are usually not seen in high-level granites. Pseudosection diagrams presented in this study have demonstrated that monzogranitic S-type magma evacuates its source region as a mixture of melt and a peritectic mineral assemblage. Phase-equilibrium modelling shows that constituents of the peritectic mineral assemblage and compositions of individual minerals undergo continuous re-equilibration at different P-T conditions along a hypothetical adiabatic ascent path. Consequently, when the magma reaches shallow crustal levels, the crystal fraction of the magma will no longer compositionally resemble the high-P-T peritectic assemblage that segregated from the source region. Additionally, the pseudosection demonstrates that along the hypothetical cooling path (804 - 743 ºC, P ~ 1 kbar) the magma still has a significant volume of melt, i.e. the magma will still have the propensity to bring out-of-equilibrium crystals into equilibrium, although it is at a late stage in magma evolution.

The experiments conducted in this study corroborate the outcomes of phase-equilibrium modelling. The hypothetically entrained peritectic mineral assemblage effectively equilibrated with the magma at P-T conditions representative of emplacement levels within the upper crust. The experiments show that apart from the apparent slower reactions between the melt and garnet, the rates of equilibration of 100 - 200 µm minerals with monzogranitic S-type magma are incredibly fast. It is likely that fast magma ascent rates through fracture propagation as detailed by Clemens and Mawer (1992) would not impede the efficiency of the equilibration

process, because the rates of equilibration have been demonstrated to be sufficiently fast to occur within the required time frame for the magma to ascend. The experiments show that the magma uses a coupled dissolution-precipitation mechanism to bring into equilibrium crystals that are stable phases but out of compositional equilibrium. Crystals that are unstable in the magma undergo modification by reacting with the melt to precipitate new phases stable under magmatic P-T conditions. The equilibration process is efficient; the plagioclase and ilmenite crystals added in the starting material were replaced by new magmatic plagioclase and ilmenite. The garnet crystals were either partially replaced by biotite and biotite-hercynite reaction rims or fully replaced cordierite-biotite pseudomorphs. The assemblages that crystallized in the experimental run products have no resemblance of the high P-T phases that were added in the starting material. These results imply that garnet crystals armored by biotite or cordierite rims in high-level S-type granitic rocks were out of equilibrium with the magma upon emplacement and crystallization.

The experimental P-T conditions of this study do not allow direct comparison with natural granitic rock systems. However, the results of this study have demonstrated that a good equilibration effectively masks a very complex history of granite bodies i.e. whatever crystallizes along the ascent and cooling paths re-equilibrates. This creates the impression that the mineralogy that is seen on granite outcrops reflects a long history of magma evolution. The magmatic nature of the products of garnet breakdown i.e. biotite and cordierite create an impression of high Fe, Mg solubility in the melt. Therefore, care must be taken when using mineral compositions and textures in arguments for and/or against any model of granite petrogenesis, specifically those founded on the idea that the chemistry of crystalline granite rocks is shaped by magmas that exist as mixtures of melt and crystals. If pseudomorphs of high-P-T minerals are not present in granitic rocks, either on a hand specimen or outcrop scale, then the observed mineral assemblages and textures probably formed late in the magmatic evolution of the granites. For example the dominant macroscopic feature on outcrops of S-type granites from the Peninsula pluton, one of the igneous bodies of the CGS,

is textures created by K-feldspar megacrysts e.g. flow accumulations of K-feldspar Farina et al. (2012), see Fig. 27. Publications by (Clemens and Wall, 1981; Vernon and Paterson, 2008) documented that K-feldspar phenocrysts form very late in the crystallization sequence of granitic rocks. Similarly, the experimental and phase-equilibrium outcomes of this study have demonstrated that magmatic K-feldspar crystallizes very late at P-T conditions close to the granite solidus. This assumption is supported by the fact that K-feldspar crystallized only in the 743 ºC run, which is close to the predicted solidus (733 ºC/ 1 kbar). Furthermore, the predicted and experimental compositions of K-feldspar are similar, but they differ significantly from the composition of the K-feldspar stable in the source region. The composition of the High-P-T K-feldspar is $An_{1.96}Ab_{25.23}Or_{72.81}$,the predicted and experimental compositions are provided in table 12. Therefore, if the magma from which the S-type granites of the Peninsula pluton really did intrude between 1 and 2 kbar, then everything seen on the outcrop occurred almost at the solidus, see Fig. 28. Consequently, the complex history of the rocks, displayed by the blue shaded region in Fig. 28 would not be evident in the crystalline rocks.

Additionally, the outcomes of this study suggest that the crystal fraction of granite magmas regardless of origin i.e. restitic, early magmatic or peritectic phases will most likely suffer the same fate of losing their “original” textural and compositional characteristics along the magma ascent path even late at P-T conditions near the solidus. Due to continuous re-equilibration of the crystal load along the ascent path, when granitic magmas reach their final emplacement levels crystals of any origin would display similar magmatic characteristics.

Figure 27: Photographs showing some textures in S-type granite rocks of the Peninsula pluton.

A) Demonstrates a vertical section through a small steeply orientated pipeformed in a finer-grained and megacrysts depleted zone of the pluton.The image is taken from Farina et al. (2012). B) Displays layering defined by biotite enrichment and k-feldspar megacrysts showing preferred orientation parallel to the layering, the image is taken from Ramphaka (2013).

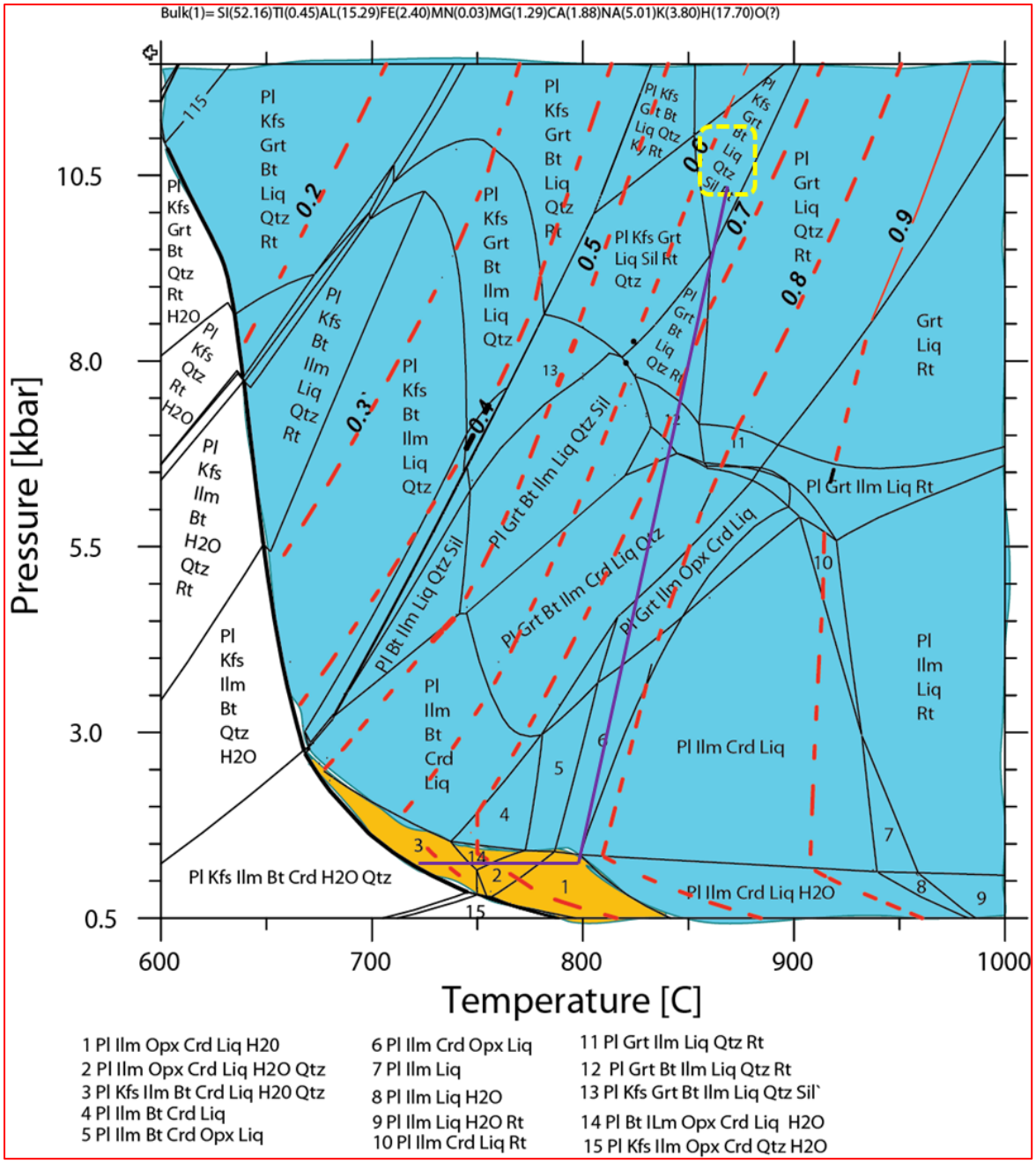

Figure 28: Pseudosection diagram illustrating hypothetical magma intrusion level of S-type magma (yellow shaded region) and the subsequent "hidden" history of the bulk rock (blue shaded region).

The hypothetical intrusion region is demonstrated by the yellow shaded area and the "hidden history" of the rock is shown by the blue shaded region. The yellow dashed square indicates the magma source region; the purple line demonstrates a hypothetical adiabatic ascent and cooling path.

10 Conclusions

The fates of a hypothetical, entrained peritectic mineral assemblage in a monzogranitic S-type magma composition, emplaced within the upper crust, were determined by means of an experimental investigation. The experimental results were compared with outcomes predicted by phase-equilibrium modelling. The findings demonstrate that experimental mineral assemblages, phase proportions, and mineral compositions are similar to those predicted by phase-equilibrium modelling. However, the presence of metastable phases in the experimental run products generates errors in the modelling. The experimental results have demonstrated that the “fate” of entrained peritectic minerals that are out of equilibrium with an S-type monzogranitic magma, emplaced at a pressure of 1 kbar and temperature range of 804 - 743 ºC is controlled by the ability of the magma to either fully or partially bring out of equilibrium crystals into equilibrium. The results have shown that a coupled dissolution-precipitation mechanism and mineral-melt reactions facilitate equilibration. Apart from the apparent slower reaction between garnet and melt, the equilibration process is rapid.

The proposed equilibration process between granitic magmas and entrained crystals explain the apparent scarcity of peritectic, restitic and early magmatic phases in high-level granitic rocks. In addition, these findings demonstrate that the growth of large crystals or development of coarse-grained textures in granitic rocks does not require long crystallization times, slow cooling rates or crystallization at any great depth. This research has also revealed that it is incorrect to assume that what is seen in high-level granitic rocks reveal significant details about the histories of those rocks. Unless textures such as pseudomorphs or reaction textures are visible, everything seen in the outcrops relates to late processes. In conclusion, this study assumed instantaneous magma ascent from deep crustal levels to emplacement in the shallow crust. However, ideally, a natural magma would pass through numerous P-T points before reaching its emplacement level. It is possible that had the bulk composition used in this study been exposed to various high-P-T points along an ascent path, the garnet would have reacted completely. Therefore, it is proposed that magmas crystallizing at similar P-T

conditions as those investigated in this study, if they are recording minerals such as garnet the magmas must have ascended and cooled rapidly.

11 Recommendations

For future research looking into the fates of peritectic mineral assemblage in granitic systems, I suggest the following to be taken into consideration:

- Experiments must be carried out at various P-T conditions along the magma ascent path, ranging from near source conditions to emplacement levels. This will give a full scope of the processes that facilitate equilibration of the entrained crystals in a cooling magma.
- The type of experimental equipment used restricted the investigated P-T range. To counteract such limitations, I suggest that a variety of experimental apparatus be used.
- To ascertain detailed dissolution or equilibration rates, it would be a good idea to vary experimental run duration. Keep the P-T conditions constant and size of the crystals uniform.
- It may also be a good idea to use more than one phase equilibrium modelling package.

12 References

Acosta-Vigil, A., London, D., Morgan, VI., G.B., 2006a. Experimental partial melting of a leucogranite at 200 MPa H_2O and 690–800 °C: compositional variability of melts during the onset of H_2O-saturated crustal anatexis. Contributions to Mineralogy and Petrology, 151, 539-557.

Altherr, R., Siebel, W., 2002. I-type plutonism in a continental back-arc setting: Miocene granitoids and monzonites from the central Aegean Sea, Greece. Contributions to Mineralogy and Petrology, 143, 397-415.doi:10.1007/s00410-002-0352-y

Anderson, G.M., 2002. Stable and metastable equilibrium: The third constraint. The Geochemical Society, Special Publications, 7, 181-187.

Ayres, M., Harris, N., 1997. REE fractionation and Nd-isotope disequilibrium during crustal anatexis: constraints from Himalayan leucogranites. Chemical Geology, 139, 249-269.

Bateman, R., 1984. On the role of diapirism in the segregation, ascent and final emplacement of granitoid magmas. Tectonophysics, 110, 211–231.

Bea, F., 1996. Controls on the trace element composition of crustal melts. Transactions of the Royal Society of Edinburgh, 87, 33-41.

Beard, J.S., Ragland, P.C., Crawford, M.L., 2005. Reactive bulk assimilation: a model for crust–mantle mixing in silicic magmas. Geology, 33 (8), 681. doi:10.1130/g21470.1.

Brown, G.C., Fyfe, W.S., 1970. The production of granite melts during ultra-metamorphism. Contributions Mineralogy and Petrology, 240, 310-318.

Brown, M., Pressley, R.A., 1999. Crustal melting in nature: Prosecuting source processes. Physics and Chemistry of the Earth, 24, 305–316.

Cann, J.R., 1970. Upward movement of granitic magmas.Geological Magazine, 43, 335-340.

Cantegrel, J.M., Didier, J., Gourguad, A., 1984. Magma mixing: origin of intermediate rock and “enclaves” from volcanism to plutonism. Physics of the Earth and Planetary Interiors, 35, 63-76.

Carlson, W., 2006. Rates of Fe, Mg, Mn, and Ca diffusion in garnet. American Mineralogist, 91(1), 1-11.

Castro, A., Patino Douce, A.E., Corretge, L.G., de la Rosa, J.D., El-Biad, M., El-Hmidi, H., 1999. Origin of peraluminous granites and granodiorites, Iberian massif, Spain: an experimental test of granite petrogenesis. Contributions to Mineralogy and Petrology,135, 255-276.

Cesare, B., Acosta-vigil, A., Ferrero, S., Bartoli, O., 2011. Melt inclusions in migmatites and granulites. In: The Science of Microstructure–Part II, Journal of the Virtual Explorer (eds Forster, M.A. & Fitz Gerald, J.D.). The Virtual Explorer Pty Ltd, Canberra, Electronic Edition, ISSN 1441-8142. 38, paper 2.

Chappell, B.W., White, A.J.R., 1974. Two contrasting granite types. Pacific Geology, 8, 173–174.

Chappell, B.W., White, A.J.R., Wyborn,D., 1987.The importance of residual source material (restite) in granite petrogenesis.Journal of Petrology, 28, 1111-1138.

Chappell, B. W., Stephens, W. E., 1988. Origin of infracrustal (I-type) granite magmas. Transactions of the Royal Society of Edinburgh:Earth Sciences, 79, 71–86.

Chappell, B.W., 1996. Compositional variation within granite suites of the Lachlan Fold Belt: Its causes and implications for the physical state of granite magma. Transactions of the Royal Society of Edinburgh, 87, 159-170.

Chappell, B.W., White, A.J.R., Williams, I.S., Wyborn, D., Wyborn, L.A.I., 2000. Lachlan Fold Belt granites revised: high- and low-temperature granites and their implications. Australian Journal of Earth Science, 47, 123-138.

Chappell, B.W., White, A.R.J., 2001.Two contrasting granite types: 25 years later.Australian Journal of Earth Sciences,48, 489-499.

Chappell, B.W., 2004.Towards a unified model for granite genesis. Earth Sciences, 95,1-10.

Clarke, D.B., 2007. Assimilation of xenocrysts in granitic magmas: principles, processes, proxies and problems. Canadian Mineralogist, 45, 5-30.

Clemens, J.D., Wall, V. J., 1981. Crystallization and origin of some peraluminous (S-type) granitic magmas, Canadian Minealogist, 19, 111–131.

Clemens, J.D., 1981. The origin and evolution of some peraluminous acid magmas (experimental, geochemical and petrological investigations). Ph.D. Thesis, Monash University, Clayton, Vic. (unpublished).

Clemens, J.D., Wall, V.J., 1984. Origin and evolution of a peraluminous silicic ignimbrite suite: the Violet Town Volcanics. Contributions to Mineralogy and Petrology, 88: 354-371.

Clemens, J. D., Vielzeuf, D., 1987. Constraints on melting andmagma production in the crust, Earth and Planetary Science Letters, 86, 287–306.

Clemens, J.D., 1990 The granulite-granite connexion. In: Vielzeuf, D, Vidal Ph (eds) Granulites and crustal evolution. Kluwer Academic Publishers, Dordrecht, 25-36.

Clemens, J. D., Mawer, C. K., 1992. Granitic magma transport by fracture propagation. Tectonophysics, 204, 339-360.

Clemens, J.D., Petford, N., ,Mawer, C.K., 1997. Ascent mechanisms of granitic magmas: causes and consequences, in Deformation-enhanced fluid transport in the Earth's crust and mantle.(ed. M. Holness), Chapman & Hall, London, 144–171.

Clemens, J.D., Droop, G.T.R., 1998. Fluids, P–T paths and the fates of anatectic melts in the Earth's crust.Lithos, 44, 21-36.

Clemens, J.D., Watkins, J.M., 2001. The fluid regime of high-temperature metamorphism during granitoid magma genesis. Contributions to Mineralogy and Petrology, 140, 600-606.

Clemens, J.D., 2003. S-type granitic magmas—petrogenetic issues, models and evidence. Earth-Science Reviews, 61(1-2), 1-18.

Clemens, J.D., Darbyshire, D.P.F., Flinders, J., 2009. Sources of post-orogenic calcalkaline magmas: the Arrochar and Garabal Hill–Glen Fyne complexes, Scotland. Lithos, 112 (3-4), 524–542. doi:10.1016/j.lithos.2009.03.026.

Clemens, J.D., Helps, P.A., Stevens, G., 2010. Chemical structure in granitic magmas — a signal from the source?. Earth and Environmental Science Transactions of the Royal Society of Edinburgh, 100 (1-2), 159–172. doi:10.1017/s1755691009016053.

Clemens, J.D., Stevens, G., Farina, F., 2011.The enigmatic sources of I-type granite: The peritectic connexion. Lithos,126, 174-181.

Clemens, J.D., 2012. Granitic magmatism from source to emplacement : a personal view. Applied Earth Sciences, 121 (3), 107-136.

Clemens, J.D., Stevens, G., 2012.What controls chemical variation in granitic magmas? . Lithos, 134, 317-329.

Clemens, J.D., Stevens, G., 2016. Melt segregation and magma interactions during crustal melting:Breaking out of the matrix. Earth Science Reviews, 160, 333-349.

Coleman, D.S., Gray, W., Glazner, A.F., 2004. Rethinking the emplacement and evolution of zoned plutons: geochronologic evidence for incremental assembly of the Tuolumne Intrusive Suite, California. Geology, 32, 433-436.

Collins, W.J., 1996. Lachlan Fold Belt granitoids: Products of three-component mixing. Transactions of the Royal Society of Edinburgh, 87, 171–181.

Connolly, J. A. D., Kerrick, D. M., 1987. An algorithm and computer program for calculating composition phase diagrams. Calphad, 11, 1-55.

Couch S., 2003. Experimental investigation of crystallization kinetics in a haplogranitesystem. American Mineralogist, 88,1471-1485.

de Capitani, C., Petrakakis, K., 2010. The computation of equilibrium assemblage diagrams with Theriak/Domino software. American Mineralogist, 95(7), 1006-1016.

Deer, W.A., Howie, R.A., Zussman, J., 1992. An introduction to the rock-forming minerals. Harlow, Pearson Prentice Hall.

De Paolo, D. J., 1981. Trace element and isotopes effects of combined wallrock assimilation and fractional crystallization. Earth and Planetary Science Letters, 53,189-202.

Didier, J., 1984. The problem of enclaves in granitic rocks, a review of recent ideas on their origin. in Geology of Granites and their Metallogenic Relations. K. T. Xu, G (Ed.). Beijing, Science Press, 137-144.

Dini, A., Innocenti, F., Rocchi, S., Tonarini, S., Westerman, D.S., 2002. The magmatic evolution of the laccolith–pluton–dyke complex of the Elba Island, Italy. Geological Magazine, 139, 257–279.

Donaldson, C.,1 985. The Rates of Dissolution of Olivine, Plagioclase, and Quartz in a Basalt Melt. Mineralogical Magazine, 49(354), 683-693.

Downes, H., Shaw, A., Williamson, B.J., Thirlwall, M.F., 1997. Sr, Nd a136(1997) 99-122 Hercynian granodiorites and monzogranites, Massif Central, France. Chemical Geology, 136 , 99-122.

Downes, H., Duthou, J.L., 1988. Isotopic and trace element arguments for the lower crustal origin of Hercynian granitoids and pre-Hercynian orthogneisses, Massif Central (France). Chemical Geology, 68, 29--308.

England, R. W., 1990. The identification of granitic diapirs. Journal of the Geological Society. London, 147, 931–933.

Farina, F., Stevens, G., 2011. Source controlled $^{87}Sr/^{86}Sr$ isotope variability in granitic magmas: the inevitable consequence of mineral-scale isotopic disequilibrium in the protolith. Lithos, 122, 189-200.

Ferrero, S., Bartoli, O., Cesare, B., Salvioli-Mariani, E., Acosta-vigil, A., Cavallo, A., Groppo, C., Battiston, S., 2012. Microstructures of melt inclusions in anatectic metasedimentary rocks. Journal of Metamorphic Geology, 30, 303-322.

Glazner, A., Bartley, J., Coleman, D., Gray, W. Taylor, R., 2004. Are plutons assembled over millions of years by amalgamation from small magma chambers?. GSA Today, 14 (4), 4 -11.

Glazner, A.F., 2007. Thermal limitations on incorporation of wall rock into magma.Geology, 35 (4), 319. doi:10.1130/g23134a.1.

Garcia-Arias, M., Stevens, G., 2016. Phase-equilibrium modelling of granite magma petrogenesis: A. An evaluation of the magma compositions produced by crystal entrainment in the source, Lithos (2016), http://dx.doi.org/10.1016/j.lithos.2016.09.028.

Gray, C.M., 1984. An isotopic mixing model for the origin of granitic rocks in southeastern Australia. Earth and Planetary Science Letters, 70, 47-60.

Green, T.H., 1976. Experimental generation of cordierite or garnet bearing granitic liquids from a pelitic composition. Geology, 4, 85-88. Doi: 10.1130/0091-7613(1976)4<85:EGOCGG>2.0.CO;2.

Griffin, T.J., White, A.J.R., Chappell, B.W., 1978. The Moruya batholith and geochemical contrasts between the Moruya and Jindabyne suites. Geological Society of Australia Journal, 25, 235-247.

Hamilton, D.L., Henderson, C.M.B., 1968. The preparation of silicate compositions by a gelling method. Mineralogical Magazine, 36, 832-838.

Hawkesworth, C.J., Blake, S., Evans, P., Hughes, R., Macdonald, R., Thomas, L.E., Turner, S., Zellmer,G., 2000. Time scales of on magma chambers—integrating physical, isotopic and geochemical perspectives. Journal of Petrology, 41, 991-1006.

Hine, R., Williams, I.S., Chappell, B.W., White, A.J.R., 1978. Contrasts between I- and S-type granitoids of the Kosciusko Batholith. Journal of the Geological Society of Australia: An

International Geoscience Journal of the Geological Society of Australia, 25 (3-4), 219-234.doi: 10.1080/00167617808729029.

Holland, T.J.B., Powell, R., 1998. An internally consistent thermodynamic data set for phases of petrological interest. Journal of metamorphic Geology, 16, 309-343.

Holland, T.J.B., Powell, R., 2003. Activity composition relations for phases in petrological calculations: an asymmetric multicomponent formulation. Contributions to Mineralogy and Petrology, 145(4), 492-501.

Huppert, H.E., Sparks, R.S.J., Turner, J.S., 1984. Some effects of viscosity on the dynamics of replenished magma chambers. Journal of Geophysical Research, 89, 6857-6877.

Inger, S., Harris, N., 1993. Geochemical constraints on leucogranite magmatism in the Langtang valley, Nepal Himalaya. Journal of Petrology, 34, 345-368.

Johannes, W., 1980. Metastable melting in the granite system Qz-Or-Ab-An-H2O. Contributions to Mineralogy and Petrology, 72, 73-80.

Johnson, T.E., Hudson, N.F.C., Droop, G.T.R.,2001. Partial melting of the Inzie Head gneisses: The role of water and a petrogenetic grid in KFMASH applicable to anatectic pelitic migmatites. Journal of Metamorphic Geology, 19, 99-118. doi: 10.1046/j.0263-4929. 2000.00292.x.

Johnson, T.E., Gibson, R.L., Brown, M., Buick, I.S., Cartwright, I., 2003. Partial melting of metapelitic rocks beneath the Bushveld Complex. South Africa. Journal of Petrology, 44, 789-813.

Kalsbeek, F., Jepsen, H.F., Jones, K.A., 2001. Geochemistry and petrogenesis of S-type granites in the East Greenland Caledonides. Lithos, 57,91-109.

Keay S., Steele, D., Compston W., 1999. Identifying granite sources by SHRIMP UPb zircon geochronology: an application to the Lachlan fold belt. Contributions to Mineral and Petrology, 137, 323-341.

Keay, S., Collins, W.J., McCulloch, M.T., 1997. A three-component Sr-Nd isotopic mixing model for granitoid genesis, Lachlan fold belt, eastern Australia. Geology; 25 (4); 307-310.

Kirkpatrick, R.J., Klein, L., Uhlmann, D.R., Hays, J.F., 1979. Rates and processes of crystal growth in the system anorthite-albite. Journal of Geophysical Research, 84, 3671-3676.

Kretz, R., 1983. Symbols for rock-forming minerals. American Mineralogist, 68, 277-279.

Liu, S., Hua, R., Gao, S., Feng ,C., Huang, Z., Lai, S., Yuan H., Liu X., Coulson, I.M., Feng G., Wanga, T., Qi, Y., 2009. U–Pb zircon, geochemical and Sr–Nd–Hf isotopic constraints on the age and origin of Early Palaeozoic I-type granite from the Tengchong–Baoshan Block, Western Yunnan Province, SW China. Journal of Asian Earth Sciences, 36, 168-182.

Lofgren, G. E.,1974a. An experimental study of plagioclase crystal morphology: isothermal crystallization. American Jurnal of Science., 274, 243-273.

London, D., Morgan VI, G.B., Acosta-Vigil, A., 2012. Experimental simulations of anatexis and assimilation involving metapelite andgranitic melt. Lithos, 153, 292-307.

MaalØe, S., Wyllie, P.J., 1975. Water content of a granite magma deduced from the sequence of crystallization determined experimentally wiyh water-undersaturated conditions. Contibutions to Petrology and Mineralogy, 52, 175-191.

Maas, R., Nicholls, I., Legg, C., 1997. Igneous and Metamorphic Enclaves in the S-type Deddick Granodiorite, Lachlan Fold Belt, SE Australia: Petrographic, Geochemical and Nd-Sr Isotopic Evidence for Crustal Melting and Magma Mixing. Journal of Petrology, 38(7), 815-841.

Maliva, R.G., Siever, R., 1988a. Diagenetic replacement controlled by force of crystallization. Geology, 16, 688-91.

Miller, C.F., Stoddard, E.F., Bradfish, L.J., Dollase, W.A., 1981. Composition of plutonic muscovite: genetic implications. Canadian Mineralogist, 19, 25-34.

Midllemost, E.A.K., 1994. Naming materials in the magma/igneous rock system. Earth Science Reviews, 37 (3-4), 215-224.

Montel, J., Vielzeuf, D., 1997. Partial melting of metagreywackes, Part II. Compositions of minerals and melts. Contributions to Mineralogy and Petrology, 128, 176-196.

Muncill, G.E., Lasaga, A.C., 1987. Crystal-growth kinetics of plagioclase in igneous systems:One-atmospheree xperimentsa nd application of a simplified growth model. American Mineralogist, 72, 299-311.

Nicoli, G., Stevens, G., Moyen, J.-F., Frei, D., 2014. Rapid evolution from sediment to anatectic granulite in an Archean continental collision zone: the example of the Bandelierkop Formation metapelites, South Marginal Zone, Limpopo Belt, South Africa. Journal of Metamorphic Geology. doi:10.1111/jmg.12116.

Patiño-Douce, A.E., Johnston, A.D., 1991. Phase equilibria and melt productivity in the pelitic system: implications for the origin of peraluminous granitoids and aluminous granites. Contributions to Mineralogy and Petrology, 107, 202-218.

Patiño-Douce, A.E., Harris, N., 1998. Experimental constraints on Himalayan anatexis. Journal of Petrology, 39, 689-710.

Petford, N., Cruden, A.R., McCaffrey, K.J.W., Vigneresse, J.L., 2000. Granite magma formation, transport and emplacement in the Earth's crust. Nature, 408, 669-673.

Petford, N., Kerr, R.C., Lister, J.R., 1993. Dike transport of granitic magmas. Geology, 21, 843–845.

Pichavant, M., Costa, F., Burgisser, A., Scaillet, B., Martel, C., Poussineau, S., 2007. Equilibration Scales in Silicic to Intermediate MagmasçImplications for Experimental Studies. Journal of Petrology, 48 (10), 1955-1972. doi:10.1093/petrology/egm045

Pickering, J.M., Johnston, A.D., 1998. Fluid-absent melting behavior of a two-mica metapelite: Experimental constraints on the origin of the Black Hills granite. Journal of Petrology, 39,1787-1804.

Piwinskiii, A.J., 1967. The attainment of equilibrium in hydrothermal experiments with granite rocks. Earth and Planetary Science Letters, 2, 161-192.

Piwinskiii, A.J, 1968. Experimental Studies of Igneous Rock Series Central Sierra Nevada Batholith, California. The Journal of Geology, 76(5), 548-570.

Platen v, H.,1965. Kristallisation granitischer Schmelzen. Contibutions to Petrology and Mineralogy, 11, 334-381.

Powell, R., Holland, T. J. B., 1988. An internally consistent dataset with uncertainties and correlations: Applications to geobarometry, worked examples and a computer program. Journal of Metamorphic Geology, 6(2), 173-204.

Powell, R., Holland, T. J. B. H., Worley, B., 1998. Calculating phase diagrams involving solid solutions via non-linear equations, with examples using THERMOCALC. Journal of Metamorphic Geology, 16(4), 577-588.

Putins, A., 2002. Mineral replacement reactions: from macroscopic observations to microscopic mechanisms. Mineralogical Magazine, 66(5). 689-708.

Putins, A., 2009. Mineral replacement reactions. Reviews in Mineralogy and Geochemistry, 20, 87-124.

Puziewicz, J., Johannes, J., 1988. Phase equilibria and compositions of Fe-Mg- Al minerals and melts in water-saturated peraluminous granitic systems. Contributions to Mineralogy and Petrology, 100,156-168. doi: 10.1007/BF00373582.

Ramphaka, P.L., 2013. The origin of rhythmic magmatic layering in coarse-grained porphyritic S-type granite of the Peninsula pluton, Cape Granite Suite, South Africa. Unpublished masters thesis, Stellenbosch University.

Reid J.B., Evans O.C., Fates D.G., 1983. Magma mixing in granitic rocks of the central Sierra Nevada, California. Earth and Planetary Science Letters, 66, 243-261.

Ruiz-Agudo, E., Putnis, C., Putnis, A., 2014. Coupled dissolution and precipitation at mineral-fluid interfaces. Chemical Geology, 383, 132-146.

Sawyer, E.W., 1996. Melt segregation and magma flow in migmatites: Implications for the generation of granite magmas. Transactions of the Royal Society of Edinburgh. 87, 85-94.

Scaillet, B., France-Lanord, C., Le Fort, P., 1990. Badrinath-Gangotri plutons (Garhwal, India. petrological and geochemical evidence for fractionation processes in a High Himalayan leucogranite. Journal of VolcanoIogy and Geothermal Research, 44,163-188.

Scheepers, R., and Armstrong, R., 2002. New U-Pbzircon ages of the Cape Granite Suite: Implications for the magmatic evolution of the Saldania Belt. South African Journal of Geology, 105, 241-256.

Skinner, J., 1956. Physical properties of garnet group. American Mineralogist, 41, 428-436.

Sparks, R.S.J., Marshall, L.A., 1986. The thermal and mechanical constraints on mixing between mafic and silicic magmas. Journal of Volcanology and Geothermal Research ,29, 99-124.

Stevens, G., Van Reenen, D.D., 1992a. Partial melting and the origin of metapelitic granulites in the Southern Marginal Zone of the Limpopo Belt, South Africa. Precambrian Research. 55, 303-319.

Steves, G., Clemens, J.D., 1993. Fluid-absent melting and the roles of fluids in the lithosphere: a slanted summary? Chemical Geology, 108, 1-17.

Stevens, G., Clemens, J.D., Droop, G.T.R., 1997. Melt productionduring granulite-facies anatexis: experimental data from ‘primitive’ metasedimentary protoliths. Contributions to Mineralogy and Petrology, 128, 352-370.

Stevens, G.,Vilaros, A., Moyen, J.F., 2007.Selective peritectic garnet entrainment as the origin of geochemicl diversity in S-type granite. Geology, 35, 9-12.

Stevens, G., Villaros, A., Moyen, J.F., 2007. Selective peritectic garnet entrainment as the origin of geochemical diversity in S-type granites. Geology, 35 (1), 9-12.

Swanson, S. E., 1974 The effect of crystal growth rate and nucleation density on the texture of granodiorites (abstract.). Geolical Sociecty of American Abstracts and programs, 6, 979.

Swanson, S.E., 1977. Relation of nucleation and crystal-growth rate to the development of granitic textures. American Mineralogist, 62, 966-978.

Taylor, J., Stevens, G., 2010. Selective entrainment of peritectic garnet into S-type granitic magmas: evidence from Archaean mid-crustal anatectites. Lithos, 120(3), 277-292.

Tropper, P., Hauzenberger, C., 2015. How well do pseudosection calculations reproduce simple experiments using natural rocks: an example from high-PP high-TT granulites of the Bohemian Massif. Australian Journal of Earth Sciences, 108 (1), 123-138. doiI: 10.17738/ajes.2015.0008.

Tropper, P., Konzett, J., Finger, F., 2005. Experimental Constraints on the formation of high-P/high-T granulites in the Southern Bohemian Massif. European Journal of Mineralogy, 17, 343-356. doi.org/10.1127/0935-1221/2005/0017-0343.

Tuttle, O.F., 1949, Two pressure vessels for silicate-water studies: Geological Society of America Bulletin, 60, 1727-1729.

Tuttle, O.F., Bowen, N.L., 1958, Origin of granite in light of experimental studies in the system NaAlSi3Os-KAlSiaOs-SiO2-HO20: Geological Sociecty of America Memoirs, 74, 5-98.

van der Molen, I., Paterson, M.S., 1979. Experimental deformation of partially melted granite. Contributions to Mineralogy and Petrology, 70, 299-318.

Vernon, R.H., 2007. Problems in identifying restite in S-type granites of southeastern Australia, with speculations on sources of magma and enclaves. The Canadian Mineralogist, 45 (1),147-178.

Vernon, R.H., Paterson, S.R., 2008. How late are K-feldspar megacrysts in granites?. Lithos, 104, 327-336.

Vielzeuf, D., Montel, J.M., 1994. Partial melting of metagreywackes, Part I. Fluid-absent experiments and phase relationships. Contributions to Mineralogy and Petrology, 117 375-393.

Vielzeuf, D., Clemens, J.D., Pin, C., Moinet, E., 1990. Granites,granulites and crustal differentiation, in Granulites and crustal differentiation, (ed. D. Vielzeuf and P. Vidal), Dordrecht, Kluwer Academic Publishers.

Vielzeuf, D., Holloway, J.R., 1988. Experimental determination of the fluid-absent melting reactions in the pelitic system. Consequences for crustal differentiation. Contributions to Mineralogy and Petrology, 98, 257-276.

Vielzeuf, D., Baronnet, A., Perchuk, A.L., Laporte, D., Baker, M.B., 2007. Calcium diffusivity in alumina-silicate garnets: an experimental and ATEM study. Contributions to Mineralogy and Petrology, 154, 153-170.

Vigneresse, J.L., Barbey, P., Cuney, M., 1996. Rheological transitions during partial melting and crystallization with application to felsic magma segregation and transfer. Journal of Petrology, 37,1579-600.

Villaros, A., Stevens, G., Moyen, J.F., Buick, I.S., 2009a.The trace element compositions of S-type granites: Evidence for disequilibrium meltind and accesory phase entrainment in the source. Contributions to Mineralogy and Petrology, 158, 543-561.

Villaros, A., Stevens, G., Buick, I.S., 2009b. Tracking S-type granite from source to emplacement: clues from garnet in the Cape Granite Suite. Lithos, 112, 217–235.

Waight, T.E., Dean, A.A., Maas, R., Nicholls, I.A., 2000a. Sr and Nd isotopic investigations towards the origin of feldspar megacrysts in microgranular enclaves in two I-type plutons of the Lachlan Fold Belt, southeast Australia. Australian Journal of Earth Scences, 47, 1105-1112.

Waight, T.E., Maas, R., Nicholls, I.A., 2001. Geochemical investigations of microgranitoid enclaves in the S-type Cowra Granodiorite, Lachlan Fold Belt, SE Australia. Lithos, 56, 165-186.

Waight, T.E., Maas, R., Nicholls, I.A., 2000b. Fingerprinting feldspar phenocrysts using crystal isotopic composition stratigraphy: implications for crystal transfer and magma mingling in S-type granites. Contributions to Mineralogy and Petrology, 139, 227-239.

Wall, V.J., Clemens, J.D., Clarke, D.B., 1987. Models forgranitoid evolution and source compositions. Journal of Geology., 95, 731–750.

White, A.J.R., Chappell, B.W., 1977. Ultrametamorphism and granitoid genesis. Tectonophysics, 43, 7-22.

White, A., Chappell, B., Wyborn, D., 1999. Application of the Restite Model to the Deddick Granodiorite and its Enclaves -a Reinterpretation of the Observations and Data of Maas et al. (1997). Journal of Petrology, 40(3), 413-421.

White, R. W., Powell, R., Holland, T. J. B., Worley, B. A., 2000. The effect of TiO_2 and Fe_2O_3 on metapelitic assemblages at greenschist and amphibolite facies conditions: mineral equilibria calculations in the system K_2O-FeO-MgO-Al_2O_3-SiO_2-H_2O-TiO_2-Fe_2O_3. Journal of Metamorphic Geology, 18, 497-512.

White, R., Powell, R., Clarke, G., 2002. The interpretation of reaction textures in Fe-rich metapelitic granulites of the Musgrave Block, central Australia: constraints from mineral equilibria calculations in the system K_2O-FeO-MgO-Al_2O_3-SiO_2-H2O-TiO_2-Fe_2O_3. Journal of Metamorphic Geology, 20(1), 41-55.

White, R.W., Powell, R., Holland, T.J.B., 2007. Progress relating to calculation of partial melting equilibria for metapelites. Journal of Metamorphic Geology, 25, 511-527.

Williamson B.J., Downes, H., Thirlwall, M.F., Beard, A., 1997. Geochemical constraints on restite composition and unmixing in the Velay anatectic granite, French Massif Central. Lithos, 40, 295-319.

Winkler, H.G.F., Platen, H.v., 1960. Experimentelle Gesteinmetamorphose III. Anatektische Ultrametamorphose kalkhaltiger Tone. Geochimica et Cosmochimica Acta, 18, 294-316.

Winkler, H.G.F., Platen, H.v., 1961. Experimentelle Gesteinmetamorphose IV. Bildung anatektischer Schmelzen aus metamorphisierten Grauwacken. Geochimica et Cosmochimica Acta, 24, 48-69.

Winter, J.D., 2014. Principles of Igneous and Metamorphic Pertrology. Second edition. Edinburgh : Pearson education limited, 109-110.

Wu, F., Jahn, B., Wilde, S.A., Lod, C., Yui, T., Lin, Q., Ge, W., Sun, D., 2003. Highly fractionated I-type granites in NE China (I):geochronology and petrogenesis. Lithos, 66, 241-273.

Zarrebini, S.K., 2016. An experimental investigation into the ‘fate’ of entrained peritectic minerals in I-type granite magmas intruded at below 2kbar. Masters Thesis, Stellenbosch University.Unpublished.

Zhang, Y., Walker, D., Lesher, C.E., 1989. Diffusive crystal dissolution. Contributions to Mineralogy and Petrology,102, 492-513.

13 Appendices

Appendix 1: Synthesis of starting material

Preparation of silicate gel, as outlined by Hamilton and Henderson (1968).

The alkali carbonates, TiO_2 and MgO reagents were dried in a furnace heated at 110 ºC for atleast an hour prior to use. The above-mentioned oxides were weighed, transferred into a beaker and it was covered with a watch glass and placed in a fume cupboard. Nitric acid and distilled water were added to the beaker in a 1:1 ratio, using a squirt bottle to dissolve all the powdered reagents. After most of the reagents had dissolved, a little more nitric acid was added and the solution was placed on a hot plate heated at ~ 70 ºC to evaporate the solution to almost dryness. The resultant crystals were re-dissolved in cold deionized water and re-evaporated to almost dryness. This step was repeated three times to rid the solution of any traces of nitric acid.

The resultant nitrate solids were dissolved in cold deionized water (DI), (volume DI water ≤ volume of required TEOS). The required amount of TEOS was sucked up in a syringe and weighed into a small Teflon beaker; approximately the same volume of ethanol was added into the beaker and stirred to homogenize the solution. The TEOS/ethanol solution was transferred into the large beaker containing the nitrate solution. The sides of the beaker were washed with ethanol (Vol. ethanol = Vol. TEOS), thus the total amount of added ethanol must be more or less the same as the combined volume of added TEOS and nitrate solution. This solution was stirred with a glass rod until it appeared homogeneous. While stirring, 0.88 ammonium hydroxide was slowly added into the TEOS ethanol nitrate solution until a stiff gel formed. The “gel” was left overnight to allow the gelling reaction to run to completion.

After the gelling reaction had taken place, the gel was dried on a hot plate heated at ~70 ºC with the stirring rod inside the beaker. Thereafter the beaker was transferred to a furnace heated at 110ºC to dry for 1 full day. The gel was removed from the furnace and using a spatula all the adhering pieces of the gel was scrapped off the stirring rod and sides of the

beaker. The gel was transferred into an agate mortar and it was grind down. The fine powdered gel was transferred to a platinum crucible; it was heated over a low Bunsen burner until all the brownish NO_2 fumes disappeared. Then the remaining nitrates were converted into oxides by transferring the crucible with dried gel into a furnace heated at 1000 ºC. After removal from the furnace, the gel was, regrind and mixed with appropriate amounts of kaolinite and fayalite. The bulk composition was completed by adding 30 wt% peritectic assemblage (garnet, ilmenite and plagioclase) into the silicate gel. The bulk composition was stored in a vacuum desiccator.

Fayalite synthesis

The synthetic fayalite was synthesized from a mixture of pure SiO_2, Fe metal powder and Fe_2O_3 powder in correct stoichiometric proportions. This mixture was ground in an agate mortar under acetone and left to dry in a furnace heated at ~100 ºC. Thereafter, the mixture was pressed into pellets using a hydraulic press. These pellets were placed into a SiO_2 glass tube with a sealed base. Then the tube was flushed with argon gas, and the open end of the tube was sealed by melting it under a vacuum. The tube was tested for leaks and the synthesis process was completed by placing tubes that were properly sealed in a muffle furnace heated at 900 ºC for 3 days.

Appendix 2: SEM Mineral Standards (Astimex Scientific limited, MINM25-53 #05-010).

Mineral	Standard	Element	Mineral	Standard	Element
Plagioclase and k-feldspar	Albite	Na , Si	Cordierite	Albite	Si
	Pyrope-garnet	Mg		Plagioclase An 65	Al
	Plagioclase An 65	Al		Pyrope Garnet	Mg
	Sanadine	K		Sanadine	K
	Ilmenite	Fe, Ti, Mn		Ilmenite	Fe, Mn
	Diopside	Ca	Garnet	Pyrope Garnet	Si, Al,Mg
Ilmenite	Pyrope garnet	Si, Mg, Al		Ilmenite	Fe, Mn
	Ilmenite	Ti,Fe,Mn		Biotite	K,Ti
Biotite	Biotite	Si, K, Ti		Anorthite 65	Na
	Pyrope Garnet	Al, Mg		Diopside	Ca
	Plagioclase An 65	Ca, Na	Quartz	quartz	Si
	Almandine Garnet	Mn, Fe	Melt	quartz	Si
				Biotite	Ti
				Ilmenite	Fe, Mn
				Albite	Na
				Sanadine	K
				Anorthite 65	Al, Mg
				Diopside	Ca

Appendix 3: Additional Ilmenite electron microbe data

Exp	1	1	1	1	1	2	2	2	2	2	3	3	3	3	3	3
P(Kbar)	1	1	1	1	1	1	1	1	1	1	1	1	1	1	1	1
T(°C)	804	804	804	804	804	754	754	754	754	754	743	743	743	743	743	743
	1	2	3	4	5	1	2	3	4	5	1	2	3	4	5	6
SiO_2	0.89	0.86	0.63	0.50	0.43	0.46	0.74	3.10	0.28	0.19	0.80	0.80	0.73	0.71	0.94	0.81
TiO_2	42.05	42.68	42.80	44.00	43.07	49.27	48.12	47.42	49.36	48.98	53.01	52.97	53.06	53.13	52.25	52.08
Al_2O_3	0.77	0.69	0.60	0.50	0.65	0.35	0.48	0.41	0.35	0.28	0.60	0.54	0.61	0.56	0.60	0.73
Fe_2O_3	20.97	19.61	21.96	17.87	19.20	7.73	8.30	3.31	5.70	7.09	-	-	-	-	-	-
FeO	31.69	33.17	30.58	34.54	33.42	40.30	39.46	43.18	41.33	40.79	44.31	44.10	44.11	43.99	44.70	44.55
MnO	0.59	0.79	0.52	0.70	0.60	-	0.20	0.16	0.17	0.35	0.20	0.34	0.26	0.26	0.21	0.34
MgO	2.01	2.00	2.97	2.44	2.66	1.75	1.69	1.70	1.81	1.76	1.07	1.29	1.22	1.28	1.31	1.48
Na_2O	0.46	0.28	0.47	-	-	0.25	0.24	-	-	-	-	-	-	-	-	-
K_2O	0.29	0.20	0.23	0.19	0.15	0.10	0.12	-	-	-	-	-	-	-	-	-
Total	99.72	100.28	100.76	100.74	100.18	100.22	99.36	99.26	99.00	99.44	99.99	100.04	99.98	99.93	100.01	99.99
xO2	3	3	3	3	3	3	3	3	3	3	3	3	3	3	3	3
Si	0.02	0.02	0.02	0.01	0.01	0.01	0.02	0.08	0.01	0.00	0.02	0.02	0.02	0.02	0.02	0.02
Ti	0.81	0.81	0.80	0.82	0.81	0.92	0.90	0.89	0.93	0.92	0.99	0.99	0.99	0.99	0.97	0.97
Al	0.02	0.02	0.02	0.01	0.02	0.01	0.01	0.01	0.01	0.01	0.02	0.02	0.02	0.02	0.02	0.02
Fe3+	0.35	0.34	0.38	0.33	0.34	0.14	0.16	0.06	0.11	0.13	-	-	-	-	-	-
Fe2+	0.68	0.70	0.64	0.71	0.71	0.84	0.82	0.90	0.87	0.86	0.92	0.91	0.91	0.91	0.93	0.92
Mn2+	0.01	0.02	0.01	0.01	0.01	0.00	0.00	0.00	0.00	0.01	0.00	0.01	0.01	0.01	0.00	0.01
Mg	0.07	0.07	0.11	0.09	0.10	0.06	0.06	0.06	0.07	0.07	0.04	0.05	0.04	0.05	0.05	0.05
Na	0.02	0.01	0.02	-	-	0.01	0.01	-	-	-	-	-	-	-	-	-

K	0.01	0.01	0.01	0.01	-	0.00	0.00	-	-	-	-	-	-	-	-	-
Σcation	2.00	2.00	2.00	2.00	2.00	2.00	2.00	2.00	2.00	2.00	1.98	1.99	1.99	1.99	1.99	2.00
Mg#	6.63	6.57	9.50	7.92	8.57	6.19	6.04	6.15	6.50	6.24	4.13	4.98	4.69	4.93	4.97	5.60

Appendix 4: Additional plagioclase electron microbe data

Exp	1	1	1	1	1	1	2	2	2	2	2	2	2	3	3	3	3	3
P(Kbar)	1	1	1	1	1	1	1	1	1	1	1	1	1	1	1	1	1	1
T(°C)	804	804	804	804	804	804	754	754	754	754	754	754	754	743	743	743	743	743
	1	2	3	4	5	6	1	2	3	4	5	6	7	1	2	3	4	5
SiO_2	57.11	57.31	56.66	56.19	57.74	56.68	58.26	57.26	58.45	58.93	58.90	59.30	58.41	61.08	60.06	60.00	60.00	61.03
TiO_2	0.26	0.13	0.19	0.80	0.17	0.12	-	-	-	-	-	-	-	0.16	0.00		0.17	0.15
Al_2O_3	25.84	25.90	26.92	25.98	25.32	25.89	25.49	25.99	24.78	25.53	24.80	25.32	25.33	21.32	22.74	24.93	22.36	21.37
FeO	0.28	0.26	0.20	0.24	0.35	0.35	0.97	0.81	0.82				0.85	3.58	3.49		3.43	3.31
MgO	-	-	-	-	-	-	-	-	-	-	-	-	-	0.58	0.57	0.00	0.36	0.33
CaO	10.89	10.60	10.65	10.52	9.99	11.00	8.97	8.99	8.83	7.23	8.64	7.59	7.50	6.81	6.31	7.60	6.97	6.93
Na_2O	5.21	5.30	4.99	4.94	5.61	5.05	6.32	6.10	6.57	7.25	6.76	7.25	7.03	6.58	6.68	7.01	6.68	6.85
K_2O	0.86	0.85	0.89	1.49	0.93	0.90	0.34	0.44	0.31	0.31	0.43	0.26	0.37	0.44	0.49	0.50	0.40	0.39
Total	100.45	100.34	100.50	100.16	100.11	99.99	100.35	99.59	99.76	99.25	99.53	99.73	99.50	100.55	100.34	100.04	100.38	100.37
xO2	8	8	8	8	8	8	8	8	8	8	8	8	8	8	8	8	8	8
Si	2.57	2.58	2.54	2.54	2.60	2.56	2.61	2.59	2.64	2.65	2.65	2.65	2.63	2.75	2.70	2.68	2.71	2.75
Ti	0.01	0.00	0.01	0.03	0.01	0.00	-	-	-	-	-	-	-	0.01	0.00	0.00	0.01	0.01
Al	1.37	1.37	1.42	1.39	1.34	1.38	1.35	1.38	1.32	1.35	1.32	1.34	1.35	1.13	1.21	1.31	1.19	1.13
Fe^{2+}	0.01	0.01	0.01	0.01	0.01	0.01	0.04	0.03	0.03	0.00	0.00	0.00	0.03	0.13	0.13	0.00	0.13	0.12
Mg	-	-	-	-	-	-	-	-	-	-	-	-	-	0.04	0.04	0.00	0.02	0.02
Ca	0.53	0.51	0.51	0.51	0.48	0.53	0.43	0.44	0.43	0.35	0.42	0.36	0.36	0.33	0.30	0.36	0.34	0.33

Na	0.45	0.46	0.43	0.43	0.49	0.44	0.55	0.53	0.57	0.63	0.59	0.63	0.61	0.57	0.58	0.61	0.58	0.60
K	0.05	0.05	0.05	0.09	0.05	0.05	0.02	0.03	0.02	0.02	0.02	0.02	0.02	0.03	0.03	0.03	0.02	0.02
Σcation	4.99	4.99	4.98	5.00	4.99	4.99	5.00	5.00	5.00	5.00	5.00	5.00	5.01	4.98	5.00	4.99	5.00	4.99
XAn	51.04	49.98	51.35	49.55	47.02	51.87	43.12	43.77	41.88	34.91	40.39	36.09	36.30	35.40	33.25	36.40	35.68	35.00
XAb	44.17	45.26	43.57	42.11	47.78	43.10	54.93	53.70	56.37	63.32	57.20	62.42	61.57	61.88	63.68	60.75	61.87	62.63
XOr	4.78	4.76	5.09	8.34	5.20	5.03	1.95	2.52	1.76	1.77	2.41	1.49	2.13	2.71	3.07	2.85	2.46	2.37

Appendix 5: Additional k-feldspar electron microbe data

Exp	3	3	3	3	3	3	3
P(Kbar)	1	1	1	1	1	1	1
T(°C)	743	743	743	743	743	743	743
	1	2	3	4	5	6	7
SiO_2	65.29	65.08	65.04	65.28	64.99	65.06	65.07
TiO_2	0.21	0.20	0.29	0.30	0.34	0.35	0.27
Al_2O_3	18.60	18.66	18.60	17.90	18.45	18.62	18.45
MgO	0.11	0.00	0.26	0.00	0.00	0.26	0.19
Na_2O	2.91	2.99	3.41	2.96	3.63	3.40	2.88
K_2O	11.51	11.51	11.00	11.92	10.97	10.94	11.70
Total	100.34	100.11	100.13	99.75	99.9	100.38	100.17
XO2	8	8	8	8	8	8	8
Si	2.97	2.97	2.96	2.99	2.97	2.96	2.97
Ti	0.01	0.01	0.01	0.01	0.01	0.01	0.01
Al	1.00	1.00	1.00	0.97	0.99	1.00	0.99
Fe^{2+}	0.03	0.03	0.02	0.02	0.02	0.03	0.03
Mg	0.01	0.00	0.02	0.00	0.00	0.02	0.01
Ca	0.05	0.04	0.04	0.04	0.05	0.05	0.04
Na	0.26	0.26	0.30	0.26	0.32	0.30	0.25
K	0.67	0.67	0.64	0.70	0.64	0.63	0.68
Σcation	4.99	4.99	5.00	4.99	5.00	5.00	4.99
XAn	4.99	4.44	4.45	4.36	4.69	4.93	4.05
XAb	26.40	27.05	30.62	26.24	31.9	30.52	26.09
XOr	68.61	68.51	64.93	69.4	63.41	64.55	69.86

Appendix 6: Additional garnet electron microbe data

Exp	1	1	1	1	1	1	2	2	2	2	3	3	3	3	3	3
P(Kbar)	1	1	1	1	1	1	1	1	1	1	1	2	1	1	1	1
T(°C)	804	804	804	804	804	804	754	754	754	754	743	743	743	743	743	743
	1	2	3	4	5	6	1	2	3	4	1	2	3	4	5	6
SiO_2	39.32	39.78	39.76	39.78	39.41	39.75	39.40	39.31	38.60	39.71	39.94	40.24	40.05	39.78	40.04	40.09
Al_2O_3	21.96	21.71	22.63	22.12	21.71	21.58	22.37	22.41	21.96	22.48	22.40	22.72	22.60	22.46	22.65	22.61
Cr_2O_3	0.00	0.00	0.18	0.00	0.00	0.20	0.12	0.00	0.00	0.00	0.23	0.00	0.28	0.17	0.10	0.19
Fe_2O_3	3.17	2.98	0.62	1.61	3.49	2.59	0.35	1.09	1.63	0.34	1.51	0.06	0.59	1.17	0.74	0.38
FeO	24.44	25.14	26.59	26.16	24.40	24.90	24.48	25.02	25.18	26.67	25.03	25.80	25.52	24.93	25.72	25.73
MnO	0.44	0.45	0.37	0.41	0.59	0.57	0.46	0.46	0.50	0.37	0.47	0.43	0.38	0.39	0.45	0.46
MgO	10.77	10.68	10.01	10.27	10.76	10.85	10.54	10.29	9.75	9.77	10.15	10.02	10.09	10.24	10.22	10.55
CaO	2.28	2.30	2.14	2.10	2.30	2.11	2.64	2.48	2.42	2.36	3.24	3.13	3.12	3.12	2.98	2.30
Total	102.38	103.04	102.29	102.45	102.65	102.55	100.34	100.94	99.88	101.67	102.82	102.40	102.57	102.14	102.28	102.27
x02	12.00	12.00	12.00	12.00	12.00	12.00	12.00	12.00	12.00	12.00	12.00	12.00	12.00	12.00	12.00	12.00
Si	2.94	2.96	2.98	2.98	2.95	2.97	3.00	2.97	2.99	3.00	2.97	3.00	2.98	2.97	2.98	2.99
Al	1.94	1.91	2.00	1.95	1.91	1.90	2.00	1.98	1.99	1.97	1.96	2.00	1.98	1.98	1.99	1.99
Cr	0.00	0.00	0.01	0.00	0.00	0.01	0.00	0.01	0.01	0.00	0.01	0.00	0.02	0.01	0.01	0.01
Fe^{3+}	0.18	0.17	0.03	0.09	0.20	0.15	0.00	0.07	0.02	0.02	0.08	0.00	0.03	0.07	0.04	0.02
Fe^{2+}	1.53	1.57	1.67	1.64	1.53	1.56	1.61	1.56	1.60	1.63	1.56	1.61	1.59	1.56	1.60	1.60
Mn	0.03	0.03	0.02	0.03	0.04	0.04	0.03	0.02	0.03	0.03	0.03	0.03	0.02	0.02	0.03	0.03
Mg	1.20	1.19	1.12	1.15	1.20	1.21	1.11	1.14	1.17	1.13	1.13	1.11	1.12	1.14	1.15	1.17
Ca	0.18	0.18	0.17	0.17	0.18	0.17	0.25	0.25	0.18	0.22	0.26	0.25	0.25	0.25	0.20	0.18
Σcation	8.00	8.00	8.00	8.00	8.00	8.00	8.00	8.00	8.00	8.00	8.00	8.00	8.00	8.00	8.00	8.00

Mg#	0.41	0.40	0.39	0.40	0.41	0.41	0.40	0.41	0.41	0.40	0.40	0.40	0.41	0.41	0.41	0.41
XAlm	51.98	52.84	55.93	54.98	51.77	52.38	53.62	52.40	53.66	54.12	52.41	53.62	53.28	52.40	53.71	53.66
XPyp	40.86	40.02	37.53	38.50	40.71	40.71	37.14	38.37	39.22	37.55	37.89	37.14	37.57	38.37	38.54	39.22
XSpss	0.94	0.95	0.79	0.87	1.27	1.21	0.91	0.83	0.98	0.95	1.00	0.91	0.80	0.83	0.95	0.98
XGrs	6.22	6.19	5.76	5.65	6.25	5.69	8.32	8.40	6.14	7.38	8.70	8.32	8.35	8.40	6.80	6.14

Appendix 7: Additional Hercynite electron microbe data

Exp	1	1	1	1	1	1	1	1	1	1	1	1
P(Kbar)	1	1	1	1	1	1	1	1	1	1	1	1
T(°C)	804	804	804	804	804	804	804	804	804	804	804	804
	1	2	3	4	5	6	7	8	9	10	11	12
SiO_2	0.29	0.21	0.25	0.00	0.28	0.00	0.19	0.20	0.21	0.24	0.18	0.29
Al_2O_3	55.34	58.22	56.66	56.48	55.49	57.80	57.28	58.20	57.84	56.53	56.87	54.80
Fe_2O_3	9.56	5.66	7.21	8.88	7.85	6.01	5.60	4.30	6.51	7.55	7.46	9.73
FeO	26.27	27.18	27.52	26.75	28.17	27.62	29.23	29.23	27.79	27.82	27.72	26.97
MnO	0.33	0.34	0.38	0.29	0.24	0.32	0.35	0.35	0.41	0.38	0.34	0.39
MgO	8.07	7.96	7.41	7.45	8.28	7.56	7.71	7.77	7.74	7.33	7.52	8.22
Na_2O	0.50	0.41	0.43	0.60	0.00	0.35	0.00	0.00	0.38	0.42	0.41	0.35
Total	100.36	99.98	99.86	100.45	100.31	99.66	100.36	100.05	100.88	100.27	100.50	100.75
XO2	4.00	4.00	4.00	4.00	4.00	4.00	4.00	4.00	4.00	4.00	4.00	4.00
Si	0.01	0.01	0.01	0.00	0.01	0.00	0.01	0.01	0.01	0.01	0.01	0.01
Al	1.81	1.89	1.86	1.85	1.82	1.89	1.87	1.90	1.87	1.85	1.86	1.79
Fe^{3+}	0.20	0.12	0.15	0.19	0.16	0.13	0.12	0.09	0.13	0.16	0.16	0.20
Fe^{2+}	0.61	0.63	0.64	0.62	0.66	0.64	0.68	0.68	0.64	0.65	0.64	0.63
Mn	0.01	0.01	0.01	0.01	0.01	0.01	0.01	0.01	0.01	0.01	0.01	0.01
Mg	0.33	0.33	0.31	0.31	0.34	0.31	0.32	0.32	0.32	0.30	0.31	0.34
Na	0.03	0.02	0.02	0.03	0.00	0.02	0.00	0.00	0.02	0.02	0.02	0.02
Σcation	3.00	3.00	3.00	3.00	3.00	3.00	3.00	3.00	3.00	3.00	3.00	3.00
XFe	53.33	58.50	58.27	55.69	56.33	59.38	60.86	62.25	58.58	58.33	57.95	53.53
Mg#	29.20	30.55	27.99	27.67	29.53	28.99	28.64	29.51	29.08	27.41	28.02	29.08

Appendix 8: Additional cordierite electron microbe data

Exp	1	1	1	1	1	1	1	1	1	1	1	1	1	1	1	1
P(Kbar)	1	1	1	1	1	1	2	2	2	2	2	3	3	3	3	3
T(°C)	804	804	804	804	804	804	754	754	754	754	754	743	743	743	743	743
	1	2	3	4	5	6	1	2	3	4	5	1	2	3	4	5
SiO_2	47.59	48.06	47.89	47.87	48.41	47.71	49.20	49.55	45.96	47.99	48.14	45.42	48.08	45.35	47.85	48.26
Al_2O_3	32.62	32.75	32.66	33.23	33.68	33.16	33.91	33.99	33.07	32.96	33.34	33.02	32.09	32.92	33.42	32.11
FeO	6.90	7.29	6.87	6.88	6.36	6.31	7.36	7.20	7.22	7.13	7.20	10.05	10.73	10.01	9.56	9.06
MnO	0.15	0.00	0.00	0.00	0.00	0.00	0.14	0.16	0.00	0.00	0.16	0.19	0.00	0.18	0.00	0.00
MgO	9.52	9.63	9.59	9.57	9.87	9.64	9.32	9.15	8.86	9.07	9.09	7.54	6.08	7.90	6.97	7.59
CaO	0.26	0.10	0.11	0.16	0.28	0.25	0.18	0.17	0.19	0.00	0.13	0.38	0.00	0.23	0.00	0.00
Na_2O	0.44	0.20	0.20	0.27	0.48	0.46	0.24	0.19	0.48	0.13	0.28	0.45	0.40	0.31	0.40	0.39
K_2O	0.40	0.29	0.30	0.37	0.30	0.32	0.15	0.16	0.26	0.11	0.12	0.57	0.32	0.37	0.31	0.28
Total	97.88	98.32	97.62	98.35	99.39	97.85	100.49	100.56	96.04	97.38	98.46	97.62	97.71	97.28	98.51	97.69
xO2	18.00	18.00	18.00	18.00	18.00	18.00	18.00	18.00	18.00	18.00	18.00	18.00	18.00	18.00	18.00	18.00
Si	4.93	4.95	4.95	4.92	4.91	4.92	4.95	4.97	4.85	4.97	4.94	4.80	5.05	4.80	4.96	5.03
Ti	0.00	0.00	0.00	0.00	0.00	0.00	0.00	0.00	0.00	0.00	0.00	0.00	0.00	0.00	0.00	0.00
Al	3.98	3.97	3.98	4.02	4.03	4.03	4.02	4.02	4.12	4.02	4.03	4.12	3.97	4.11	4.08	3.94
Fe^{2+}	0.60	0.63	0.59	0.59	0.54	0.54	0.62	0.60	0.64	0.62	0.62	0.89	0.94	0.89	0.83	0.79
Mn	0.01	0.00	0.00	0.00	0.00	0.00	0.01	0.01	0.00	0.00	0.01	0.02	0.00	0.02	0.00	0.00
Mg	1.47	1.48	1.48	1.47	1.49	1.48	1.40	1.37	1.39	1.40	1.39	1.19	0.95	1.25	1.08	1.18
Ca	0.03	0.01	0.01	0.02	0.03	0.03	0.02	0.02	0.02	0.00	0.01	0.04	0.00	0.03	0.00	0.00

Na	0.09	0.04	0.04	0.05	0.10	0.09	0.05	0.04	0.10	0.03	0.06	0.09	0.08	0.06	0.08	0.08
K	0.05	0.04	0.04	0.05	0.04	0.04	0.02	0.02	0.03	0.01	0.02	0.08	0.04	0.05	0.04	0.04
Σcation	11.16	11.11	11.10	11.12	11.14	11.13	11.08	11.05	11.16	11.04	11.08	11.22	11.03	11.20	11.06	11.06
Mg#	70.65	70.18	71.35	71.26	73.43	73.16	68.92	68.93	68.65	69.38	68.74	56.76	50.27	58.02	56.53	59.90
XFe	28.70	29.82	28.65	28.74	26.57	26.84	30.50	30.40	31.35	30.62	30.55	42.44	49.73	41.23	43.47	40.10

Appendix 9: Additional biotite electron microbe data

Exp	1	1	1	1	1	1	1	1	1	3	3	3	3	3	3	3	3	3
P(Kbar)	1	1	1	1	1	1	1	1	1	1	1	1	1	1	1	1	1	1
T(°C)	804	804	804	804	804	804	804	804	804	743	743	743	743	743	743	743	743	743
	1	2	3	4	5	6	7	8	9	3	4	5	6	7	8	9	10	11
SiO2	40.18	41.31	40.09	40.43	40.66	41.35	39.26	39.66	40.35	36.12	35.96	35.31	36.72	37.17	36.49	35.96	34.77	38.19
TiO2	1.36	0.98	1.61	1.53	1.19	0.58	1.96	1.19	1.59	-	-	-	-	-	-	-	-	-
Al2O3	19.41	20.25	19.82	19.96	19.52	20.17	19.32	20.05	19.87	21.44	21.54	21.02	22.70	22.88	21.47	20.85	20.69	22.17
FeO	14.09	14.38	13.71	13.72	14.21	14.60	15.05	14.62	14.10	17.67	17.20	19.65	16.50	17.84	17.62	18.28	16.56	17.53
MnO	0.00	0.13	0.18	0.00	0.00	0.00	0.22	0.00	0.00	-	-	-	-	-	-	-	-	-
MgO	10.55	11.65	10.76	10.56	10.02	10.25	12.42	10.02	10.25	11.60	11.94	10.60	12.70	12.23	11.49	10.40	10.75	11.98
CaO	0.21	0.54	0.18	0.36	0.19	0.30	0.00	0.19	0.30	-	-	-	-	-	-	-	-	-
Na2O	0.70	0.92	0.87	1.03	0.85	1.02	0.90	0.85	0.62	0.37	0.51	0.44	0.42	0.41	0.42	0.35	0.37	0.42
K2O	8.30	8.82	8.93	8.65	8.66	8.10	9.01	8.99	8.81	9.01	9.14	9.20	9.26	9.28	9.01	8.96	8.97	9.04
Total	94.79	98.99	96.15	96.24	95.29	96.36	98.14	95.56	95.88	96.21	96.29	96.21	98.30	99.82	96.49	94.80	92.12	99.33
XO2	22	22	22	22	22	22	22	22	22	22	22	22	22	22	22	22	22	22
Si	5.88	5.81	5.80	5.83	5.92	5.94	5.61	5.80	5.85	5.36	5.33	5.31	5.29	5.30	5.39	5.43	5.38	5.45
Ti	0.15	0.10	0.17	0.17	0.13	0.06	0.21	0.13	0.17	0.00	0.00	0.00	0.00	0.00	0.00	0.00	0.00	0.00
Al	3.35	3.35	3.38	3.39	3.35	3.41	3.26	3.46	3.39	3.75	3.76	3.72	3.86	3.85	3.74	3.71	3.78	3.73
Fe2+	1.72	1.69	1.66	1.65	1.73	1.75	1.80	1.79	1.71	2.19	2.13	2.47	1.99	2.13	2.18	2.31	2.14	2.09
Mn2+	0.00	0.02	0.02	0.00	0.00	0.00	0.03	0.00	0.00	0.00	0.00	0.00	0.00	0.00	0.00	0.00	0.00	0.00
Mg	2.30	2.44	2.32	2.27	2.18	2.19	2.65	2.18	2.21	2.56	2.64	2.38	2.73	2.60	2.53	2.34	2.48	2.55
Ca	0.03	0.08	0.03	0.06	0.03	0.05	0.00	0.03	0.05	-	-	-	-	-	-	-	-	-
Na	0.20	0.25	0.24	0.29	0.24	0.28	0.25	0.24	0.17	0.11	0.15	0.13	0.12	0.11	0.12	0.10	0.11	0.12

K	1.55	1.58	1.65	1.59	1.61	1.48	1.64	1.68	1.63	1.70	1.73	1.76	1.70	1.69	1.70	1.73	1.77	1.64
Σcation	15.17	15.33	15.28	15.25	15.19	15.18	15.37	15.30	15.18	15.67	15.73	15.77	15.69	15.68	15.65	15.63	15.67	15.57
Mg#	57.16	59.09	58.32	57.84	55.69	55.59	59.54	54.99	56.45	53.91	55.32	49.03	57.85	55.00	53.76	50.35	53.64	54.93
XFe	42.84	40.91	41.68	42.16	44.31	44.41	40.46	45.01	43.55	46.09	44.68	50.97	42.15	45.00	46.24	49.65	46.36	45.07

Appendix 10: Additional Electron Microbe analysis of quenched experimental melts, normalized to 100% anhydrous.

Table 1: Experiment 1

Exp	1	1	1	1	1	1	1	1	1
P(Kbar)	1	1	1	1	1	1	1	1	1
T(°C)	804	804	804	804	804	804	804	804	804
	1	2	3	4	5	6	7	8	9
SiO_2	76.09	76.32	76.26	76.99	76.34	76.56	77.04	76.83	76.65
TiO_2	0.38	0.41	0.37	0.22	0.24	0.31	0.33	0.25	0.33
Al_2O_3	15.52	15.71	15.05	14.75	14.75	14.68	14.49	14.60	15.28
FeO	0.77	0.84	0.83	0.80	0.82	0.91	0.87	0.82	0.86
MgO	0.56	0.54	0.65	0.50	0.40	0.50	0.52	0.50	0.57
CaO	0.64	0.60	0.71	0.63	0.60	0.55	0.55	0.58	0.54
Na_2O	1.22	1.27	1.26	1.37	1.65	1.51	1.16	1.41	1.45
K_2O	4.82	4.30	4.87	4.75	5.20	4.97	5.03	5.03	4.31
Total	100.00	100.00	100.00	100.00	100.00	100.00	100.00	100.00	100.00
Si	1.27	1.27	1.27	1.28	1.27	1.27	1.28	1.28	1.28
Ti	0.00	0.01	0.00	0.00	0.00	0.00	0.00	0.00	0.00
Al	0.15	0.15	0.15	0.14	0.14	0.14	0.14	0.14	0.15
Fe^{2+}	0.01	0.01	0.01	0.01	0.01	0.01	0.01	0.01	0.01
Mg	0.01	0.01	0.02	0.01	0.01	0.01	0.01	0.01	0.01
Ca	0.01	0.01	0.01	0.01	0.01	0.01	0.01	0.01	0.01
Na	0.02	0.02	0.02	0.02	0.03	0.03	0.02	0.02	0.02
K	0.05	0.05	0.05	0.05	0.06	0.05	0.05	0.05	0.05
Mg#	0.57	0.53	0.58	0.53	0.46	0.49	0.52	0.52	0.54
ASI	1.84	1.99	1.73	1.72	1.55	1.64	1.72	1.65	1.89
Mg + Fe	0.02	0.03	0.03	0.02	0.02	0.03	0.02	0.02	0.03

Table 2: Experment 2

Exp	2	2	2	2	2	2	2	2
P(Kbar)	1	1	1	1	1	1	1	1
T(°C)	754	754	754	754	754	754	754	754
	1	2	3	4	5	6	7	8
SiO_2	76.73	75.40	76.91	76.52	75.62	75.80	75.70	76.30
TiO_2	0.32	0.27	0.29	0.31	0.30	0.27	0.31	0.30
Al_2O_3	14.64	14.75	14.71	14.50	14.46	14.25	14.54	14.33
FeO	0.90	0.92	0.82	0.81	0.95	0.84	0.93	0.81
MgO	0.59	0.40	0.40	0.65	0.44	0.55	0.46	0.45
CaO	0.58	0.63	0.53	0.60	0.54	0.56	0.66	0.52
Na_2O	1.15	1.71	1.40	1.13	1.57	1.63	1.63	1.40
K_2O	5.08	5.92	4.94	5.49	6.12	6.10	5.78	5.87
Total	100.00	100.00	100.00	100.00	100.00	100.00	100.00	100.00
Si	1.28	1.25	1.28	1.27	1.26	1.26	1.26	1.27
Ti	0.00	0.00	0.00	0.00	0.00	0.00	0.00	0.00
Al	0.14	0.14	0.14	0.14	0.14	0.14	0.14	0.14
Fe^{2+}	0.01	0.01	0.01	0.01	0.01	0.01	0.01	0.01
Mg	0.01	0.01	0.01	0.02	0.01	0.01	0.01	0.01
Ca	0.01	0.01	0.01	0.01	0.01	0.01	0.01	0.01
Na	0.02	0.03	0.02	0.02	0.03	0.03	0.03	0.02
K	0.05	0.06	0.05	0.06	0.06	0.06	0.06	0.06
Mg#	0.54	0.43	0.47	0.59	0.45	0.54	0.47	0.50
ASI	1.72	1.41	1.70	1.62	1.41	1.37	1.42	1.48
Mg + Fe	0.03	0.02	0.02	0.03	0.02	0.03	0.02	0.02

Table 3: Experiment 3

Exp	3	3	3	3	3	3	3
P(Kbar)	1	1	1	1	1	1	1
T(°C)	743	743	743	743	743	743	743
	1	2	3	4	5	6	7
SiO_2	77.86	77.86	77.86	77.03	77.36	78.05	77.35
TiO_2	0.13	0.15	0.14	0.18	0.16	0.18	0.17
Al_2O_3	13.28	13.25	13.68	13.87	13.29	13.29	13.72
FeO	0.98	0.93	1.00	1.02	1.00	1.03	0.98
MgO	0.31	0.33	0.46	0.36	0.49	0.44	0.42
CaO	0.44	0.48	0.63	0.49	0.57	0.44	0.52
Na_2O	1.89	1.89	1.10	1.69	1.76	1.42	1.74
K_2O	5.10	5.11	5.12	5.37	5.37	5.16	5.11
Total	100.00	100.00	100.00	100.00	100.00	100.00	100.00
Si	1.30	1.30	1.30	1.28	1.29	1.30	1.29
Ti	0.00	0.00	0.00	0.00	0.00	0.00	0.00
Al	0.13	0.13	0.13	0.14	0.13	0.13	0.13
Fe^{2+}	0.01	0.01	0.01	0.01	0.01	0.01	0.01
Mg	0.01	0.01	0.01	0.01	0.01	0.01	0.01
Ca	0.01	0.01	0.01	0.01	0.01	0.01	0.01
Na	0.03	0.03	0.02	0.03	0.03	0.02	0.03
K	0.05	0.05	0.05	0.06	0.06	0.05	0.05
Mg#	0.36	0.39	0.45	0.38	0.47	0.43	0.43
ASI	1.40	1.38	1.60	1.45	1.35	1.51	1.46
Mg + Fe	0.02	0.02	0.03	0.02	0.03	0.03	0.02